

DISTRIBUTION AGREEMENT

In presenting this thesis or dissertation as a partial fulfillment of the requirements for an advanced degree from Emory University, I hereby grant to Emory University and its agents the non-exclusive license to archive, make accessible, and display my thesis or dissertation in whole or in part in all forms of media, now or hereafter known, including display on the world wide web. I understand that I may select some access restrictions as part of the online submission of this thesis or dissertation. I retain all ownership rights to the copyright of the thesis or dissertation. I also retain the right to use in future works (such as articles or books) all or part of this thesis or dissertation.

Virginia Vachon

Date

APPROVAL SHEET

Modulation of host cell innate immune proteins by viral non-coding RNAs

By: Virginia K. Vachon

Doctor of Philosophy

Graduate Division of Biological and Biomedical Sciences

Graeme L. Conn, PhD

Advisor

Anita H. Corbett, PhD

Committee Member

Charles P. Moran Jr., PhD

Committee Member

Eric A. Ortlund, PhD

Committee Member

Samuel H. Speck, PhD

Committee Member

Accepted:

Lisa A. Tedesco, PhD

Dean of the James T. Laney School of Graduate Studies

_____Date

Modulation of host cell innate immune proteins by viral non-coding RNAs

By

Virginia Vachon

BA, Agnes Scott College, 2007

Advisor: Graeme L. Conn, Ph.D.

An abstract of

A dissertation submitted to the Faculty of the
James T. Laney School of Graduate Studies of Emory University

In partial fulfillment of the requirements for the degree of

Doctor of Philosophy

In

Graduate Division of Biological and Biomedical Sciences

Microbiology and Molecular Genetics

2015

ABSTRACT

Modulation of host cell innate immune proteins by viral non-coding RNAs

By

Virginia Vachon

Precise control of protein synthesis is essential for regulation of normal cellular processes and responses to cell stress. In addition, the innate immune response exploits varied strategies of translational control in order to limit viral protein synthesis and thus replication. The double-stranded RNA-activated protein kinase (PKR) and 2'-5'-oligoadenylate synthetases (OAS) sense cytosolic double-stranded RNA, a molecular hallmark of virus infection, to initiate a general shut down of protein synthesis. The central importance of PKR and OAS is highlighted by numerous diverse strategies employed by a range of viruses to thwart their effects. Among them, the Adenovirus non-coding (nc)RNA transcript, VA RNA₁, accumulates to high levels in later stages of infection, and is critical for efficient adenoviral replication. VA RNA₁ is well recognized for its inhibition of dsRNA-activated protein kinase (PKR)-mediated shut-down of general translation but, counterintuitively, VA RNA₁ *activates* rather than inhibits OAS1. The fundamental basis for control of these proteins by VA RNA₁ and other viral or cellular non-coding RNAs, including the range of RNA sequences and structures capable of regulating their activity remains underexplored.

Here, VA RNA₁ is used as a model to further our understanding of RNA-mediated regulation of PKR and OAS1. Following a review of the current state of knowledge surrounding the multifaceted roles of VA RNA₁, a description is provided of methods developed for solution-based probing of VA RNA₁ and other short RNA structures. These methods are then applied to a study on the role of VA RNA₁ structure in PKR inhibition. Finally, using VA RNA₁ as a starting point, discovery and characterization of a general, novel motif for optimal activation of OAS1 is presented.

Defining the molecular signatures which govern the activities of PKR and OAS1 is essential to understanding how these proteins maximize their protective role against a broad range of pathogens while accurately discriminating between foreign and self molecules to avoid inadvertent activation. Detailed knowledge of specific pathogen-associated molecular patterns recognized by proteins of the innate immune system is also an essential foundation for development of therapeutic strategies that either directly target viral pathogens or enhance the host cell response to them.

Modulation of host cell innate immune proteins by viral non-coding RNAs

By

Virginia Vachon

BA, Agnes Scott College, 2007

Advisor: Graeme Conn, Ph.D.

A dissertation submitted to the Faculty of the
James T. Laney School of Graduate Studies of Emory University

In partial fulfillment of the requirements for the degree of

Doctor of Philosophy

In

Graduate Division of Biological and Biomedical Sciences

Microbiology and Molecular Genetics

2015

ACKNOWLEDGEMENTS

I would like to thank the members of my committee for their continued encouragement and support.

Many thanks to the members of the Conn Lab for their willingness to teach, troubleshoot, and discuss all aspects of science.

I would also like to thank Greg Gessler for making life as a scientist and parent look easy, and Olive Gessler for loving the ‘science lab,’ and taking her tubes of ‘protein’ to show-and-tell.

Finally, I would like to thank Graeme Conn for convincing me to come solve puzzles in his lab.

TABLE OF CONTENTS

ABSTRACT	iv
ACKNOWLEDGEMENTS	vi
CHAPTER 1:	1
Introduction	1
BACKGROUND	2
RESEARCH GOALS	14
REFERENCES	17
CHAPTER 2:	31
Adenovirus VA RNA: An essential pro-viral non-coding RNA	31
ABSTRACT	32
INTRODUCTION	33
<i>Expression, Localization, and Structure of AdV VA RNAs</i>	35
Cellular Localization of VA RNA₁	39
VA RNA Structure	41
<i>VA RNAs Usurp Multiple Cellular Functions</i>	46
VA RNA interference with RNAi machinery	46
<u>Competition for nuclear export by Exportin 5 (Exp 5)</u>	48
<u>Dicer Saturation</u>	48
<u>mivaRNA incorporation into RISC: a mechanism of viral control of host cell gene expression?</u>	50
VA RNA ₁ -mediated inhibition of PKR	54

VA RNA _I regulation of 2'-5' oligoadenylate synthetase-1 (OAS1).....	61
Pro-viral roles of Apical Stem–Central Domain fragment from Dicer-processing of VA RNA _I	65
<i>VA RNA_I induces type-I interferon late in infection</i>	68
<i>Considerations for Ad vectors</i>	69
CONCLUSIONS	70
ACKNOWLEDGEMENTS	71
REFERENCES	71
CHAPTER 3:	91
Plasmid template design and <i>in vitro</i> transcription of short RNAs within a ‘structure cassette’ for structure probing experiments.....	91
ABSTRACT	92
INTRODUCTION	93
MATERIALS.....	97
<i>Generating a structure cassette plasmid containing a target RNA sequence.</i>	97
<i>Cloning Method 1: PCR.</i>	98
<i>Cloning Method 2: Direct ligation of chemically synthesized DNA oligonucleotides.</i>	99
<i>Analysis of transcribed RNA.</i>	99
METHODS	100
<i>Generating structure cassette plasmids with new target RNAs.</i>	100

<i>Cloning Method 1: PCR</i>	102
<i>Cloning Method 2: Direct ligation of chemically synthesized DNA oligonucleotides</i>	103
<i>Analysis and preparation of transcribed RNA for probing experiments</i>	104
NOTES.....	106
ACKNOWLEDGEMENTS.....	110
REFERENCES.....	110
CHAPTER 4:	112
Dissection of the adenoviral VA RNA_I Central Domain structure reveals minimal requirements for RNA-mediated inhibition of PKR	112
ABSTRACT.....	113
INTRODUCTION	113
EXPERIMENTAL PROCEDURES.....	116
RESULTS AND DISCUSSION.....	121
REFERENCES	146
ACKNOWLEDGEMENTS.....	151
FUNDING.....	151
CHAPTER 5:	152
A novel RNA molecular signature for activation of 2'-5' oligoadenylate synthetase-1.	152
ABSTRACT.....	153

INTRODUCTION	153
MATERIAL AND METHODS	155
RESULTS	159
DISCUSSION	173
ACKNOWLEDGEMENT	177
FUNDING.....	177
SUPPLEMENTAL FIGURES	178
REFERENCES	183
CHAPTER 6:	189
Conclusions	189
VA RNA ₁ INHIBITION OF PKR: OPEN QUESTIONS	190
DICER PROCESSING OF VA RNA ₁	194
FUNCTIONAL IMPLICATIONS OF THE 3'-SSPY MOTIF	196
ADDITIONAL POTENTIAL PROVIRAL ROLES FOR VA RNA ₁	202
THE FUNCTIONS OF EBV EBER-1 REMAIN UNCLEAR.....	203
CONCLUSION.....	204

LIST OF TABLES

CHAPTER 11

TABLE 1. Proteins Responsible For Detection Of Viral dsRNA During Infection.....3

CHAPTER 5152

TABLE 1. Influence Of 3'-ssPy On OAS1 Activity..... 165

TABLE OF FIGURES

CHAPTER 1

Figure 1. PKR-mediated antiviral response to cytoplasmic dsRNA.....5

Figure 2. PKR mediated antiviral response to cytoplasmic dsRNA7

Figure 3. Viral non-coding RNA secondary structures.....9

Figure 4. Model of viral non-coding RNAs VA RNA₁ and EBER-1 interaction with dsRNA-activated innate immune proteins PKR and OAS1.....11

CHAPTER 2

Figure 1. VA RNA₁ gene organization and transcript secondary structure.....37

Figure 2. Predicted structure of additional 3'-end sequence in VA RNA₁ produced at the 'backup terminator' (T2).....40

Figure 3. Structural model for AdV VA RNA₁ and the role of the Central Domain in PKR inhibition.....44

Figure 4. Overview of known activities of VA RNAs against host cell components.....47

Figure 5. Activity of the Dicer-derived Apical Stem-Central Domain (AS-CD) fragment against
PKR and OAS1).....67

CHAPTER 3

Figure 1. A plasmid system for in vitro transcription of RNAs within a “structure cassette.”
.....95

Figure 2. Denaturing polyacrylamide gel analysis of target RNAs within the structure
cassette.....103

Figure 3. Native polyacrylamide gel analysis of RNAs within the structure cassette.....105

CHAPTER 4

Figure 1. The VA RNA_I Central Domain contains putative tertiary interactions that are
stabilized by low pH, Mg²⁺ and PKR.....124

Figure 2. Identification of tertiary interactions and Mg²⁺ binding sites within the VA RNA_I
Central Domain.....127

Figure 3. A123 is the protonated nucleotide within the VA RNA_I Central Domain.131

Figure 4. Loop III nucleotides 123-127 are sufficient to form the Central Domain
pseudoknot structure.133

Figure 5. SHAPE analysis of TSΔ25+1 and TSΔ25 RNAs.....135

Figure 6. The intact VA RNA_I Central Domain tertiary structure is not required for PKR
inhibition or binding.....137

Figure 7. Role of the Central Domain 5'-strand nucleotides and three-helix junction in
optimal PKR inhibition.....140

CHAPTER 5

Figure 1. Activation of OAS1 by adenovirus VA RNA ₁ requires its single-stranded pyrimidine-rich 3'-end.	162
Figure 2. The 3'-ssPy motif potentiates OAS1 activation by a simple dsRNA duplex containing an OAS1 consensus sequence.	164
Figure 3. Kinetic analysis of OAS1 activation by RNAs with and without a 3'-ssPy motif.	165
Figure 4. The 3'-ssPy motif causes an increase in OAS1 activity but not an altered accumulation of specific product lengths.....	167
Figure 5. 3'-end modifications have minor effects on 3'-ssPy activity, and are relatively unaltered by 5'-ppp on the reverse strand of 18 bp RNA.	169
Figure 6. OAS1 G157 is a critical mediator of 3'-ssPy motif action..	172
Figure 7. Model for 3'-ssPy motif action.	174
Supplementary Figure S1. Human OAS1 produced by cleavage of the SUMO-OAS1 fusion is active and shows only minimal prep-to-prep variation.....	178
Supplementary Figure S2. Secondary and domain structures of the non-coding RNAs used in this study.	179
Supplementary Figure S3. Full activation of OAS1 by structured viral and cellular non-coding RNAs requires their 3'-end single-stranded pyrimidine-rich sequence (3'-ssPy motif).....	180
Supplementary Figure S4. ssRNA sequences corresponding to the 18 bp dsRNA do not activate OAS1.	180

Supplementary Figure S5. A 5'-triphosphate group on the reverse strand of the model 18 bp dsRNA has little effect on 3'-ssPy motif activity.....181

Supplementary Figure S6. Consurf analysis of OAS1.182

CHAPTER 6

Figure 1. Updated model of viral non-coding rRNAs VA RNA₁ and EBER-1 interaction with dsRNA-activated innate immune proteins PKR and OAS1.....191

Figure 2. The Dicer-processed VA RNA₁ is not identical to TSA₂₁.....195

Figure 3. OAS1 binding orientation and potency is derived from the context-specific effects of the activation consensus sequence and the 3'-ssPy motif.....198

Figure 4. A 40 nt hairpin RNA construct containing the 18 bp model duplex RNA for cell-based studies.199

CHAPTER 1:

Introduction

BACKGROUND

The innate cellular immune system is critical for host survival of invading pathogens. Upon detection of foreign molecules, or pathogen-associated molecular patterns (PAMPs) of infection (1), this system elicits a range of responses that limit virus replication and spread, and initiates response by the adaptive immune system. The collection of innate immune proteins that detect foreign nucleic acids, including cytoplasmic double-stranded RNA (dsRNA), is especially important for limiting virus replication. Cytoplasmic dsRNA can be produced as a consequence of RNA virus genome replication, transcription of overlapping reading frames in both RNA and DNA viruses, and formation of viral mRNA or RNA genome secondary structure. In order to maximize the range of their protective effect, innate immune proteins must be somewhat promiscuous, and thus able to detect dsRNA from multiple pathogenic sources, while still maintaining a level of stringency required for avoiding inadvertent activation.

The proteins responsible for detection of cytoplasmic dsRNA during virus infection include the dsRNA-activated protein kinase (PKR) (2), retinoic acid-inducible gene I (RIG-I) (3), melanoma differentiation-associated gene 5 (MDA5) (4), and the 2'-5' oligoadenylate synthetase (OAS) family (5). Each of these proteins possesses specific, though often overlapping, requirements for activation; including dsRNA length, the degree to which base-pair mismatches are tolerated, the importance of sequence content, tolerance of RNA modifications, and the presence of a 5'-triphosphate (Table 1). Mice lacking either PKR or a functional OAS pathway exhibit virus-specific susceptibility to infection and only minimal susceptibility to uncontrolled cell proliferation (6-11).

Table 1: Proteins responsible for detection of viral dsRNA during infection, activating dsRNAs, targets of activated proteins, and the viruses against which the activities of these proteins are required for optimal host defense.

Protein	Activating RNA	Target	Required for defense: Virus
RIG-I	Blunt dsRNA of between 10-20 and 4000 nt (80-82) ssRNA greater than 25 nt Must have 5'-ppp (83) ssRNA >300bp can activate without 5'-ppp (81)	Induces aggregation of MAVS on mitochondrial membrane, inducing a signal cascade which results in expression of Type 1 interferons and production of anti-viral genes (16).	Paramyxovirus, influenza (12) Negative strand viruses (84) Japanese encephalitis virus (12) Hepatitis C virus (85) Measles (86) West Nile Virus (87)
MDA5	dsRNA > 2000 nt (81) No reported 5' or 3' end specificity	Expression of Type 1 interferon and anti-viral genes through the same pathways as RIG-I (16). Formation of filaments on dsRNA also promotes formation of polar MAVS filaments (88)	Picornaviruses (12)
PKR	Can bind a minimum of 16 bp perfectly base-paired RNA (89). Activation requires ~33bp (90,91). A-G mismatches and secondary structure effect tolerated as long as A-form RNA maintained (92).	Phosphorylation of eIF2 results in shut down of general translation PKR also affects transcription of antiproliferative, anti-viral, and stress-response genes, nuclear translocation of NFκB, and apoptosis (reviewed in (18,20)).	Vaccinia Viruses (93) Additional roles reviewed in (94)
OAS1	Minimum of 18 bp Consensus sequences reported: NNWW(N ₆)WGN (62). APyAPy(N)nCC and UU(N)nACCC (in different parts of the RNA) (63).	Activation results in synthesis of 2'-5' oligoadenylates (A(2'-5'A) _n). Oligoadenylate trimers (or longer) activate only known target RNase L, causing degradation of cellular, viral and rRNAs (9).	Dengue Virus (95) Flaviviruses (96) West Nile Virus (97) Additional roles reviewed in (9)

Similarly, MDA5 and RIG-I have overlapping roles in defense against some viruses, and may be singly dispensable in a virus-dependent manner (12,13). Mice deficient in both PKR and the OAS/ RNase L pathway or RIG-I and MDA5 show considerable susceptibility to a larger range of viruses than do mice deficient in single proteins (14,15). In spite of having some overlapping ability to detect dsRNA and elicit host immune responses, the virus-dependent susceptibility of mice in which these proteins are absent indicates that this overlap in function is incomplete (12).

PKR and the OAS family of proteins regulate cellular protein synthesis

Unlike MDA5 and RIG-I, whose activation results primarily in stimulation of Type-I interferon genes (16,17), PKR and OAS activation by cytoplasmic dsRNA results in a shut down of protein synthesis (Table 1) (18,19). Though PKR has a range of other inflammatory and stress response functions, reviewed extensively by others (18,20), its effect on general translation is severely limiting to virus replication.

Upon detection of cytoplasmic dsRNA, PKR dimerizes and *trans* autophosphorylates on multiple serine/threonine residues, resulting in an activated kinase with reduced dependence on dsRNA. Activated PKR then phosphorylates its target, the α subunit of the translation initiation factor eIF2 on residue serine 51 (21). eIF2 α -Ser51 phosphorylation increases the affinity of eIF2 for its guanosine nucleotide exchange factor eIF2B, effectively rendering it unable to exchange GDP for GTP, and sufficiently depleting eIF2•GTP to halt translation. Because GTP hydrolysis is the rate-limiting step for formation of the ternary complex during translation initiation, PKR phosphorylation

of eIF2 results in a shut down of general translation, thereby preventing synthesis of viral and host proteins, halting virus spread (Figure 1; 22,23).

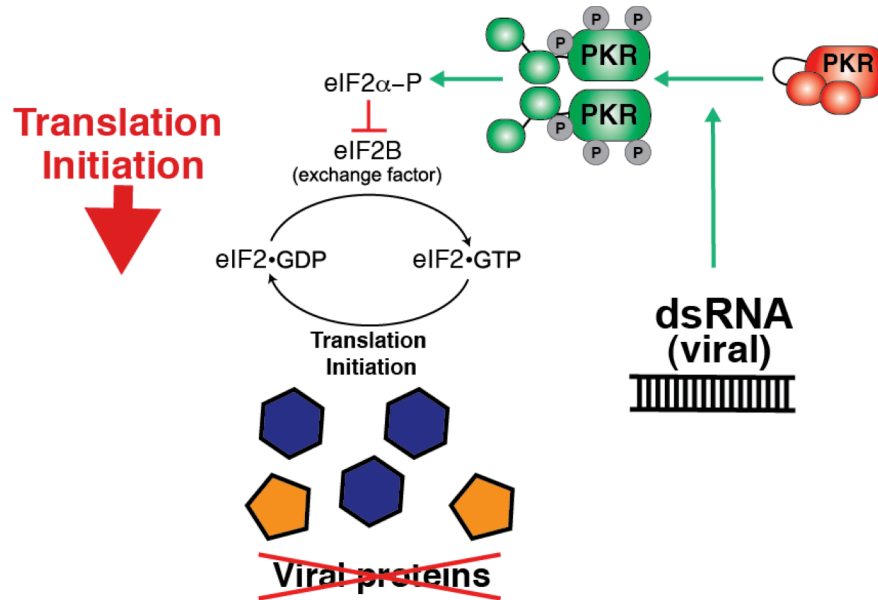


Figure 1: PKR-mediated antiviral response to cytoplasmic dsRNA. Upon detection of dsRNA produced as a consequence of viral replication, PKR monomers (red) dimerize (green) and phosphorylates their target, the α subunit of translation initiation factor eIF2. This phosphorylation increases the affinity of eIF2 for its guanosine nucleotide exchange factor eIF2B, effectively rendering it unable to exchange GDP for GTP, and sufficiently depleting eIF2•GTP to halt translation. Through this avenue, PKR phosphorylation of eIF2 results in a shut down of general translation, thereby preventing synthesis of viral and host proteins, halting virus spread.

The OAS family of proteins also limits virus replication through shut down of protein synthesis. The OAS family is comprised of 8 distinct proteins, derived from four different genes. Three of the four genes, *OAS1*, *OAS2*, and *OAS3*, are located together on chromosome 12, and each contains the indicated number of repeating core units (24,25). *OAS1* is expressed as four splice variants (p41, p44, p46, and p48), *OAS2* as two splice variants (p69 and p71), and *OAS3* as a single variant (p100) (25). The fourth gene, *OASL*,

contains a single, catalytically inactive core unit, is located at a distant site on chromosome 12, and possesses an additional exon homologous to ubiquitin (26). Though OASL is catalytically inactive, it serves an antiviral role by modulating the activity of RIG-I by mimicking the polyubiquitin required by dsRNA-bound RIG-I to induce transcriptional initiation of Type-I interferon (27).

Upon binding dsRNA, the catalytically active OAS forms (OAS1, OAS2, and OAS3) synthesize 2'-5' linked oligoadenylate ($A(2'-5'A)_n$), in a non-processive fashion (28,29). These second messengers, when comprised of three or more adenylates ($pppA(2'-5'A)_{n>2}$), activate their only known target, the latent cellular endoribonuclease L (RNase L) (30). By tethering RNase L monomers together to form a functional dimer, activated RNase L degrades single-stranded RNA (31), primarily after UU and UA dinucleotides (32) present in loops or bulges in otherwise highly structured RNAs (33), thereby halting protein translation (Figure 2) . While overexpression of RNase L, or activation of the enzyme by copious quantities of $pppA(2'-5'A)_n$ results in cleavage of ribosomal RNA, the true targets of RNase L in are unknown (34). The effects of OAS are thought to be local, and the response of RNase L dose-dependent (35), raising the possibility that in the context of infection, RNase L may have more specific targets, such as specific viral RNAs bound to the ribosome. Indeed, there are conflicting reports of whether RNase L specifically targets viral mRNA, RNA genome, or cellular ribosomal RNA (36-39).

Members of the OAS family of enzymes have been reported to have optimal catalytic activity at different pHs and distinct subcellular localization (40,41), suggesting that they

may be compartmentalized within the cell. Additionally, different OAS genes and variants have been reported to have distinct roles in limiting infection by different viruses (41-44). In this work, the most studied OAS1 variant, p42 (UniProt accession # P00973-2) is used to dissect the RNA features required for activation of this protein.

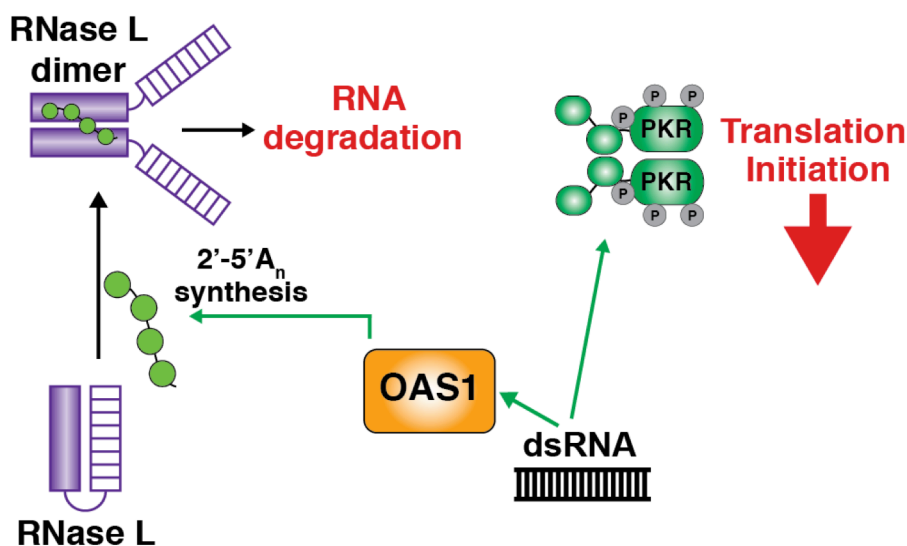


Figure 2: OAS1 mediated antiviral response to cytoplasmic dsRNA. In addition to PKR (green), the antiviral protein OAS1 (orange) also responds to cytoplasmic dsRNA to shut down translation. Upon binding dsRNA, active OAS1 synthesizes 2'-5' linked oligoadenylate ($A(2'-5'A)_n$) (green), in a non-processive fashion. These second messengers, activate latent RNase L (purple) by tethering RNase L monomers together to form a functional dimer. Activated RNase L degrades single-stranded RNA, thereby halting protein translation.

Viral countermeasures against PKR and the OAS/ RNase L pathway

An extensive array of viral countermeasures highlights the importance of PKR- and OAS-mediated translational shut down as a defense against virus infection, reviewed in (9,45). Strategies for thwarting the effects of PKR include direct inhibition, sequestration of dsRNA, and the synthesis of eIF2 α mimics. Similarly, the numerous virus strategies for escape from the effects of OAS1 include direct inhibition, synthesis of 2'-5'

phosphodiesterases which cleave and thereby inactivate 2'-5' linked oligoadenylates, and direct inhibitors of RNase L. Further evidence of the importance of these two systems is the fact that many of these mechanisms are thought to have evolved independently within disparate classes of viruses (45,46).

Both Adenovirus and Epstein-Barr virus synthesize two short (~170 nt) non-coding RNA Polymerase III (Pol III) transcripts, VA RNA_I/ VA RNA_{II} and EBER-1/ EBER-2, respectively. Each of these RNAs accumulates to extraordinarily high levels in late stages in infection, with approximately 10⁶-10⁸ copies per cell (47). In the case of Adenovirus, VA RNAs are required for efficient virus replication (48). In Epstein-Barr virus, however, the importance of EBERs is less clear, although recent reports indicate that they are necessary for efficient transformation of lymphocytes (49). VA RNA_I and EBER-1 are structurally very similar (Figure 3) (50), and Epstein-Barr virus EBERs are capable of functionally substituting for VA RNAs during Adenovirus infection. Even so, their functions cannot be entirely identical, as the converse is not true: VA RNAs are unable to complement an Epstein-Barr virus strain in which the EBERs are deleted (51). Though comparatively little is known about the function of the secondary species, VA RNA_{II} and EBER-2, VA RNA_I and EBER-1 are well characterized. The structures of Adenovirus VA-RNA_I and the Epstein-Barr RNA EBER-1, and how these RNAs interact with and regulate the activity of both PKR and OAS1, are the focus of this work. Both VA RNA_I and EBER-1 bind to PKR and inhibit its activity by preventing dimerization and autophosphorylation, and thus, phosphorylation of eIF2 α (Figure 2; 47,52).

Counterintuitively, each of these RNAs *activate*, rather than inhibit, OAS1 *in vitro* (Figure 4) (53,54). Why a single RNA, in two instances, would inhibit one *and* also activate a second parallel host anti-viral pathways is perplexing and requires further detailed investigation.

VA RNA_I is a multi-functional pro-viral RNA

VA RNA_I is a highly structured RNA comprised of three structurally independent domains: the Terminal Stem (TS), Central Domain (CD), and Apical Stem (AS) (Figure 1) (55). In spite of the fact that the largely base-paired Apical Stem provides at least 20 bp of dsRNA that could potentially activate PKR, this RNA potently inhibits PKR (47). Previous work in our lab utilizing systematic deletion of VA RNA_I showed that a mutant lacking the entire Terminal Stem (TS Δ 21 RNA) retains full inhibitory function against PKR (56).

During Adenovirus infection, the RNA interference (RNAi) pathway enzyme Dicer cleaves VA RNA_I to produce an approximately 23 bp fragment that is loaded onto the RNA-induced silencing complex (RISC) and a truncated VA RNA_I similar in size to TS Δ 21 RNA (56,57). Though Dicer processes only a small fraction of the VA RNA_I present late in Adenovirus infection, this processing is thought to saturate both Dicer and the RISC complex, preventing processing of antiviral micro RNAs (58). The role and importance of the RISC-associated VA RNA_I remain unclear (59,60). However, the sequence of the Adenovirus type 2 (Ad2) Dicer-processed 23 bp fragment is unnecessary for efficient virus replication (61). That a single RNA can serve to saturate the cellular

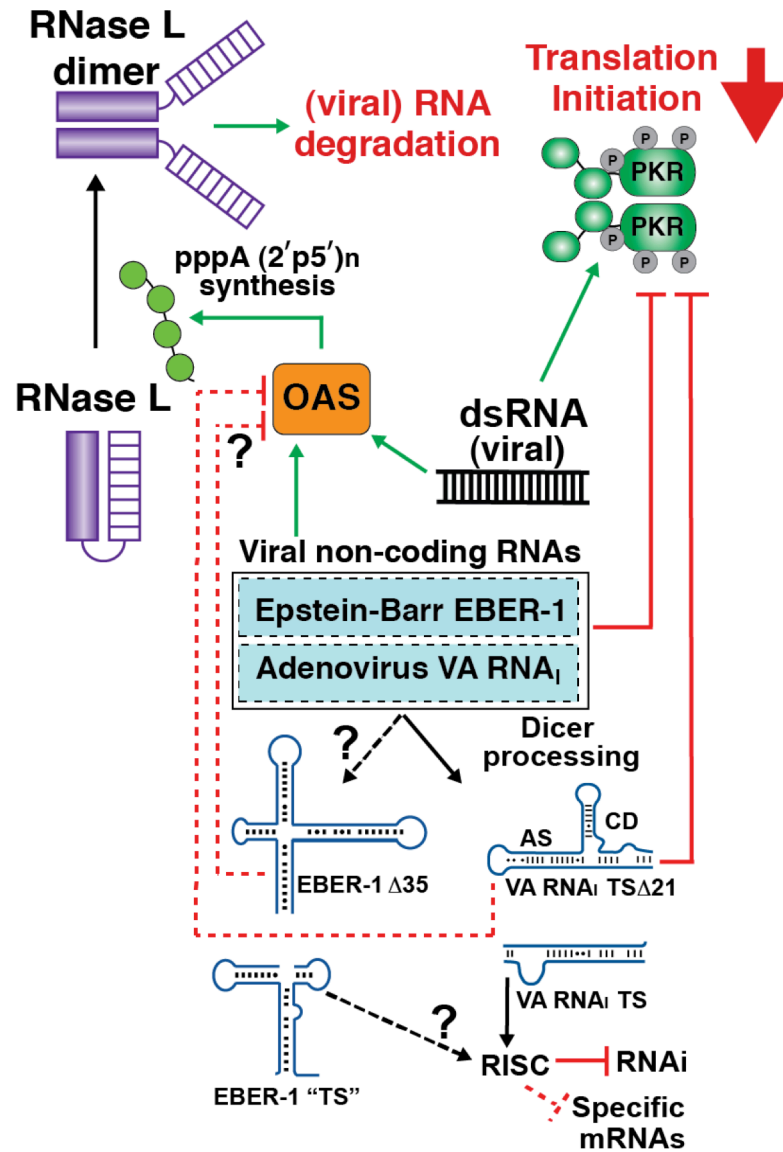


Figure 4. Model for viral non-coding RNAs VA RNA₁ and EBER-1 regulation of dsRNA-activated innate immune proteins PKR (green) and OAS1 (orange). PKR activation by dsRNA leads to translational arrest. Activated OAS1 synthesizes pppA(2'p-5)_{n≥2} second messengers which activate the latent endoribonuclease RNase L leading to cleavage of virus and host RNAs. Dicer processing of VA RNA₁ generates an RNA that retains its activity against PKR (TS_{Δ21}) but has unknown activity against OAS1. The processed VA RNA₁ Terminal Stem is loaded onto the RISC complex; the role of these fragments is unknown. It is also unknown if EBER-1 is processed by Dicer, or if any truncated fragment produced retains activity against PKR or OAS1.

RNAi machinery and efficiently inhibit PKR (56) indicates that this transcript possesses multiple functions, all of which are explored further in the detailed review of VA RNA_I biology in Chapter 2.

VA RNA_I activation of OAS1

VA RNA_I activates OAS1 *in vitro* but the sequence and structural qualities of this RNA that define it as an activator of OAS are unknown (54). At the outset of this work, two publications reported specific but dissimilar OAS1 activation sequences (62,63). In one case, where single-stranded RNA aptamers were retrieved through SELEX, the consensus sequence is degenerate, and the experiments complicated by the propensity for the ligand adapter sequences to activate OAS and the likelihood that the single-stranded RNAs were folding to form secondary structures. For these reasons, though each type of consensus sequence is present in both VA RNA_I and EBER-1, efforts in this work were focused on the more clearly defined activation consensus sequence WW(N₉)WG (where W is A or U, and N is any nucleotide). This sequence is present at two locations in VA RNA_I (Figure 3); once in the Terminal Stem region missing in TSΔ21 RNA, and again in the Central Domain. We hypothesized that Dicer processing may generate an RNA with reduced or ablated activity against OAS1. Therefore, defining the activity of TSΔ21 RNA, in conjunction with mutagenesis-based studies of VA RNA_I would inform our understanding of the comparative importance of the consensus sequences and the structural features present in this RNA for regulation of OAS1.

Pro-viral functions of EBER-1 may mirror those of VA RNA_I

Though the structures of VA RNA_I and EBER-1 are quite similar, and their common inhibitory activity against PKR is established, there is some ambiguity as to EBER-1's localization during infection (64-67). Because both PKR and OAS1 are cytoplasmic, the biological relevance of both VA RNA_I and EBER-1 interaction with these proteins is shaped by its localization. While the cytoplasmic localization of VA RNA_I is established, some groups report EBER-1 to be present in the cytoplasm of infected cells (64), while others insist that it is present exclusively in the nucleus (66,67). Further complicating the matter is the fact that Epstein–Barr virus is capable of both acute and latent infection (68), and that EBER-1 localization may be dependent on the context of virus life cycle or upon cell cycle. Additionally, the hybridization sites for probes used in studies showing EBER-1 to be localized to the nucleus are located in a region of the RNA analogous to VA RNA_I's Terminal Stem. This raises the possibility that a Dicer-processed EBER-1 fragment may be present, but remain undetected due to the absence of the necessary ssRNA sequences for fluorescent probe hybridization. Should this be the case, the activities of truncated EBER-1 against PKR and OAS1 could inform our understanding of how Epstein–Barr virus interacts with this arm of the innate immune system.

PKR and OAS/ RNase L anti-proliferative functions

In addition to the antiviral effects of these proteins, an increasing appreciation for their anti-proliferative functions outside of the context of virus infection has emerged. Both PKR and the OAS/ RNase L pathway have been identified as important in mediating the inflammation associated with diabetes, controlling cell proliferation during

differentiation, and have been implicated in various types of cancers (reviewed in 18,20,69,70). In addition to its role in limiting virus infection, RNase L has also been implicated in context-specific targeting of cellular mRNAs, defending against intracellular bacteria (71-74) and as an oncogene in hereditary prostate cancer (75). Improving our understanding of how these proteins are regulated during virus infection is therefore applicable not only to our understanding of host-pathogen interactions, but also to the numerous important processes of which these proteins are a part.

RESEARCH GOALS

This work began with two primary questions on the nature of VA RNA_I and EBER-1 structures and the activities of these RNAs against PKR and OAS1 (Figure 4).

Specifically, my work aimed to address the questions:

1. What are the features of VA RNA_I that define it as an *inhibitor* of PKR?

Following a detailed review of VA RNA_I structure and function in **Chapter 2**, the next two chapters describe development of new methods for ‘Selective 2’-Hydroxyl Acylation Analyzed by Primer Extension’ (SHAPE) (76,77) and their application to my analysis of VA RNA_I inhibition of PKR (**Chapter 3, Chapter 4**); (76). This latter chapter describes a study which aimed to dissect the VA RNA_I tertiary structure to determine its contribution to PKR inhibition. However, these studies uncovered that PKR inhibition does not require this tertiary structure and thus the structural requirements for inhibition by RNA are far simpler than previously appreciated.

2. What are the features of VA RNA_I that define it as an *activator* of OAS1?

Initially, I asked if the Dicer-processed VA RNA_I TSΔ21 retains its ability to activate OAS1. During initial comparisons between full-length VA RNA_I and TSΔ21 activity against OAS1, I was unable to reproduce published data for full-length VA RNA_I (54,78). Upon close comparison of our VA RNA_I construct with those used by other groups, we identified the only difference to be the absence (in our construct) of the RNA's 3'-UUUU tail, generated by Pol III transcription termination. While this 3'-CUUU sequence is entirely dispensable in studies of PKR, it is required for optimal VA RNA_I activation of OAS1. This initial observation began an investigation in which we uncovered a novel motif for activation of OAS1, the 3'-single-stranded pyrimidine (3'-ssPy), described in **Chapter 5**.

Following the discovery of the 3'-ssPy motif, we sought to better understand its function through experiments utilizing a simple 18 bp system that contains two overlapping activation consensus sequences. Using this system, we plan to investigate the key question of how the presence of the 3'-ssPy adjacent to an activation consensus sequence affects its ability to activate OAS1 using a future experimental approach outlined in **Chapter 6**. Using the results of these experiments, we hope to explain the ability of VA RNA_I features other than the 3'-ssPy to influence OAS1 activity. In the context of the full length RNA, to which the 3'-CUUU sequence is appended, preliminary results show that mutations to distant 3'-ends of activation consensus sequences dampen the effect of the RNA on OAS1. This preliminary result, in conjunction with our findings in **Chapter 5**, raise questions about how RNA structure and affinity for OAS1 may shape the activating potential of any given RNA molecule.

3. Does EBER-1 activity against PKR and OAS1 mirror that of VA RNA_I?

Though there is some ambiguity surrounding EBER-1's cellular localization, its structural similarity to VA RNA_I and its ability to inhibit PKR and activate OAS1 prompt the question of whether there are additional similarities between these two RNAs (52,53,79). We first asked if truncated EBER-1 would retain its ability to capable inhibit PKR but become a pseudo inhibitor of OAS1 as VA RNA_I does. Before testing the activity of a truncated EBER-1, we asked if EBER-1 is indeed processed *in vitro* by Dicer *in vitro* (Figure 4). Preliminary results indicate that this RNA is processed, and experiments addressing the activity of this RNA and its Dicer-processed fragment against both PKR an OAS1 will be important next steps as outlined in **Chapter 6**.

Collectively these studies shape our current understanding of how VA RNA_I exerts its activity against PKR and OAS. The structural requirements for VA RNA_I inhibition of PKR are simpler than previously appreciated; shedding light on how structurally dissimilar VA RNA_I's from varying serotypes are able to maintain inhibitory activity against PKR. The discovery of the 3'-ssPy motif as necessary for optimal activation of OAS1 is the first report of an RNA feature responsible for potentiation of OAS1 unrelated to a search for a canonical activation sequences. While these findings are explored individually in their respective chapters, together they have led to formation of new hypotheses regarding the relationship between the PKR and OAS/ RNase L pathways and how the activities of these proteins are governed by RNA structures, sometimes found within the same RNA, as with VA RNA_I (Figure 3). Understanding

how these proteins interact with dsRNA will allow for a more complete understanding of host-pathogen interactions as well as how the cell avoids their inadvertent activation.

REFERENCES

1. Akira, S., Uematsu, S. and Takeuchi, O. (2006) Pathogen recognition and innate immunity. *Cell*, **124**, 783-801.
2. Meurs, E., Chong, K., Galabru, J., Thomas, N.S., Kerr, I.M., Williams, B.R. and Hovanessian, A.G. (1990) Molecular cloning and characterization of the human double-stranded RNA-activated protein kinase induced by interferon. *Cell*, **62**, 379-390.
3. Yoneyama, M., Kikuchi, M., Natsukawa, T., Shinobu, N., Imaizumi, T., Miyagishi, M., Taira, K., Akira, S. and Fujita, T. (2004) The RNA helicase RIG-I has an essential function in double-stranded RNA-induced innate antiviral responses. *Nat Immunol*, **5**, 730-737.
4. Kang, D.C., Gopalkrishnan, R.V., Wu, Q., Jankowsky, E., Pyle, A.M. and Fisher, P.B. (2002) mda-5: An interferon-inducible putative RNA helicase with double-stranded RNA-dependent ATPase activity and melanoma growth-suppressive properties. *Proc Natl Acad Sci U S A*, **99**, 637-642.
5. Roberts, W.K., Hovanessian, A., Brown, R.E., Clemens, M.J. and Kerr, I.M. (1976) Interferon-mediated protein kinase and low-molecular-weight inhibitor of protein synthesis. *Nature*, **264**, 477-480.
6. Abraham, N., Stojdl, D.F., Duncan, P.I., Methot, N., Ishii, T., Dube, M., Vanderhyden, B.C., Atkins, H.L., Gray, D.A., McBurney, M.W. *et al.* (1999)

- Characterization of transgenic mice with targeted disruption of the catalytic domain of the double-stranded RNA-dependent protein kinase, PKR. *J Biol Chem*, **274**, 5953-5962.
7. Carr, D.J., Wuest, T., Tomanek, L., Silverman, R.H. and Williams, B.R. (2006) The lack of RNA-dependent protein kinase enhances susceptibility of mice to genital herpes simplex virus type 2 infection. *Immunology*, **118**, 520-526.
 8. Nott, M.R. and Briffa, A.C. (1992) The Humphrey ADE, Magill and Lack breathing systems. *Anaesthesia*, **47**, 1105-1106.
 9. Silverman, R.H. (2007) Viral encounters with 2',5'-oligoadenylate synthetase and RNase L during the interferon antiviral response. *J Virol*, **81**, 12720-12729.
 10. Zhang, P. and Samuel, C.E. (2007) Protein kinase PKR plays a stimulus- and virus-dependent role in apoptotic death and virus multiplication in human cells. *J Virol*, **81**, 8192-8200.
 11. Zhou, A., Paranjape, J., Brown, T.L., Nie, H., Naik, S., Dong, B., Chang, A., Trapp, B., Fairchild, R., Colmenares, C. *et al.* (1997) Interferon action and apoptosis are defective in mice devoid of 2',5'-oligoadenylate-dependent RNase L. *EMBO J*, **16**, 6355-6363.
 12. Kato, H., Takeuchi, O., Sato, S., Yoneyama, M., Yamamoto, M., Matsui, K., Uematsu, S., Jung, A., Kawai, T., Ishii, K.J. *et al.* (2006) Differential roles of MDA5 and RIG-I helicases in the recognition of RNA viruses. *Nature*, **441**, 101-105.
 13. Loo, Y.M., Fornek, J., Crochet, N., Bajwa, G., Perwitasari, O., Martinez-Sobrido, L., Akira, S., Gill, M.A., Garcia-Sastre, A., Katze, M.G. *et al.* (2008) Distinct RIG-I and MDA5 signaling by RNA viruses in innate immunity. *J Virol*, **82**, 335-345.

14. Errett, J.S., Suthar, M.S., McMillan, A., Diamond, M.S. and Gale, M., Jr. (2013) The essential, nonredundant roles of RIG-I and MDA5 in detecting and controlling West Nile virus infection. *J Virol*, **87**, 11416-11425.
15. Zhou, A., Paranjape, J.M., Der, S.D., Williams, B.R. and Silverman, R.H. (1999) Interferon action in triply deficient mice reveals the existence of alternative antiviral pathways. *Virology*, **258**, 435-440.
16. Loo, Y.M. and Gale, M., Jr. (2011) Immune signaling by RIG-I-like receptors. *Immunity*, **34**, 680-692.
17. Yoneyama, M., Kikuchi, M., Matsumoto, K., Imaizumi, T., Miyagishi, M., Taira, K., Foy, E., Loo, Y.M., Gale, M., Jr., Akira, S. *et al.* (2005) Shared and unique functions of the DExD/H-box helicases RIG-I, MDA5, and LGP2 in antiviral innate immunity. *J Immunol*, **175**, 2851-2858.
18. Garcia, M.A., Gil, J., Ventoso, I., Guerra, S., Domingo, E., Rivas, C. and Esteban, M. (2006) Impact of protein kinase PKR in cell biology: from antiviral to antiproliferative action. *Microbiol Mol Biol Rev*, **70**, 1032-1060.
19. Hovanessian, A.G., Brown, R.E. and Kerr, I.M. (1977) Synthesis of low molecular weight inhibitor of protein synthesis with enzyme from interferon-treated cells. *Nature*, **268**, 537-540.
20. Williams, B.R. (1999) PKR; a sentinel kinase for cellular stress. *Oncogene*, **18**, 6112-6120.
21. Cole, J.L. (2007) Activation of PKR: an open and shut case? *Trends Biochem Sci*, **32**, 57-62.

22. Krishnamoorthy, T., Pavitt, G.D., Zhang, F., Dever, T.E. and Hinnebusch, A.G. (2001) Tight binding of the phosphorylated alpha subunit of initiation factor 2 (eIF2alpha) to the regulatory subunits of guanine nucleotide exchange factor eIF2B is required for inhibition of translation initiation. *Mol Cell Biol*, **21**, 5018-5030.
23. Rowlands, A.G., Panniers, R. and Henshaw, E.C. (1988) The catalytic mechanism of guanine nucleotide exchange factor action and competitive inhibition by phosphorylated eukaryotic initiation factor 2. *J Biol Chem*, **263**, 5526-5533.
24. Eskildsen, S., Justesen, J., Schierup, M.H. and Hartmann, R. (2003) Characterization of the 2'-5'-oligoadenylate synthetase ubiquitin-like family. *Nucleic Acids Res*, **31**, 3166-3173.
25. Justesen, J., Hartmann, R. and Kjeldgaard, N.O. (2000) Gene structure and function of the 2'-5'-oligoadenylate synthetase family. *Cell Mol Life Sci*, **57**, 1593-1612.
26. Hartmann, R., Olsen, H.S., Widder, S., Jorgensen, R. and Justesen, J. (1998) p59OASL, a 2'-5' oligoadenylate synthetase like protein: a novel human gene related to the 2'-5' oligoadenylate synthetase family. *Nucleic Acids Res*, **26**, 4121-4128.
27. Zhu, J., Zhang, Y., Ghosh, A., Cuevas, R.A., Forero, A., Dhar, J., Ibsen, M.S., Schmid-Burgk, J.L., Schmidt, T., Ganapathiraju, M.K. *et al.* (2014) Antiviral activity of human OASL protein is mediated by enhancing signaling of the RIG-I RNA sensor. *Immunity*, **40**, 936-948.
28. Kerr, I.M., Brown, R.E. and Hovanessian, A.G. (1977) Nature of inhibitor of cell-free protein synthesis formed in response to interferon and double-stranded RNA. *Nature*, **268**, 540-542.

29. Justesen, J., Ferbus, D. and Thang, M.N. (1980) Elongation mechanism and substrate specificity of 2',5'-oligoadenylate synthetase. *Proc Natl Acad Sci U S A*, **77**, 4618-4622.
30. Hovanessian, A.G., Wood, J., Meurs, E. and Montagnier, L. (1979) Increased nuclease activity in cells treated with pppA2'p5'A2'p5' A. *Proc Natl Acad Sci U S A*, **76**, 3261-3265.
31. Han, Y., Whitney, G., Donovan, J. and Korennykh, A. (2012) Innate immune messenger 2-5A tethers human RNase L into active high-order complexes. *Cell Rep*, **2**, 902-913.
32. Wreschner, D.H., McCauley, J.W., Skehel, J.J. and Kerr, I.M. (1981) Interferon action--sequence specificity of the ppp(A2'p)nA-dependent ribonuclease. *Nature*, **289**, 414-417.
33. Malathi, K., Saito, T., Crochet, N., Barton, D.J., Gale, M., Jr. and Silverman, R.H. (2010) RNase L releases a small RNA from HCV RNA that refolds into a potent PAMP. *RNA*, **16**, 2108-2119.
34. Silverman, R.H., Skehel, J.J., James, T.C., Wreschner, D.H. and Kerr, I.M. (1983) rRNA cleavage as an index of ppp(A2'p)nA activity in interferon-treated encephalomyocarditis virus-infected cells. *J Virol*, **46**, 1051-1055.
35. Nilsen, T.W. and Baglioni, C. (1979) Mechanism for discrimination between viral and host mRNA in interferon-treated cells. *Proc Natl Acad Sci U S A*, **76**, 2600-2604.
36. Andersen, J.B., Mazan-Mamczarz, K., Zhan, M., Gorospe, M. and Hassel, B.A. (2009) Ribosomal protein mRNAs are primary targets of regulation in RNase-L-induced senescence. *RNA Biol*, **6**, 305-315.

37. Baglioni, C., De Benedetti, A. and Williams, G.J. (1984) Cleavage of nascent reovirus mRNA by localized activation of the 2'-5'-oligoadenylate-dependent endoribonuclease. *J Virol*, **52**, 865-871.
38. Li, X.L., Blackford, J.A. and Hassel, B.A. (1998) RNase L mediates the antiviral effect of interferon through a selective reduction in viral RNA during encephalomyocarditis virus infection. *J Virol*, **72**, 2752-2759.
39. Wreschner, D.H., James, T.C., Silverman, R.H. and Kerr, I.M. (1981) Ribosomal RNA cleavage, nuclease activation and 2-5A(ppp(A2'p)nA) in interferon-treated cells. *Nucleic Acids Res*, **9**, 1571-1581.
40. Marie, I., Blanco, J., Rebouillat, D. and Hovanessian, A.G. (1997) 69-kDa and 100-kDa isoforms of interferon-induced (2'-5')oligoadenylate synthetase exhibit differential catalytic parameters. *Eur J Biochem*, **248**, 558-566.
41. Lin, R.J., Yu, H.P., Chang, B.L., Tang, W.C., Liao, C.L. and Lin, Y.L. (2009) Distinct antiviral roles for human 2',5'-oligoadenylate synthetase family members against dengue virus infection. *J Immunol*, **183**, 8035-8043.
42. Mossman, K.L., Macgregor, P.F., Rozmus, J.J., Goryachev, A.B., Edwards, A.M. and Smiley, J.R. (2001) Herpes simplex virus triggers and then disarms a host antiviral response. *J Virol*, **75**, 750-758.
43. Dugan, J.W., Albor, A., David, L., Fowlkes, J., Blackledge, M.T., Martin, T.M., Planck, S.R., Rosenzweig, H.L., Rosenbaum, J.T. and Davey, M.P. (2009) Nucleotide oligomerization domain-2 interacts with 2'-5'-oligoadenylate synthetase type 2 and enhances RNase-L function in THP-1 cells. *Mol Immunol*, **47**, 560-566.

44. Brehin, A.C., Casademont, I., Frenkiel, M.P., Julier, C., Sakuntabhai, A. and Despres, P. (2009) The large form of human 2',5'-Oligoadenylate Synthetase (OAS3) exerts antiviral effect against Chikungunya virus. *Virology*, **384**, 216-222.
45. Langland, J.O., Cameron, J.M., Heck, M.C., Jancovich, J.K. and Jacobs, B.L. (2006) Inhibition of PKR by RNA and DNA viruses. *Virus Res*, **119**, 100-110.
46. Zhang, R., Jha, B.K., Ogden, K.M., Dong, B., Zhao, L., Elliott, R., Patton, J.T., Silverman, R.H. and Weiss, S.R. (2013) Homologous 2',5'-phosphodiesterases from disparate RNA viruses antagonize antiviral innate immunity. *Proc Natl Acad Sci U S A*, **110**, 13114-13119.
47. Mathews, M.B. and Shenk, T. (1991) Adenovirus virus-associated RNA and translation control. *J Virol*, **65**, 5657-5662.
48. Thimmappaya, B., Weinberger, C., Schneider, R.J. and Shenk, T. (1982) Adenovirus VAI RNA is required for efficient translation of viral mRNAs at late times after infection. *Cell*, **31**, 543-551.
49. Ahmed, W. and Khan, G. (2014) The labyrinth of interactions of Epstein-Barr virus-encoded small RNAs. *Rev Med Virol*, **24**, 3-14.
50. Rosa, M.D., Gottlieb, E., Lerner, M.R. and Steitz, J.A. (1981) Striking similarities are exhibited by two small Epstein-Barr virus-encoded ribonucleic acids and the adenovirus-associated ribonucleic acids VAI and VAII. *Mol Cell Biol*, **1**, 785-796.
51. Bhat, R.A. and Thimmappaya, B. (1983) Two small RNAs encoded by Epstein-Barr virus can functionally substitute for the virus-associated RNAs in the lytic growth of adenovirus 5. *Proc Natl Acad Sci U S A*, **80**, 4789-4793.

52. Clarke, P.A., Sharp, N.A. and Clemens, M.J. (1990) Translational control by the Epstein-Barr virus small RNA EBER-1. Reversal of the double-stranded RNA-induced inhibition of protein synthesis in reticulocyte lysates. *Eur J Biochem*, **193**, 635-641.
53. Sharp, T.V., Raine, D.A., Gewert, D.R., Joshi, B., Jagus, R. and Clemens, M.J. (1999) Activation of the interferon-inducible (2'-5') oligoadenylate synthetase by the Epstein-Barr virus RNA, EBER-1. *Virology*, **257**, 303-313.
54. Desai, S.Y., Patel, R.C., Sen, G.C., Malhotra, P., Ghadge, G.D. and Thimmapaya, B. (1995) Activation of interferon-inducible 2'-5' oligoadenylate synthetase by adenoviral VAI RNA. *J Biol Chem*, **270**, 3454-3461.
55. Coventry, V.K. and Conn, G.L. (2008) Analysis of adenovirus VA RNAI structure and stability using compensatory base pair modifications. *Nucleic Acids Res*, **36**, 1645-1653.
56. Wahid, A.M., Coventry, V.K. and Conn, G.L. (2008) Systematic deletion of the adenovirus-associated RNAI terminal stem reveals a surprisingly active RNA inhibitor of double-stranded RNA-activated protein kinase. *J Biol Chem*, **283**, 17485-17493.
57. Andersson, M.G., Haasnoot, P.C., Xu, N., Berenjian, S., Berkhout, B. and Akusjarvi, G. (2005) Suppression of RNA interference by adenovirus virus-associated RNA. *J Virol*, **79**, 9556-9565.
58. Xu, N., Segerman, B., Zhou, X. and Akusjarvi, G. (2007) Adenovirus virus-associated RNAII-derived small RNAs are efficiently incorporated into the rna-

- induced silencing complex and associate with polyribosomes. *J Virol*, **81**, 10540-10549.
59. Furuse, Y., Ornelles, D.A. and Cullen, B.R. (2013) Persistently adenovirus-infected lymphoid cells express microRNAs derived from the viral VAI and especially VAI RNA. *Virology*, **447**, 140-145.
60. Aparicio, O., Carnero, E., Abad, X., Razquin, N., Guruceaga, E., Segura, V. and Fortes, P. (2010) Adenovirus VA RNA-derived miRNAs target cellular genes involved in cell growth, gene expression and DNA repair. *Nucleic Acids Res*, **38**, 750-763.
61. Kamel, W., Segerman, B., Punga, T. and Akusjarvi, G. (2014) Small RNA sequence analysis of adenovirus VA RNA-derived miRNAs reveals an unexpected serotype-specific difference in structure and abundance. *PLoS One*, **9**, e105746.
62. Kodym, R., Kodym, E. and Story, M.D. (2009) 2'-5'-Oligoadenylate synthetase is activated by a specific RNA sequence motif. *Biochem Biophys Res Commun*, **388**, 317-322.
63. Hartmann, R., Norby, P.L., Martensen, P.M., Jorgensen, P., James, M.C., Jacobsen, C., Moestrup, S.K., Clemens, M.J. and Justesen, J. (1998) Activation of 2'-5' oligoadenylate synthetase by single-stranded and double-stranded RNA aptamers. *J Biol Chem*, **273**, 3236-3246.
64. Schwemmle, M., Clemens, M.J., Hilse, K., Pfeifer, K., Troster, H., Muller, W.E. and Bachmann, M. (1992) Localization of Epstein-Barr virus-encoded RNAs EBER-1 and EBER-2 in interphase and mitotic Burkitt lymphoma cells. *Proc Natl Acad Sci U S A*, **89**, 10292-10296.

65. Iwakiri, D., Zhou, L., Samanta, M., Matsumoto, M., Ebihara, T., Seya, T., Imai, S., Fujieda, M., Kawa, K. and Takada, K. (2009) Epstein-Barr virus (EBV)-encoded small RNA is released from EBV-infected cells and activates signaling from Toll-like receptor 3. *J Exp Med*, **206**, 2091-2099.
66. Howe, J.G. and Steitz, J.A. (1986) Localization of Epstein-Barr virus-encoded small RNAs by in situ hybridization. *Proc Natl Acad Sci U S A*, **83**, 9006-9010.
67. Fok, V., Friend, K. and Steitz, J.A. (2006) Epstein-Barr virus noncoding RNAs are confined to the nucleus, whereas their partner, the human La protein, undergoes nucleocytoplasmic shuttling. *J Cell Biol*, **173**, 319-325.
68. Young, L.S. and Rickinson, A.B. (2004) Epstein-Barr virus: 40 years on. *Nat Rev Cancer*, **4**, 757-768.
69. Ezelle, H.J. and Hassel, B.A. (2012) Pathologic effects of RNase-L dysregulation in immunity and proliferative control. *Front Biosci (Schol Ed)*, **4**, 767-786.
70. Bisbal, C. and Silverman, R.H. (2007) Diverse functions of RNase L and implications in pathology. *Biochimie*, **89**, 789-798.
71. Chakrabarti, A., Jha, B.K. and Silverman, R.H. (2011) New insights into the role of RNase L in innate immunity. *J Interferon Cytokine Res*, **31**, 49-57.
72. Li, X.L., Ezelle, H.J., Kang, T.J., Zhang, L., Shirey, K.A., Harro, J., Hasday, J.D., Mohapatra, S.K., Crasta, O.R., Vogel, S.N. *et al.* (2008) An essential role for the antiviral endoribonuclease, RNase-L, in antibacterial immunity. *Proc Natl Acad Sci U S A*, **105**, 20816-20821.
73. Bisbal, C., Silhol, M., Laubenthal, H., Kaluza, T., Carnac, G., Milligan, L., Le Roy, F. and Salehzada, T. (2000) The 2'-5' oligoadenylate/RNase L/RNase L inhibitor

- pathway regulates both MyoD mRNA stability and muscle cell differentiation. *Mol Cell Biol*, **20**, 4959-4969.
74. Al-Ahmadi, W., Al-Haj, L., Al-Mohanna, F.A., Silverman, R.H. and Khabar, K.S. (2009) RNase L downmodulation of the RNA-binding protein, HuR, and cellular growth. *Oncogene*, **28**, 1782-1791.
75. Wiklund, F., Jonsson, B.A., Brookes, A.J., Stromqvist, L., Adolfsson, J., Emanuelsson, M., Adami, H.O., Augustsson-Balter, K. and Gronberg, H. (2004) Genetic analysis of the RNASEL gene in hereditary, familial, and sporadic prostate cancer. *Clin Cancer Res*, **10**, 7150-7156.
76. Merino, E.J., Wilkinson, K.A., Coughlan, J.L. and Weeks, K.M. (2005), *J Am Chem Soc*, Vol. 127, pp. 4223-4231.
77. Vachon, V.K. and Conn, G.L. (2012) Plasmid template design and in vitro transcription of short RNAs within a "structure cassette" for structure probing experiments. *Methods Mol Biol*, **941**, 157-169.
78. Meng, H., Deo, S., Xiong, S., Dzananovic, E., Donald, L.J., van Dijk, C.W. and McKenna, S.A. (2012) Regulation of the interferon-inducible 2'-5'-oligoadenylate synthetases by adenovirus VA(I) RNA. *Journal of Molecular Biology*, **422**, 635-649.
79. Clarke, P.A., Schwemmler, M., Schickinger, J., Hilse, K. and Clemens, M.J. (1991) Binding of Epstein-Barr virus small RNA EBER-1 to the double-stranded RNA-activated protein kinase DAI. *Nucleic Acids Res*, **19**, 243-248.
80. Schlee, M., Hartmann, E., Coch, C., Wimmenauer, V., Janke, M., Barchet, W. and Hartmann, G. (2009) Approaching the RNA ligand for RIG-I? *Immunol Rev*, **227**, 66-74.

81. Kato, H., Takeuchi, O., Mikamo-Satoh, E., Hirai, R., Kawai, T., Matsushita, K., Hiiragi, A., Dermody, T.S., Fujita, T. and Akira, S. (2008) Length-dependent recognition of double-stranded ribonucleic acids by retinoic acid-inducible gene-I and melanoma differentiation-associated gene 5. *J Exp Med*, **205**, 1601-1610.
82. Schmidt, A., Schwerd, T., Hamm, W., Hellmuth, J.C., Cui, S., Wenzel, M., Hoffmann, F.S., Michallet, M.C., Besch, R., Hopfner, K.P. *et al.* (2009) 5'-triphosphate RNA requires base-paired structures to activate antiviral signaling via RIG-I. *Proc Natl Acad Sci U S A*, **106**, 12067-12072.
83. Hornung, V., Ellegast, J., Kim, S., Brzozka, K., Jung, A., Kato, H., Poeck, H., Akira, S., Conzelmann, K.K., Schlee, M. *et al.* (2006) 5'-Triphosphate RNA is the ligand for RIG-I. *Science*, **314**, 994-997.
84. Schlee, M., Roth, A., Hornung, V., Hagmann, C.A., Wimmenauer, V., Barchet, W., Coch, C., Janke, M., Mihailovic, A., Wardle, G. *et al.* (2009) Recognition of 5' triphosphate by RIG-I helicase requires short blunt double-stranded RNA as contained in panhandle of negative-strand virus. *Immunity*, **31**, 25-34.
85. Sumpter, R., Jr., Loo, Y.M., Foy, E., Li, K., Yoneyama, M., Fujita, T., Lemon, S.M. and Gale, M., Jr. (2005) Regulating intracellular antiviral defense and permissiveness to hepatitis C virus RNA replication through a cellular RNA helicase, RIG-I. *J Virol*, **79**, 2689-2699.
86. Plumet, S., Duprex, W.P. and Gerlier, D. (2005) Dynamics of viral RNA synthesis during measles virus infection. *J Virol*, **79**, 6900-6908.

87. Fredericksen, B.L., Keller, B.C., Fornek, J., Katze, M.G. and Gale, M., Jr. (2008) Establishment and maintenance of the innate antiviral response to West Nile Virus involves both RIG-I and MDA5 signaling through IPS-1. *J Virol*, **82**, 609-616.
88. Berke, I.C. and Modis, Y. (2012) MDA5 cooperatively forms dimers and ATP-sensitive filaments upon binding double-stranded RNA. *EMBO J*, **31**, 1714-1726.
89. Bevilacqua, P.C. and Cech, T.R. (1996) Minor-groove recognition of double-stranded RNA by the double-stranded RNA-binding domain from the RNA-activated protein kinase PKR. *Biochemistry*, **35**, 9983-9994.
90. Zheng, X. and Bevilacqua, P.C. (2004) Activation of the protein kinase PKR by short double-stranded RNAs with single-stranded tails. *RNA*, **10**, 1934-1945.
91. Manche, L., Green, S.R., Schmedt, C. and Mathews, M.B. (1992) Interactions between double-stranded RNA regulators and the protein kinase DAI. *Mol Cell Biol*, **12**, 5238-5248.
92. Bevilacqua, P.C., George, C.X., Samuel, C.E. and Cech, T.R. (1998) Binding of the protein kinase PKR to RNAs with secondary structure defects: role of the tandem A-G mismatch and noncontiguous helices. *Biochemistry*, **37**, 6303-6316.
93. Zhang, P. and Samuel, C.E. (2008) Induction of protein kinase PKR-dependent activation of interferon regulatory factor 3 by vaccinia virus occurs through adapter IPS-1 signaling. *J Biol Chem*, **283**, 34580-34587.
94. Dauber, B. and Wolff, T. (2009) Activation of the Antiviral Kinase PKR and Viral Countermeasures. *Viruses*, **1**, 523-544.
95. Alagarasu, K., Honap, T., Damle, I.M., Mulay, A.P., Shah, P.S. and Cecilia, D. (2013) Polymorphisms in the oligoadenylate synthetase gene cluster and its

- association with clinical outcomes of dengue virus infection. *Infect Genet Evol*, **14**, 390-395.
96. Mashimo, T., Simon-Chazottes, D. and Guenet, J.L. (2008) Innate resistance to flavivirus infections and the functions of 2'-5' oligoadenylate synthetases. *Curr Top Microbiol Immunol*, **321**, 85-100.
97. Lim, J.K., Lisco, A., McDermott, D.H., Huynh, L., Ward, J.M., Johnson, B., Johnson, H., Pape, J., Foster, G.A., Kryzstof, D. *et al.* (2009) Genetic variation in OAS1 is a risk factor for initial infection with West Nile virus in man. *PLoS Pathog*, **5**, e1000321.

CHAPTER 2:

**Adenovirus VA RNA: An essential pro-viral non-coding
RNA**

The following Chapter is a draft of a review to be submitted April 15, 2015:

Vachon, V.K. and Conn, G.L. (2015). Adenovirus VA RNA: An essential pro-viral non-coding RNA. *Virus Research*

ABSTRACT

Adenovirus ‘virus-associated’ RNAs (VA RNAs) are exceptionally abundant (up to 10^8 copies per cell), heterogeneous, non-coding RNA transcripts (~150-200 nucleotides). The predominant species, VA RNA_I, is best recognized for its essential function in relieving the cellular anti-viral blockade of protein synthesis through inhibition of the double-stranded RNA-activated protein kinase (PKR). More recent evidence has revealed that VA RNAs also interferes with several other host cell processes, in part by virtue of the high level to which VA RNA_I accumulates. Following transcription by cellular RNA polymerase III, VA RNAs saturate the nuclear export protein Exportin 5 (Exp5) and the cellular endoribonuclease Dicer, interfering with pre-micro (mi)RNA export and miRNA biogenesis, respectively. Dicer-processed VA RNA fragments are incorporated into the RNA-induced silencing complex (RISC) as ‘mivaRNAs’, where they may specifically target cellular genes. VA RNA_I also interacts with other innate immune proteins, including OAS1. While intact VA RNA_I has the paradoxical effect of activating OAS1, VA RNA_I lacking the entire Terminal Stem has been reported to be a pseudoinhibitor of OAS1. However, we find here that the authentic product of Dicer-processing activates OAS1 to the same degree as full-length VA RNA_I while retaining activity against PKR. These findings underscore that the impact of VA RNA_I on the outcome of Adenovirus infection beyond that of well-established PKR inhibition is underexplored. Further, any additional contributions of VA RNA_I heterogeneity resulting from variations in transcription initiation and termination to each of these functions remain open questions that are discussed here.

INTRODUCTION

Adenoviruses (AdVs) are naked, icosahedral, double-stranded DNA viruses that have been extensively studied for well over 60 years. Human AdVs include approximately 56 types divided into eight classes, A-G (1). AdVs are pathogenic, and can cause a variety of different diseases including gastroenteritis, keratoconjunctivitis, hemorrhagic cystitis and acute respiratory disease. Class C AdVs, which include the most widely studied Ad2 and Ad5, are the most frequent cause of myocarditis in children under the age of one year and are a common cause of respiratory illness in children (2,3). However, in between 50-90% of cases, Class C AdV primary infections are asymptomatic (1,2). In addition to acute infection, AdVs are capable of both persistent (4) and true latent infection (5,6). In spite of their complex biology, our depth of knowledge of Adenovirus coupled with its ease of genetic manipulation, ability to infect a wide range of tissues, including both dividing and senescent cells, has led to its development as a promising candidate for gene and oncotherapy (7,8).

The AdV genome is ~36 kilobases long with inverted terminal repeats. Genes are organized into early and late transcriptional units, and are transcribed from both strands of the DNA genome. All human AdV serotypes encode at least one highly structured, approximately 160 nucleotide (nt), non-coding “virus-associated RNA” (VA RNA) (9,10). Approximately 80% of all AdVs, including Ad2 and Ad5, encode two distinct VA RNA transcripts, VA RNA_I and VA RNA_{II} (9). VA RNAs from serotypes with only a single VA RNA gene most resemble the Class C VA RNA_I. VA RNA_I is essential for efficient virus replication: In Ad5, deletion of VA RNA_I led to an approximately 20-fold

decrease in virus titer (11). While deletion of VA RNA_{II} caused no measurable decrease in AdV5 viability, deletion of both VA RNA_I and VA RNA_{II} decreased titers 60 fold (12). This greater impact compared to the single VA RNA_I deletion suggests that while VA RNA_{II} can partly compensate for the absence of VA RNA_I, VA RNA_I plays the predominant pro-viral role. For this reason, the majority of research into the function of the Adenovirus VA RNAs has focused on VA RNA_I and it is therefore the main focus of this review. Where the collective activities of both VA RNA_I and VA RNA_{II} are discussed, the term VA RNA will be used, while the individual VA RNAs will be referred to specifically as VA RNA_I and VA RNA_{II}.

During Adenovirus infection, VA RNA_I and VA RNA_{II} accumulate in the cytoplasm beginning at ~18 hours post infection, and by late in the lytic infection cycle (24 hours), these RNAs have accumulated to extraordinarily high levels, 10^8 and 10^6 copies per cell, respectively (10). Like many viral RNAs, VA RNA_I interacts with multiple cellular proteins and likely have multiple functions during infection. The most established and best understood role of VA RNA_I is as an efficient inhibitor of the innate immune protein double-stranded (ds)RNA-activated kinase (PKR). Through this activity, VA RNA_I allows AdV to escape a key cellular response to dsRNA, a potent pathogen-associated molecular pattern (PAMP), and confers AdV's observed resistance to interferon (10,13). In addition to binding and inhibiting PKR, VA RNA_I interacts with the other innate immune system dsRNA-detecting proteins, RIG-I and OAS1 (14,15), as well as the host RNA interference (RNAi) machinery through the cellular endoribonuclease Dicer and Argonaute-2 (Ago-2) within the RNA-induced silencing complex (RISC) (16,17). While

most functions of VA RNA_I are associated with its accumulation late in infection, recent work has revealed a novel role for VA RNA_I early in infection as a repressor of Hepatoma-Derived Growth Factor (18). Understanding the interactions of this RNA with host proteins during AdV infection will add to the growing body of knowledge of the multifaceted roles of non-coding RNAs (ncRNAs), improve our understanding of host-pathogen recognition, and promote effective development of AdV-based technologies. Of particular importance is building an understanding of how particular RNA features are critical for activation and inhibition of dsRNA-detecting innate immune proteins. Such proteins are responsible for the general detection of viruses and thus represent a potential target for influencing the outcome of infection. The ability to modulate and selectively activate these proteins is of particular interest for developing general antiviral therapies effective against viruses that rely upon manipulation of dsRNA-detecting innate immune proteins but for which there are no vaccines or treatments (19,20). For example, selective activation of PKR or the OAS/ RNase L pathway in infected cells has already been demonstrated as a viable way to inhibit replication of a range of viruses including respiratory syncytial virus, encephalomyocarditis virus, and human parainfluenza virus 3 (21-23).

Expression, Localization, and Structure of AdV VA RNAs

VA RNA gene structure and transcription

The VA RNA genes encode transcripts of ~150-200 nt in length. Accumulation of VA RNA_I was first observed late in Ad2 infection (24), and a second RNA species, VA RNA_{II}, was later found to be present in lower amounts, at approximately a 1:40 ratio (25).

Both VA RNAs are transcribed by the cellular RNA Polymerase III (RNA Pol III) (25,26). RNA Pol III requires two intragenic promoter elements, Box A and Box B, which are highly conserved across all AdVs and in Ad2 are located approximately at positions +13 to +24 and +56 to +70, respectively (27-29) (**Fig. 1**). Mutations in these promoter regions reduce VA RNA transcription and limit virus replication *in vivo* (9). Accumulation of VA RNAs is a function of AdV genome copy number (18) and in viruses which possess VA RNA_I and VA RNA_{II}, the RNAs compete for transcription by RNA Pol III (28). Though both VA RNAs are initially transcribed at similar levels, RNA Pol III becomes limiting following AdV genome replication, and VA RNA_I outcompetes VA RNA_{II} for transcription, resulting in the lower relative level of VA RNA_{II} observed late in infection (12).

In Ad2, transcription of VA RNA_I is initiated at one of two possible transcriptional start sites (**Fig. 1**), G(+1) or three nt upstream at A(-3) (30,31), with the former variant accounting for 75% of the total VA RNA_I pool (30,32). In contrast, Ad2 VA RNA_{II} has only a single start site corresponding to the G(+1) form (33,34), though in other AdVs, VA RNA_{II} can have alternative transcription start sites (35). While these alternative transcriptional start sites are not present in every VA RNA_I, such variation in transcription initiation is present in many serotypes (9,35). The 3'-ends of VA RNAs are unique in that they are dictated by termination of transcription itself and not by processing, as is the case for many host polymerase transcripts (36). Termination of VA RNA_I transcription by RNA Pol III is instigated by a conserved 3'-end transcription termination sequence located ~10 nt from the 3'-end of the RNA, immediately upstream of four consecutive adenosines (d(A₄); **Fig. 1**).

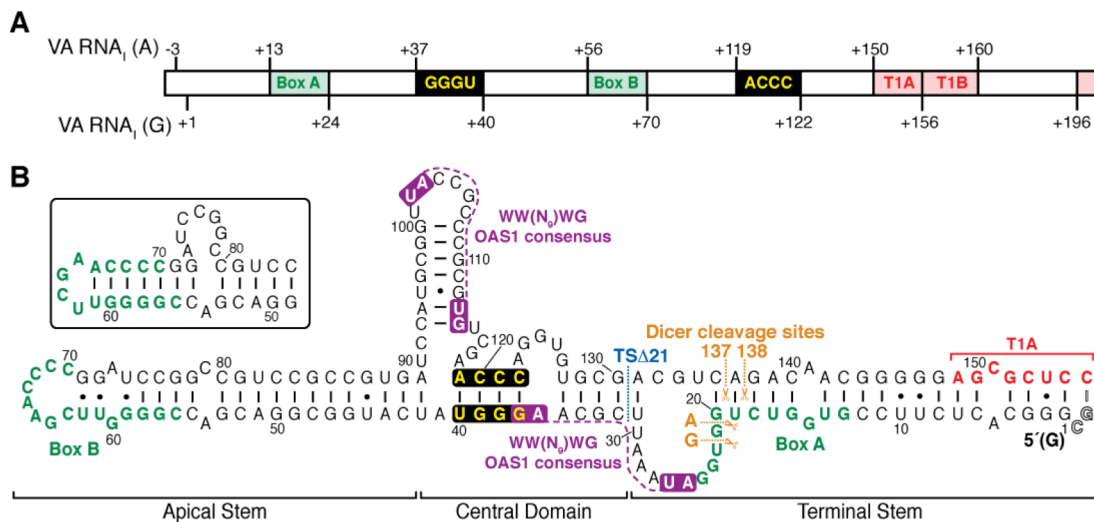


Fig. 1. VA RNA₁ gene organization and transcript secondary structure. *A*, Adenovirus VA RNA₁ is transcribed from two distinct start sites: A (-3) and G (+1) producing VA RNA₁(A) and VA RNA₁(G) transcripts, respectively. Locations of the RNA Pol III Box A and B promoter regions (green), internal terminator sequence (T1A, red), first d(A₄) terminator sequence (T1B, red), backup terminator sequence (T2, red), and pair of universally conserved complementary tetranucleotide sequences (yellow) are indicated. *B*, Secondary structure of VA RNA₁, which is comprised of three structural domains: Terminal Stem, Central Domain, and Apical Stem. The RNA Pol III promoter sequences, conserved tetranucleotides, and T1A/ T1B terminator sequences are colored as in *panel A*. Two WW(N₉)WG OAS1 consensus activation sequences (purple), sites of Dicer cleavage (orange dotted lines), and the site of TSA21 RNA truncation (blue dotted line) are mapped on the RNA secondary structure. 5'-end nucleotides arising from alternative transcription start site in VA RNA₁ (A) are shown in outline font. The VA RNA₁ Apical Stem can adopt two functionally non-equivalent structures; the alternate folding with base pairing between G57-G60 and C67-C70 which results in the formation of a loop within the helix is shown (boxed).

Unlike some other RNA Pol III transcripts, for which a d(A₄) sequence on the template strand is sufficient for transcription termination, mutations in the conserved VA RNA₁ terminator sequence upstream of its d(A₄) sequence significantly decreases termination

efficiency (36). While the exact function of the upstream terminator sequence is unclear, it has been shown to bind the cellular nuclear factor 1 (NF1), which promotes RNA Pol III termination and transcript release (36). In the absence of NF1, AdV replication is diminished as RNA Pol III is unable to properly terminate, release the VA RNA_I transcript and re-initiate transcription (37). RNA Pol III completes VA RNA_I transcription by transcribing between one and four single-stranded uridines from the d(A₄) terminator sequence and appending up to two additional non-templated uridines to the 3'-end of the VA RNA_I. This process generates a mixture of VA RNA_I transcripts appended with between one to six 3'-end uridines (**Fig. 1B**), with transcripts containing two or four 3'-end uridines being the most abundant, followed by those with one or three 3'-end uridines, and those containing five or six uridines representing an extremely small subset of the VA RNA_I pool (38).

Sequencing of the Ad2 VA RNA_I and VA RNA_{II} genes identified an additional “backup terminator” sequence at position +37 from the 3'-end of VA RNA_I (38,39) (“T2”; **Fig. 1A**). During RNA Pol III transcription of VA RNA_I, in AdV infection and *in vitro*, a subset of VA RNA_I transcripts do not terminate at position ~157-159, but rather at position ~197 using the backup terminator sequence to generate a longer VA RNA_I species, V₂₀₀ (33,40). Mammalian RNA Pol III termination is leaky and transcribed genes, such as those for tRNAs, often contain both canonical d(A₄) and non-canonical termination signals, leading to a heterogeneous transcript pool (41). In contrast, yeast tRNA genes more closely resemble the organization found for VA RNA_I, with two canonical terminators placed immediately downstream of the RNA coding sequence

(42,43). This strictly controlled termination may reflect a pressure to rapidly reinitiate transcription and produce the large quantities of tRNA necessary for a fast growing unicellular organism (41). Thus the presence of a second canonical RNA Pol III terminator at the 3'-end of some VA RNA_I genes may be needed for efficient termination and reinitiation, required to accumulate high levels of viral transcript. Additionally, this terminator redundancy may ensure the absence of a VA RNA_I and VA RNA_{II} fusion, or continued transcription into the adjacent gene in serotypes lacking VA RNA_{II}, which could potentially result in activation of dsRNA-detecting innate immune proteins.

While one or both of these scenarios may be at play in the cell, neither would preclude the possibility that VA RNA_I transcripts produced from the second terminator also perform distinct functional roles. To examine whether this additional sequence is capable of adopting a stable structure, we used Mfold (44) to examine its potential folding and found that a stable hairpin is the only predicted structure (**Fig. 2**). However, whether this structure is adopted in the context of the full VA RNA_I transcript and is capable of imparting novel activities remains to be determined. More generally, variations in RNA Pol III transcriptional start and termination sites create substantial heterogeneity at both the 5'- and 3'-ends in the VA RNA_I pool; whether this heterogeneity influences VA RNA_I function in the context of infection will require further detailed investigation.

Cellular Localization of VA RNA_I

VA RNA_I is present in both the nucleus and the cytoplasm of AdV-infected cells, but

accumulates in high copy number in the cytoplasm late in infection. The La autoantigen

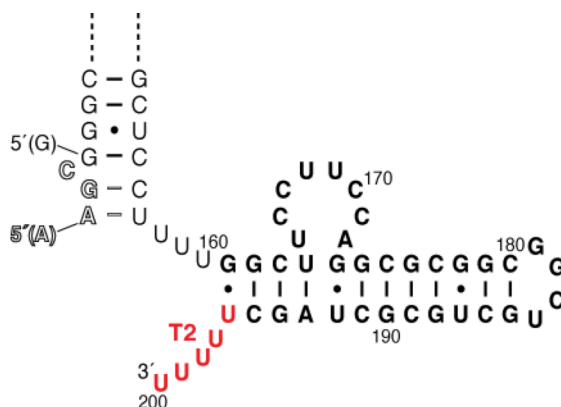


Fig. 2. Predicted structure of the additional 3'-end sequence in VA RNA₁ produced at the 'backup terminator' (T2). A small percentage of VA RNA₁ transcripts are terminated downstream of the primary terminator sequence at the 'backup terminator' (T2, red). The predicted structure of the 3'-end sequence (bold) appended to VA RNA₁ as a result of this termination is shown. The ΔG of folding for this structure predicted by Mfold is -15.40 kcal/mol.

is a protein recognized by the sera of patients with systematic lupus erythematosus (45), which binds to the 3'-end UUU-OH sequence of RNA Pol III transcripts, including tRNAs, pre-5S rRNA and VA RNA₁ (46,47). La binding facilitates proper maturation of cellular RNA Pol III transcripts, contributes to nuclear retention of small RNAs, facilitates formation of ribonucleoprotein complexes, and can promote translation of specific mRNAs (reviewed in (46)). La is essential in mammals (46), and its absence in brain tissues causes cell death (48,49). Recent work shows that La shuttles between the nucleus and cytoplasm (50), but whether La remains bound to VA RNA₁ once in the cytoplasm is unknown. However, as approximately 2×10^7 copies of La are present in the cell, most likely bound to tRNA transcripts (46), and VA RNA₁ copies alone far surpass this level at late stages in infection, it is unlikely that all VA RNA₁ molecules are bound

by La. We speculate that the rate at which VA RNA_I transcription outpaces the availability of La may play an important role in the timing of when the VA RNA_I termini are free to interact with other cellular proteins. For example, RIG-I is known to be activated by the 5'-end triphosphate (5'-ppp) group of VA RNA_I (15); occlusion of the 5'-ppp by La could thus dampen any antiviral effect that RIG-I may confer upon activation by VA RNA_I until late in infection. The degree to which La might prevent this type of interaction is unknown, as well as the number of VA RNA_I molecules required to saturate available La in the presence of its other binding partners such as tRNAs and 5S rRNA.

VA RNA Structure

VA RNA_I adopts a complex secondary structure with three distinct structural domains: The Apical Stem, Central Domain, and Terminal Stem (**Fig. 1B**) (51,52). Despite generally low sequence conservation, all VA RNAs appear to be structurally conserved and retain their overall organization into these three domains (9,52). Between AdV subgroups only two regions of VA RNA_I sequence are phylogenetically conserved: the RNA Pol III promoter sequences (Box A and Box B), and two complementary tetranucleotide sequences within the Central Domain, GGGU and ACCC (9,53) (**Fig. 1**). In addition to the proposed secondary structure formed by these tetranucleotides within the Central Domain, their specific identity may also be important for VA RNA_I inhibition of PKR, suggesting a role beyond that of maintaining stable Central Domain secondary structure.

The Apical Stem forms an unusually stable hairpin structure with an apparent thermal unfolding T_m of >80 °C (51), and which is resistant to denaturation even in 6 M urea. This latter feature causes Ad2 VA RNA_I (~155 nt) to migrate as an apparent ~220 nt RNA in denaturing polyacrylamide gels (51,54). The distal region of the Ad2 VA RNA_I Apical Stem can adopt alternate base pairings (**Fig. 1B**) that result in two structures which are functionally non-equivalent in their ability to bind and inhibit PKR (55). While PKR binding *in vitro* does not alter the relative amounts of each Apical Stem conformation, whether there are other forces at play in the cell which can drive formation of one conformation over the other, or whether the structure which inhibits PKR more weakly is retained for some other essential functional role, remains unknown.

The VA RNA_I Terminal Stem is also largely Watson-Crick base-paired but is not as stable as the Apical Stem. While the Apical Stem appears to form an independently folded structural domain, the unfolding of the Central Domain and Terminal Stem are tightly coupled, indicating that the Terminal Stem may serve to stabilize the Central Domain (51). The Terminal Stem sequence and base pairing are relatively conserved among all AdV serotypes, owing to the presence of the RNA Pol III transcription start (Box A) and termination sites (9,36) but minor substitutions which disrupt base pairing at the ends of the Terminal Stem are tolerated (56). However, the mutations tested permit maintenance of some base pairs near the very termini of the RNA, leaving open the question of whether the 5'- and 3'-ends of must be base-paired to optimally rescue translation during AdV infection. PKR also binds the Terminal Stem in isolation (57), but this region is apparently entirely dispensable for the inhibitory activity of VA RNA_I

against PKR (58). However, the finding that variants with smaller deletions, which leave portions of the Terminal Stem intact, have a reduced ability to inhibit PKR (58) suggests that aspects of Terminal Stem architecture may be important for VA RNA_I function in the context of the intact RNA.

The importance of the Terminal Stem is apparent for a more recently defined function of VA RNA_I, as a substrate of the cellular miRNA biogenesis endoribonuclease Dicer. Dicer specifically binds and processes the VA RNA Terminal Stem, making the sequence and structure of this domain indispensable for generation of VA RNA-derived miRNAs (“mivaRNAs”) (17). The reported short half-life of the Dicer-truncated VA RNA_I Apical Stem-Central Domain (AS-CD) fragment also lends some support to the idea, noted above, that the role of the Terminal Stem *in vivo* is to protect the Central Domain from degradation. However, though one group has reported that AS-CD RNA is unstable (59), detailed analysis of the fate and potential roles of the AS-CD RNA product of VA RNA_I Dicer processing has not yet been performed.

The Central Domain is the most structurally complex of the three VA RNA_I domains (60), with a secondary structure that takes the form of a three-helix junction, linking the Apical and Terminal Stems, and containing the two universally conserved, complementary tetranucleotide sequences. Additionally, a higher order tertiary structure was proposed based upon sequence complementarity and mutual insensitivity to single-strand specific ribonucleases of two loop regions within the Central Domain (9,53). This

pseudoknot interaction (dashed line) was recently experimentally verified in two independent studies.

The first built upon a prior *in vitro* identification and analysis of a truncated VA RNA₁ lacking the entire Terminal Stem (“TSΔ21 RNA”) which revealed a strong dependence of Central Domain unfolding upon solution pH (58). Stabilization at low pH is consistent with a critical protonation-dependent RNA tertiary contact, and this feature was used by

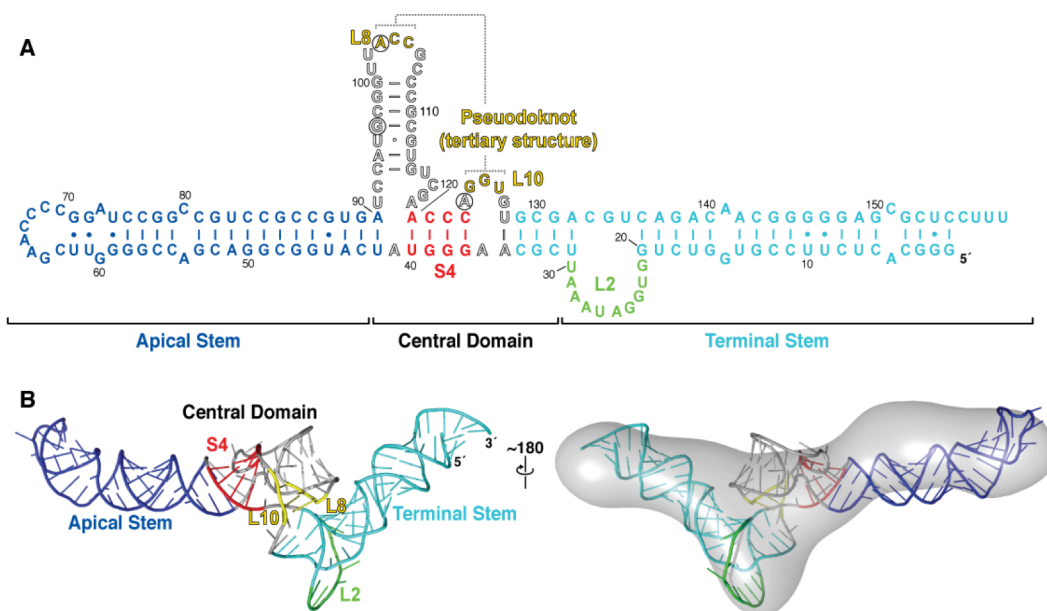


Fig. 3. A structural model for Ad VA RNA₁ and the role of the Central Domain in PKR inhibition.

A, Secondary structure of Ad2 VA RNA₁ highlighting the three major structural domains, the Central Domain pseudoknot interaction between Loops 8 and 10 (L8 and L10; yellow outline font), Loop 2 (L2; green), and the pair of conserved tetranucleotide sequences which form Stem 4 (S4; red). Putative interaction sites for Mg²⁺ (61) are indicated by the circled nucleotides. **B**, Two views of the VA RNA₁ structural model derived from solution RNA structure probing and SAXS constraints (62). Domain and structural features are colored as in panel A; the *right* view is shown with a surface representation (gray) of the *ab initio* model derived directly from the SAXS data.

Wilson *et al.* (61), in combination with solution structure probing by “selective 2'-hydroxyl acylation analyzed by primer extension” (SHAPE), to dissect the higher order structure within the Central Domain of this truncated RNA. This study identified the protonated base (A123) and provided direct experimental evidence for the pseudoknot interaction within the Central Domain (Loop 8 and Loop 10 sequences ACC:GGU; **Fig. 3**). Using Tb^{3+} -probing, potential sites of Mg^{2+} interaction within the Central Domain were also identified; two of these residues, A103 and A123, are within or immediately adjacent to the pseudoknot structure. Remarkably, however, this study also revealed that the native Central Domain tertiary structure it is not required for PKR inhibition.

Launer-Felty *et al.* (62) also applied SHAPE and dimethylsulfate (DMS) RNA structure probing to demonstrate the same Central Domain pseudoknot structure is formed within full-length Ad2 VA RNA_I. Constraints from both structure probing experiments and small angle X-ray scattering (SAXS) analysis of wild-type and mutant RNAs were used to generate a structural model for VA RNA_I. These molecular structures were compared to *ab initio* SAXS-derived molecular models with good agreement. The model of full-length wild-type VA RNA_I has an extended, almost planar structure in which the Apical and Terminal Stems are separated by a central bulge comprised of the Central Domain and the large loop at the top of the 5-side of the Terminal Stem (**Fig. 3B**). Interestingly, no change was observed in the SAXS-derived structure with addition of Mg^{2+} . While this demonstrates that divalent ion is not required for tertiary folding of the Central Domain and does not induce gross structural changes, this observation is not inconsistent with Mg^{2+} stabilization of the Central Domain tertiary structure and influence upon interaction

with PKR (63). Additionally, the model places the extended Loop 2, located at the top of the Terminal Stem, adjacent to the Central Domain suggesting that Loop 2 may be responsible for the enhanced Central Domain stability and coupling of RNA unfolding of these two domains in the intact VA RNA_I (51,58). A particularly appealing feature of the model is the compact nature of the Central Domain and the manner in which the conserved tetranucleotide sequences are positioned to stack coaxially with the Apical Stem and thus define a short extension to the primary PKR binding site (**Fig. 3**). As noted by the authors, this suggests a precise structural tuning of the PKR binding site which likely defines the molecular mechanism by which VA RNA_I exerts its inhibitory activity.

VA RNAs Usurp Multiple Cellular Functions

While VA RNA_I is best known for its essential pro-viral activity in PKR inhibition, more recent evidence has uncovered further potential roles for VA RNAs in disrupting multiple cellular processes (**Fig. 4**). In the following sections we review the current state of understanding and highlight the key areas for further investigation.

VA RNA interference with RNAi machinery

VA RNA_I interferes with cellular miRNA biogenesis on three levels: competition with cellular RNAs for Exportin 5-mediated export from the nucleus, saturation of the pre-

miRNA processing endoribonuclease Dicer, and direct interference with RISC complex assembly and function.

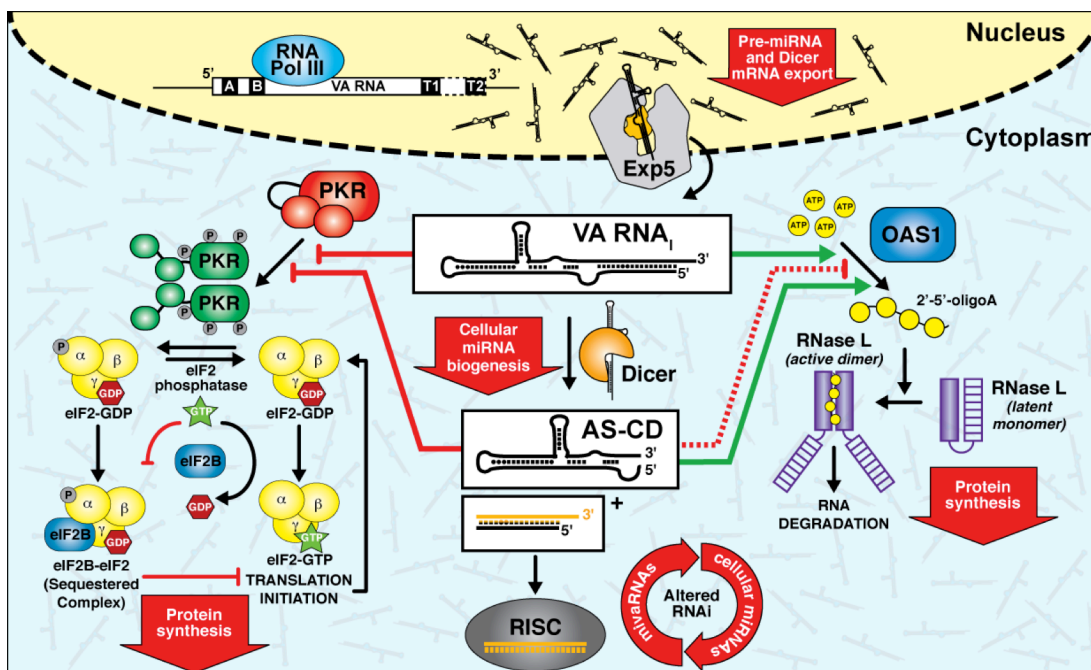


Fig. 4. Overview of known activities of VA RNAs against host cell components. VA RNA interferes with multiple cellular processes (red arrows). VA RNAs block miRNA biogenesis via saturation of nuclear RNA export by Exp5 and pre-miRNA processing by Dicer, resulting in an alteration of the population of RISC-bound miRNAs (top and center). Single-stranded segments of the VA RNA Terminal Stem are also incorporated into functional RISC complexes (as mivaRNAs). Both intact VA RNA₁ and the Dicer-derived AS-CD fragment can inhibit protein synthesis via direct inhibition of the innate immune protein PKR (left). VA RNA₁ binding to PKR prevents dsRNA-mediated PKR dimerization, activation and thus downstream phosphorylation of eIF2 which would otherwise block translation initiation. Intact VA RNA₁ and the authentic product of Dicer cleavage (AS-CD RNA fragment) activate OAS1, which could potentially activate the latent cellular ribonuclease RNase L (right). The dashed red line indicates, in contrast, that an RNA fragment with the Terminal Stem fully deleted RNA (TSΔ21) can act as a pseudoinhibitor *in vitro*.

Competition for nuclear export by Exportin 5 (Exp 5)

Following transcription by RNA Pol III, VA RNA_I is exported to the cytoplasm via Exp 5 (**Fig. 4**), a Ran-dependent GTPase important for export of nuclear RNAs, including pre-miRNAs and tRNAs (64,65). Exp 5 recognizes a ‘mini-helix,’ a ≥ 14 bp, mostly double-stranded stem with its 5’-end involved in base-pair interactions and its 3’-end comprised of 3-8 single-stranded nucleotides (66). This feature is present at the end of the VA RNA_I Terminal Stem and interacts directly with Exp 5 making it an efficient competitor against cellular pre-miRNAs for nuclear export (67). Exp5 also regulates export of Dicer mRNA into the cytoplasm, and through competition with this mRNA for export, VA RNA_I can deplete the cytoplasmic levels of Dicer protein (68). Thus, through interaction with Exp 5, VA RNA_I both alters the ability of newly synthesized pre-miRNAs to be exported to the cytoplasm and limits the cellular level of the miRNA-maturation endoribonuclease Dicer.

Dicer Saturation

Once in the cytoplasm, VA RNA further suppresses miRNA biogenesis by saturating Dicer, rendering it unavailable to process cellular pre-miRNAs, including potential antiviral miRNAs (17). Dicer binds and cleaves the Terminal Stems of VA RNA_I and VA RNA_{II} from a range of AdV serotypes (16,35). The efficiency of Dicer cleavage of VA RNA is the same as that for dsRNA of the same length (17), and produces a truncated VA RNA species and a Terminal Stem fragment from which the 22 nt miRNAs that may be incorporated into RISC are derived (**Fig. 4**) (17,32). Interestingly, VA RNA_{II} appears

to be the preferred VA RNA substrate for Dicer *in vivo*: despite ~20 fold lower expression than VA RNA_I, VA RNA_{II} is preferentially processed by Dicer and incorporated into RISC during infection (16).

Though VA RNA_{II}-derived miRNAs are more prevalent, the specific requirement of VA RNA_I for efficient AdV replication (12) has led to more numerous investigations on the interactions of VA RNA_I with the RNAi machinery. Although they differ by 3 nt in length, both G and A forms of VA RNA_I (**Fig. 1B**) are processed at the same site by Dicer, yielding VA RNA 3'-end fragments of the same size and 5'-end fragments differing in length by three nt (32). Much of the work done to identify the sites of Dicer processing in VA RNA_I used Ad5 VA RNA_I (32), for which two sites of processing were identified following nt 137 or nt 138, for both the G and A isoforms (16,32). However, another report indicated only a single cut site for Ad5 VA RNA_I after nt 138, but also showed VA RNAs from other serotypes, including Ad4 and Ad37, are cleaved at two locations (35). These conflicting reports leave open the possibility that Ad5 VA RNA_I processing may be dependent on the cell line used. Defining the precise location(s) of Dicer processing site and the factors that influence alterations in this pattern is important because variation in product length alters the seed sequences of these RNAs, and therefore the potential mRNAs targeted (69).

The importance of Dicer processing of VA RNA_I during infection is poorly understood. While some groups have reported that the phenotype of a poorly replicating Adenovirus strain lacking VA RNA_I and VA RNA_{II} can be restored by knocking down either Dicer or

Exp 5 (68), others show that knocking down Dicer has no restorative effect in this context (70). These conflicting reports raise the question of whether the importance of Dicer inhibition by VA RNA_I is serotype specific, or dependent upon the type of infection (*i.e.* acute, persistent, or latent). While much attention has focused on subsequent incorporation of Dicer processed fragments into the RISC complex and their potential targets, it remains to be seen if Adenovirus infection is affected by Dicer saturation alone. Infection with an Adenovirus containing VA RNAs resistant to Dicer processing, but which still maintain their other pro-viral functions might begin to shed light on this question.

mivaRNA incorporation into RISC: a mechanism of viral control of host cell gene expression?

Following processing by Dicer, the 3' and 5' strands of the VA RNA Terminal Stem-derived 22 bp fragment can be incorporated into RISC (17,67,71,72). These mivaRNAs are the only source of RISC-associated miRNAs of viral origin during Adenovirus infection (73). While one group reported that approximately 80% of Ago-2-containing RISC complexes late in Adenovirus infection contain mivaRNAs (16), others report a significantly lower proportion, 15% (73). Though this disparity may be attributed to differences in experimental approach, for example overexpression of Ago-2 resulting in reduced VA RNA competition with cellular RNAs (16), the extraordinary level to which VA RNA accumulates (10^8 copies per cell) (10) makes a substantial effect on the cellular miRNA population highly likely (**Fig. 4**).

The ability of a given miRNA to down regulate gene expression is not directly correlated with its overall abundance, degree of processing by Dicer, or level of incorporation into RISC. For example, despite being expressed at 20-fold lower abundance, VA RNA_{II} is the origin of the majority of RISC-associated miRNAs (~69%) (17,71). Yet among mRNAs isolated from miRNA-containing RISC during Ad5 infection, seed sequences corresponding to miRNA_{II} are underrepresented (73). Furthermore, both 3'-miRNA_I(A) and (G) more efficiently knock down reporter gene expression than miRNAs derived from VA RNA_{II} (73). Together these findings illustrate a disconnect between miRNA abundance in RISC and the likelihood that a given miRNA can knock down gene expression. This disconnect is also present among VA RNA_I-derived miRNAs. The 5'-and 3'-end strands of miRNA_I(A) and miRNA_I(G) are not incorporated into RISC in equal measure. For Ad5 VA RNA_I, while both the 5' and 3' strands of VA RNA_I(A) are incorporated, in contrast, only the 3' strand of VA RNA_I(G) is found in RISC (17,71). This preference for 5'-VA RNA_I(A) strand incorporation, in spite of miRNA_I(G) representing more than 75% of the total VA RNA pool (34), is determined by 5'-end heterogeneity, as 5'-miRNA_I(A) is three nucleotides longer than 5'-miRNA_I(G) due to their different transcriptional start sites (32,74). Although 3'-miRNA_I(A) is more likely to be found in RISC, the 3'-strand activity is only about twice that of the 5' strand (73). Curiously, a conflicting report shows that the 3'-miRNA_I(A)-associated RISC is only 2% as active as a RISC assembled upon the 5'-miRNA_I(A) *in vitro* (32). This pattern, however, is not recapitulated *in vivo*, and reporter assays demonstrate that 5'-miRNA_I(A) is not as effective in knocking down reporter expression as 3'-miRNA_I. This indicates that the

inherent activity of miRNA-associated RISC *in vitro* may not always accurately reflect miRNA function *in vivo*.

The role of miRNAs once they are incorporated into the RISC complex is unclear. The miRNAs are bound by Ago-2, the endonuclease component of RISC (75), indicating that the miRNA-loaded RISC is indeed functional. Further, sequences within the miRNAs can suppress reporter gene mRNAs containing artificial complementary sequences by approximately 20% (71), indicating that during infection these RISC-associated RNAs are indeed capable of interference. In support of the idea that the miRNAs are functional interfering RNAs, blocking the ability of VA RNA₁ Terminal Stem sequences to bind to their putative targets by supplying complementary 2'-O-methylated RNA decreases virus titer (71). This observation is consistent with earlier work demonstrating the importance of the VA RNA₁ Terminal Stem in which viruses harboring VA RNA₁ lacking 3'-half of the Terminal Stem exhibited a 10-fold reduction in virus titer (76). These discoveries sparked a search for miRNA targets during Adenovirus infection and, though some have been identified using microarray and bioinformatics approaches, the importance of knocking down these targets is unclear. While the evidence from the studies described above supports a functional role for the miRNAs, the finding that supplying miRNA mimics has no impact on virus replication in Ad5 lacking VA RNA₁ indicate that this role is not sufficient for complementing loss of PKR inhibition (73).

Recent work using microarray analysis to identify genes downregulated during AdV infection revealed 13 genes involved in DNA repair, growth, apoptosis, and RNA metabolism, that are potentially regulated by the Ad5 miRNA derived from Dicer cleavage of VA RNA_I(A) after nt 138 (miRNA_I(A)-138) (77). A single Ad5 3'-miRNA_I(A) target was subsequently verified as TIA-1 cytotoxic granule-associated RNA binding protein (34,78,79). TIA-1 is an RNA-binding protein implicated in translational control during cellular stress and alternative splicing of pro-apoptotic proteins (34,78,79). An alternate approach of RISC immunoprecipitation during Ad5 infection, and subsequent analysis of recovered RISC-associated mRNA transcripts (73), also identified potential targets of miRNAs. In this work, the miRNAs were shown to have distinct targets, including genes involved in apoptosis, membrane and mitochondria-associated processes and cell growth. Interestingly, all validated targets contained complementarity to the miRNAs in their 3'-UTRs (73). Both this and one other study identified the cell-growth protein lymphocyte antigen 6 complex (LY6K) (73,77), a protein implicated in both breast, and head and neck cancers (80,81), as a target of 3'-miRNAs (73,77).

The nature of the miRNA targets identified to date are consistent with the pro-viral role of VA RNA_I, but whether these targets are directly related to the viability of the virus is unclear. The effect of miRNAs may simply be to alter the overall population of RISC-associated miRNA, rather than to knock down specific targets (73). In fact, recent work has demonstrated that disrupting the seed sequences present in 3'- and 5' miRNAs has no effect on lytic virus growth in tissue culture (70). This finding raises the question of

whether the few genes identified as specific targets of miRNAs are important for virus replication, or incidental and therefore a side-effect of a more general inhibition (73,77). The sequence of the AdV Terminal Stem is not strictly conserved, raising the additional question of whether the same genes are down regulated during infection by different AdV serotypes, and if any such pattern is sequence-dependent. Whatever their true function, these miRNAs are also present in persistently infected lymphoid cells (82), indicating that Dicer processing of VA RNA and subsequent incorporation into RISC could have a role in both lytic and persistent infection.

Though most previous work on miRNAs utilized Ad5, VA RNAs of all human Adenoviruses serotypes are thought to be processed by Dicer and subsequently incorporated into RISC (35). Dicer processing efficiency, cut site number, and strand bias for loading miRNAs onto Ago-2 containing RISC are all serotype specific (35). Interestingly, the 5'-seed sequences in stable RISCs for each serotype examined (Ad4, Ad5, Ad11, and Ad37) have homologous seed sequences. Whether this homology has functional implications or contributes to virulence, however, remains unknown. In spite of these differences, each of the examined serotypes has maintained the ability to be processed by Dicer, indicating that serving as a substrate for Dicer may be an important pro-viral role for VA RNA_I

VA RNA_I-mediated inhibition of PKR

Shortly following the discovery that VA RNA_I is required for optimal virus replication (12), its specific role in Ad5 resistance to interferon- α and efficient translation late in

infection was revealed (11,83). The ability of VA RNA_I to promote Adenovirus protein synthesis arises from its direct inhibition of PKR, which blocks the PKR-mediated shut down of general translation (**Fig. 4**) (13,84). In the absence of viral inhibition, PKR is activated by dsRNA produced as a consequence of transcription of overlapping genes in DNA viruses, RNA genome replication in RNA viruses, or formation of RNA secondary structures (84-86). Cytoplasmic dsRNA is thus a hallmark of viral infection detected by PKR, and which promotes PKR dimerization, autophosphorylation and subsequent phosphorylation of Ser 51 on the α subunit of the eukaryotic translation initiation factor 2 (eIF2) (87,88). eIF2 phosphorylation increases affinity for the guanosine nucleotide exchange factor eIF2B, preventing exchange of GDP for GTP on eIF2. Because GTP hydrolysis is a rate-limiting step in translation initiation, PKR phosphorylation of eIF2 α leads to dramatic reduction in protein synthesis (89,90). Through its ability to bind and effectively inhibit PKR by preventing PKR dimerization, VA RNA_I thus ensures efficient production of viral proteins (91). The poor growth phenotype of Ad2 lacking VA RNAs can be complemented by growing the virus in a cell line harboring an eIF2 Ser51Ala mutation which cannot be phosphorylated and thus regulated by PKR (92). VA RNA_I transcripts from range of AdV serotypes inhibit PKR, and the degree to which they are able to do so is directly related to virus replication kinetics (52). In addition to the importance of VA RNA_I inhibition of PKR during acute infection, more recent works suggest that the ability of many AdVs to establish latent infection may be related to the abundance of VA RNA_I: for example, the low virulence and slow growth of Ad12 is due to promoter mutations which lead to low levels of VA RNA_I accumulation (93).

Collectively, these findings illustrate the importance of VA RNA_I in both acute and latent infection.

Uncovering the protein-RNA contacts that mediate PKR-VA RNA_I interaction and identifying the structural hallmarks that define VA RNA_I as an inhibitor of PKR have been the subject of extensive studies over the last several decades. While a high-resolution structure of a PKR complex with VA RNA_I (or any other RNA) has remained elusive to date, solution studies of VA RNA_I structure and *in vitro* function have revealed a wealth of important new information. Though a large majority of studies have focused specifically on the RNA molecular features and interactions that confer VA RNA_I-mediated inhibition of PKR, they have nonetheless also informed our understanding of the complex nature of VA RNA_I biology.

Binding and inhibition of PKR are the primary functions of the Apical Stem and Central Domain of VA RNA_I, respectively (94). PKR binds the Apical Stem via two N-terminal dsRNA binding motifs (95) on the same dsRNA-binding surface responsible for binding to activating RNA (96). Initially, it was hypothesized that the inability of the Apical Stem to activate PKR was due to the presence of a number of base mismatches which could potentially distort the A-form dsRNA helix. However, mutating the Apical and Terminal Stems so that they are perfectly base-paired improved both PKR binding and inhibition, rather than transforming the RNA into a PKR activator (96). In the absence of the Central Domain, the Apical Stem of VA RNA_I can activate PKR, confirming the previous finding that PKR binding and activation are distinct processes (97), and highlighting the critical

functional role of the Central Domain. Indeed, while the Apical Stem is the primary binding site for PKR, high affinity PKR-VA RNA_I interaction, and thus potent PKR inhibition requires the presence of Mg²⁺ and contacts mediated by the Central Domain (54,57,63).

The VA RNA_I Central Domain is necessary for inhibition of PKR (54,56). Following early studies which used large deletions and substitutions to show that the overall architecture of the RNA must be maintained in order to inhibit PKR (97), subsequent work focused on the role of specific sequences and substructures. The identity of the bases in the conserved Central Domain tetranucleotide sequences, GGGU and ACCC, and not simply maintenance of their base pairing, was suggested to be important for translational rescue by VA RNA_I (53). While mutation and subsequent restoration of base pairing partially recovered the ability of VA RNA variants to rescue translation, wild-type VA RNA_I activity was never fully recovered (53). This finding suggested the involvement of this conserved four bp helix (Stem 4) in the formation of a Central Domain tertiary structure (**Fig. 3**). As discussed in, two recent studies verified the presence of a pseudoknot interaction within the Central Domain using solution structure probing studies of VA RNA_I and in one case combined this data with SAXS constraints to construct a complete molecular model of VA RNA_I (61,62).

First, using the truncated T Δ 21 RNA, Wilson *et al.* (61) provided compelling evidence for the existence of a pH- and Mg²⁺-sensitive tertiary structure in the Central Domain, including a pseudoknot structure formed by the base pairing of Loop 8 and Loop 10

sequences, ACC (nts 103-105) and UGG (nts 124-136), respectively (**Fig. 3**). Contrary to expectation, however, this Central Domain tertiary structure was found to play no role in efficient inhibition of PKR by T Δ 21 RNA. Additional mutagenesis studies of the RNA revealed that PKR inhibition by VA RNA_I required only the Apical Stem and the presence of a three-helix junction, with the greatest impact on activity arising through the deletion of the 5'-half sequence at the junction between the Central Domain and Apical Stem.

A subsequent study by Launer-Felty *et al.* (62) also used SHAPE and DMS structure probing to demonstrate the same pseudoknot exists within the intact VA RNA_I. Here, mutagenesis of the pseudoknot-forming sequences revealed that formation of this tertiary structure is dependent upon the stability of the base pairing (*i.e.* with G-C but not A-U pairs) but not their specific orientation (*i.e.* G-C versus C-G). Although the impact on PKR inhibition was not directly tested, analyses of PKR-VA RNA_I binding affinity again suggested that the Central Domain tertiary structure does not play a critical role.

Specifically, perturbation of the Central Domain tertiary structure and PKR binding affinity do not appear to be directly correlated: individual mutations of each pseudoknot sequence had substantially different effects on PKR binding affinity (6- and 2.5-fold reduced upon mutation of Loop 8 and Loop 10, respectively) and a point mutant (at A103) was identified that impacted PKR affinity (4-fold reduced) while retaining the native tertiary fold. The most deleterious effects on PKR binding arose where mutations included alteration of nucleotide A103, one of three nucleotides identified by Wilson *et al.* as potential sites of Mg²⁺ binding within the Central Domain (61). The PKR-VA

RNA_I interaction is dependent upon Mg²⁺ (63), suggesting that the effects on PKR binding reflect alterations in the interaction of the divalent ion with the Central Domain and not simply disruption of the tertiary structure *per se*. Precisely how Mg²⁺ within the Central Domain tunes PKR interaction (and perhaps its inhibition), and whether the same effects are at play in the presence and absence of the Terminal Stem will require further investigation.

Both of these recent studies called into question the functional necessity for the absolute conservation of the two complementary tetranucleotide sequences which reside within the Central Domain. While previous work suggested these nucleotides and their specific orientation were important for translational rescue by VA RNA_I (53), these new studies reveal a more limited impact upon PKR binding and inhibition when these sequences are altered in the intact and Terminal Stem truncated RNAs, respectively (61,62). Although the functional basis for sequence conservation is less clear from these new works, the VA RNA_I molecular model produced by Launer-Felty *et al.* (62) suggests a clear role for the structure they form. In the model, this region of the Central Domain is coaxially stacked with the Apical Stem to add a short extension adjacent to a bulged region formed by the rest of the Central Domain and its junction with the Terminal Stem (**Fig. 3**). This model thus suggests an appealing mechanism by which the PKR binding site is precisely tuned to maximize binding without inducing PKR activation. Given that other sequences can fulfil this function *in vitro*, why are these tetranucleotides sequence absolutely conserved? As speculated by the authors of both recent studies (61,62), perhaps the conserved tetranucleotide sequences are important for other activities of VA RNA_I,

raising the intriguing possibility that the observed translational rescue by VA RNA_I may not be entirely due to PKR inhibition.

The finding that the Central Domain tertiary structure is not required for PKR inhibition and that major deletions are either fully or partially tolerated also appears inconsistent with previous reports of instances in which single mutations within the Central Domain decrease VA RNA_I inhibition of PKR (98). However, several of these point mutations, which most render VA RNA_I unable to inhibit PKR, cluster around the three-helix junction or are adjacent to putative sites of Mg²⁺ interaction (61). Thus the effects of these point mutations might be attributed to gross deformation of the Central Domain secondary structure and/ or destabilization of the three-helix junction (56,96). Therefore, while it is possible intact VA RNA_I may be more sensitive to destabilizing mutations within the Central Domain than the TSΔ21 RNA construct used by Wilson *et al.* (61), the effects of these single point mutations are not entirely inconsistent with the more general finding that the three-helix junction and the manner in which it extends the Apical Stem PKR binding site is the most critical structural feature for VA RNA_I inhibition of PKR (61,62). This more simple requirement for VA RNA_I inhibition of PKR allows a ready rationalization of the ability of VA RNAs from different AdV serotypes and other non-coding RNAs with diverse sequences and structures to inhibit PKR *in vivo*. For example, the Epstein-Barr virus, a dsRNA virus capable of both lytic and latent infection, also possesses two non-coding RNAs, EBER-I and EBER-II, which bear a broad structural similarity to the VA RNAs (99). EBER-1 binds to PKR with similar affinity to VA RNA_I, and is capable of inhibiting translation to the same degree as VA RNA_I (100).

Further, EBERs can complement a virus lacking both VA RNAs. However, VA RNAs are unable to fully complement an EBER-deleted Epstein-Barr virus, demonstrating that despite their structural similarities, the functions of these two viral non-coding RNAs are not entirely overlapping (101).

VA RNA₁ regulation of 2'-5' oligoadenylate synthetase-1 (OAS1)

Given the well-established function of VA RNA₁ as an inhibitor of PKR, it is at first glance paradoxical that this RNA can activate another arm of the innate immune system, the OAS/ RNase L pathway (14). Like PKR, the OAS family of enzymes are dsRNA-sensors. Upon detection of dsRNA, the catalytically active OAS forms (OAS1, OAS2, and OAS3) synthesize 2'-5'-linked oligoadenylate second messengers, which in turn, activate their only known target, the latent cellular endoribonuclease RNase L (102,103). Active RNase L degrades single-stranded RNA, primarily after UU and UA dinucleotides (104) present within loops or bulges of otherwise highly structured RNAs (105), thereby halting protein translation (**Fig. 4**). RNase L activity is dose-dependent (106), and its biological targets may therefore depend on 2'-5'-oligoadenylate levels; however, RNase L degrades cellular, viral, and host ribosomal rRNA (107-110). Just as viruses have developed an array of strategies for subverting the effects of PKR, they have also developed ways to circumvent the effects of OAS activation including dsRNA sequestration, direct inhibition of OAS or RNase L, or synthesis of 2'-5' phosphodiesterases (reviewed in (111)).

OAS1 has been the primary focus of most investigations concerning the identification of RNA features required for activation. While such RNA requirements are still not fully understood, the structure of OAS1 bound to an 18 bp dsRNA duplex and a single dATP revealed much about how simple dsRNAs control OAS1 activation. Upon binding to activating dsRNA the relative orientations of the OAS1 N- and C-lobes is altered in a manner which narrows the ATP-binding cleft of OAS1, and facilitates a structural rearrangement that repositions a catalytic residue to complete the enzyme active site (112). While OAS1 requires a minimum of 18 bp of duplex RNA to become active (113), not all dsRNA activates OAS1 to the same degree, indicating that there are additional RNA molecular features which contribute to activation of this enzyme. To date, most work has focused on identification of activation consensus sequences and two distinct types have been identified: WWN_9WG (113) and $AWAWN_nCC\dots UUN_nACCC$ (114). However, the dissimilarity of these sequences, coupled with the observation that not all dsRNAs which harbor them are activators, indicates that there are additional, currently unknown sequence and structural features that are important for driving activation of OAS1.

With the added complexity of RNA secondary and tertiary structures, the regions of VA RNA_I required for OAS1 activation or inhibition remains unclear. Furthermore, multiple regions of VA RNA may be bound by OAS1, either simultaneously or exclusively, with some initiating the necessary structural rearrangements to activate OAS1, and others which fail to do so and are thus unproductive. Nonetheless, initial studies of OAS1 regulation by VA RNA_I have already shown that this RNA is an excellent model system

with which to tease apart the details of RNA-mediated control of OAS1 activity. First, the OAS1-activating potential of VA RNA_I may be increased by making the Terminal Stem or Apical Stem perfectly base-paired, whereas disrupting the structure of any of the three domains reduces the effect of VA RNA_I against OAS1, even in the absence of altered binding affinity (14). However, the effect of base-pairing the Terminal Stem is greater than that of the Apical Stem (14), despite the Apical Stem being a more potent activator than the full length RNA (115). This raises the possibility that another domain, most likely the Central Domain has an inhibitory effect in the context of full-length VA RNA_I. In support of this idea, a truncated form of VA RNA_I lacking the entire Terminal Stem was recently shown to act as a pseudoinhibitor of OAS1 (115).

Second, more recent analyses of OAS1 regulation by VA RNA_I lead to the identification of the 3'-single-stranded pyrimidine (3'-ssPy, or "three prime spy") motif required for optimal activation OAS1 by both simple dsRNA and more structurally complex ncRNAs, (116). How the 3'-ssPy motif functions is not fully understood, but a single highly conserved OAS1 residue, Gly57, found in a short loop adjacent to the RNA terminus in the OAS1-dsRNA crystal structure was identified as essential for mediating the effect of the 3'-ssPy motif. Additionally, kinetic analyses with both an 18 bp dsRNA containing an OAS1 activation consensus and VA RNA_I showed that while the 3'-ssPy motif consistently increases overall OAS1 catalytic efficiency, the effects of the 3'-ssPy motif on the apparent RNA affinity are context dependent (116). Further, the idea that an activating RNA motif might enhance OAS1 activating potential by decreasing apparent RNA affinity is appealing; the comparatively weak affinity OAS1-dsRNA affinity may

be a necessary feature of the protein-RNA interaction to drive the non-processive synthetic activity of OAS1 (117-119).

Third, VA RNA_I contains two WWN₉WG activation consensus sequences (**Fig. 1B**), but their contributions to OAS1 activation have not been tested. However, in light of the insights on dsRNA-mediated activation of OAS1 gleaned from the OAS1-dsRNA crystal structure and the fact that the two consensus sequences in VA RNA_I fall outside of regular helical regions, any contribution to VA RNA_I activation of OAS1 would be remarkable and require a reassessment of the structural features that control OAS1.

The *in vivo* physiological consequences of VA RNA_I activation of OAS1 are currently underexplored; to date, all experiments that have examined VA RNA_I activity against OAS1 have been performed *in vitro*. The uncertainty surrounding VA RNA_I activation of OAS1 is compounded by the fact that VA RNA_I is only able to activate OAS1 with ~10% of the potency of perfectly double-stranded RNA of similar size (14). Whether the comparatively low OAS1-activating potential of VA RNA_I is overcome by the extraordinarily high levels to which the transcript accumulates is unknown. Further, the question of whether or not full-length VA RNA_I activation of OAS1 may be beneficial to AdV at certain stages of infection, and its activation purposeful rather than inadvertent is unknown. Perhaps appropriately timed OAS1 activation by AdV is important for establishing different types of infection. For example, could VA RNA_I activation of OAS1 promote degradation of specific viral mRNAs, and thus promote the switch between early and late gene expression? Future studies directed at examining the extent

and impacts of OAS1 activation in the context of Adenovirus infection will be required to address these questions.

In addition to the inherent ability of VA RNA_I to activate OAS1, the potency of OAS1 and therefore RNase L activity is influenced by the levels of OAS1 present in the cell. OAS1 levels are not equal between cell types due to variation in OAS1 mRNA levels (120). Therefore, if AdV tissue tropisms do not overlap with those in which OAS1 is present at a level sufficient to activate RNase L in the presence of a weak activator like VA RNA_I, the inherent activating potential of the RNA may have little bearing on the outcome of infection. To more completely understand the impact of VA RNA_I on the OAS1/RNase L pathway, future studies using cell culture to model infection are critical. Even so, demonstrations that VA RNA_I can induce RNase L-mediated degradation of cellular RNA *in vivo* would be important for understanding the effects of VA RNA_I activation of OAS1 on the cell, even absent a role in controlling infection. Understanding the consequences of VA RNA_I activation of OAS1 is an important consideration for the design of AdV vectors engineered to infect cells with higher levels of OAS1, such as liver tissue or myeloid cells (120).

Pro-viral roles of Apical Stem–Central Domain fragment from Dicer-processing of VA RNA_I

While deserved attention has been paid to the fate of the Terminal Stem-derived mivaRNAs), it is also noteworthy that the remaining Apical Stem and Central Domain-containing fragment (AS-CD RNA) arising from Dicer processing of VA RNA_I has also

been hypothesized to retain pro-viral potential. A similar RNA fragment lacking the entire Terminal Stem (TS Δ 21 RNA) retains wild-type inhibitory activity against PKR (58) and is also a pseudoinhibitor of OAS1 which binds with slightly increased affinity yet fails to activate the enzyme (115). While these studies hint that pro-viral roles exist for AS-CD RNA, TS Δ 21 RNA and the authentic Dicer-derived fragment are not identical: AS-CD RNA possesses additional 5'- and 3'-end single-stranded sequences (**Fig. 5A**). In light of the potential for short single-stranded RNA motifs to potentially regulate both PKR and OAS1 (116,121), these differences warrant more careful examination of AS-CD RNA activity. We therefore tested the activity of AS-CD RNA against PKR and OAS1 using established PKR activation and inhibition kinase assays and OAS1 chromogenic assays, respectively (61,116). We found that AS-CD RNA retains inhibitory activity against PKR, though is somewhat less potent TS Δ 21 RNA (**Fig 5B**). Surprisingly, however, we found that the authentic Dicer-derived AS-CD RNA activates OAS1 to the same degree as full-length VA RNA_I (**Fig 5C**) rather than inhibiting OAS1 as reported for TS Δ 21 RNA (115). This result casts doubt on the hypothesis that Dicer-processed AS-CD RNA serves as a pseudoinhibitor of OAS1 during AdV infection (115). The difference in activity observed between these two constructs can serve, however as a tool to begin to elucidate the structures of VA RNA_I responsible for OAS1 activation.

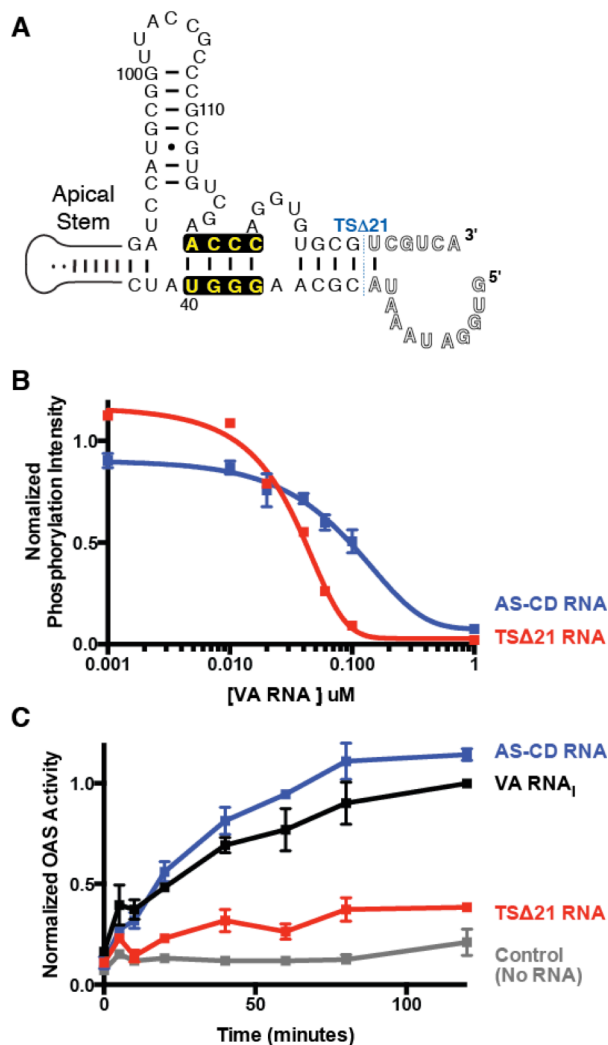


Fig. 5. Activity of the Dicer-derived Apical Stem-Central Domain (AS-CD) fragment against PKR and OAS1. *A*, Sequence and secondary structure of an authentic Dicer-derived AS-CD fragment. The site of truncation in TSA21 RNA (blue dotted line) and the pair of universally conserved tetranucleotide sequences (yellowfont with black background) are also highlighted. *B*, PKR kinase inhibition assays show that the authentic Dicer-derived AS-CD fragment (blue) inhibits PKR, though to a lesser degree than TSA21 RNA (red), corresponding to wild-type VA RNA₁ activity. PKR autophosphorylation were performed in the presence of γ -³²P ATP and poly(I):poly(C) activator RNA as previously described (61). *C*, Chromogenic assays of OAS1 activation show that the authentic Dicer-derived AS-CD fragment (blue) activates OAS1 to the same degree as wild-type VA RNA₁ (black), in contrast to TSA21 RNA (red) which acts as a pseudoinhibitor. The chromogenic assay measures levels of PP_i produced as a consequence of 2'-5' oligoadenylate synthesis, and data are normalized to full length VA RNA₁ activity as previously described (116).

VA RNA_I induces type-I interferon late in infection

In addition to the effects on PKR and OAS1, AdV infection induces expression of type I interferon in two distinct phases: the first between 12 and 24 hours, and later at between 48 and 60 hours post infection. VA RNA_I is involved only in the latter phase during the late stages of infection (15,122). While the late-stage induction is reported in some cases to occur in a RIG-I-dependent manner (15), others show that the identity of the pattern recognition receptor (PRR) on which induction depends is cell-type specific (122).

RIG-I is a cytoplasmic dsRNA-sensing innate immune protein activated by dsRNA with a triphosphate (5'-ppp) group (123,124). As the VA RNA_I Terminal Stem is largely double-stranded and possesses a 5'-ppp, this domain of VA RNA_I is potentially capable of activating RIG-I. However, not all VA RNA_I transcripts generated during infection contain a 5'-ppp: 50% are reported to have a 5'-ppp, 40% possess a di-phosphate and 10% a monophosphate (30). The determinants of this ratio are unclear, as are the functional consequences of disrupting the distributions. However, it is likely that VA RNA_I with 5'-ppp is the only form capable of activating RIG-I, suggesting that RIG-I activation may be governed by the proportion of VA RNA_I with 5'-ppp. Additional support for 5'-end phosphorylation state as a driver of RNA activity can be found by examining the 5'-ends of miRNAs incorporated into the RISC complex: because functional miRNAs produced by Dicer must contain 5'-monophosphates at their 5'-ends, one might hypothesize that only 10% of VA RNAs can serve as functional miRNAs (125). Indeed, the majority of 5'-mivRNAI(A) incorporated into the RISC complex contain 5'-monophosphates rather than 5'-ppp, while the large majority of RISC-

associated, non-functional 5'-mivaRNAs derived from VA RNA_I(G) have 5'-ppp (32). Additionally, RIG-I activation may be further controlled by the ratio of VA RNA_I with more than two 3'-end single-stranded nucleotides, as recent works on RIG-I activation by miRNAs indicate that 3'-single-stranded overhangs of between 2 and 3 nt render dsRNAs unable to efficiently activate RIG-I (126). As a large majority of VA RNA_I transcripts possess a 3'-overhang of at least 2 nt (38), most VA RNA_I transcripts are likely unable to efficiently activate RIG-I. In spite of the small fraction of total VA RNA_I which possess the RIG-I-activating 5'-ppp, the high copy number to which VA RNA_I accumulates late in infection may nonetheless explain the observed activation of RIG-I late in infection.

One alternative hypothesis is that OAS1/ RNase L activation by VA RNA_I late in infection generates RNA fragments which amplify the host-immune response through activation of RIG-I, as has been demonstrated for the degradation products of self mRNAs (127). As is the case with VA RNA_I activation of OAS, it is unclear whether RIG-I activation has an impact on the outcome of virus infection, as mutations which interfere with PKR activity are the sole requirement for restoring infectivity of AdV lacking VA RNA_I. However, like OAS1 activation, the consequences of RIG-I activation may be tissue-specific, and an important consideration for AdV-based technologies (120).

Considerations for Ad vectors

Understanding the multiple ways in which VA RNA_I affects cellular processes has been critical for the efficient development of AdV-based technologies for gene therapy, oncotherapy, and vaccine development (8,128,129). While the efficiency with which VA

RNA_I inhibits PKR has made this RNA a valuable tool for ensuring effective translation of transfected proteins (Promega), VA RNAs can be detrimental to experimental or therapeutic introduction of small hairpin RNA (shRNA) for gene silencing because of the way in which VA RNA interacts with Dicer and associates with the RISC complex (130). While development of AdV vectors lacking VA RNAs was initially limited by the low titers associated with the absence of these RNAs, more recent work has utilized cell lines which express VA RNA_I (129) or viruses in which VA RNA_I is flanked by flippase recognition target (FRT) sequences in a recombinase (Flp) expressing cell line to efficiently generate AdV vectors lacking these sequences (8). In addition to avoiding VA RNA interference with miRNA biogenesis and inadvertent activation of innate immunity, VA RNA deleted vectors also have a naturally restricted range, which includes specific types of cancer cells in which PKR function is diminished due to upregulation of the rat sarcoma oncogene (RAS), making VA RNA_I-deleted AdV vectors an attractive option for oncolytic virotherapy of specific cancer cell types (131).

CONCLUSIONS

VA RNA_I is a remarkable, multifaceted and essential pro-viral ncRNA transcript capable of modulating many host cell defenses against viruses and interfering with cellular processes such nuclear RNA export, protein synthesis and miRNA biogenesis. However, the specific impact of many of these potential activities of VA RNA_I on the outcome of AdV infection remains underexplored. Our limited understanding in this area is further complicated by the fact that there are several different VA RNA_I subspecies resulting from 5'- and 3'-end heterogeneity present during infection that may have disparate

impacts on each of these pathways. Additionally, the seemingly opposing activity of VA RNA_I in activating RIG-I and OAS1 may be tissue specific. Therefore, these activities may be of no consequence to AdV or a currently poorly defined mode by which the virus fine tunes its own replication and spread. While experiments thus far have demonstrated that PKR inhibition is the only function of VA RNA_I sufficient to ensure optimal virus replication (11), *in vivo* experiments that systematically disrupt interactions with each individual pathway will be central in establishing the relative importance of each role of VA RNA_I is capable of performing. Even in the absence of concrete functional data, VA RNA_I can serve as an excellent model RNA for understanding how highly structured non-coding RNAs regulate innate cellular immune proteins.

ACKNOWLEDGEMENTS

We gratefully acknowledge Samantha Schwartz for assistance with the PKR kinase inhibition assays reported in this work, and Drs. James L. Cole and Katherine Launer-Felty for providing the molecular images used in the preparation of Figure 3B. We also thank Dr. Anita H. Corbett for reviewing and providing comments on the manuscript.

REFERENCES

1. Knipe, D.M. and Howley, P.M. (2013) *Fields virology*. 6th ed. Wolters Kluwer/Lippincott Williams & Wilkins Health, Philadelphia, PA.
2. Edwards, K.M., Thompson, J., Paolini, J. and Wright, P.F. (1985) Adenovirus infections in young children. *Pediatrics*, **76**, 420-424.

3. Bowles, N.E., Ni, J., Kearney, D.L., Pauschinger, M., Schultheiss, H.P., McCarthy, R., Hare, J., Bricker, J.T., Bowles, K.R. and Towbin, J.A. (2003) Detection of viruses in myocardial tissues by polymerase chain reaction. evidence of adenovirus as a common cause of myocarditis in children and adults. *Journal of the American College of Cardiology*, **42**, 466-472.
4. Fox, J.P., Hall, C.E. and Cooney, M.K. (1977) The Seattle Virus Watch. VII. Observations of adenovirus infections. *American journal of epidemiology*, **105**, 362-386.
5. Neumann, R., Genersch, E. and Eggers, H.J. (1987) Detection of adenovirus nucleic acid sequences in human tonsils in the absence of infectious virus. *Virus research*, **7**, 93-97.
6. Garnett, C.T., Talekar, G., Mahr, J.A., Huang, W., Zhang, Y., Ornelles, D.A. and Gooding, L.R. (2009) Latent species C adenoviruses in human tonsil tissues. *Journal of virology*, **83**, 2417-2428.
7. Choi, J.W., Lee, J.S., Kim, S.W. and Yun, C.O. (2012) Evolution of oncolytic adenovirus for cancer treatment. *Advanced drug delivery reviews*, **64**, 720-729.
8. Maekawa, A., Pei, Z., Suzuki, M., Fukuda, H., Ono, Y., Kondo, S., Saito, I. and Kanegae, Y. (2013) Efficient production of adenovirus vector lacking genes of virus-associated RNAs that disturb cellular RNAi machinery. *Scientific reports*, **3**, 1136.
9. Ma, Y. and Mathews, M.B. (1996) Structure, function, and evolution of adenovirus-associated RNA: a phylogenetic approach. *Journal of virology*, **70**, 5083-5099.

10. Mathews, M.B. and Shenk, T. (1991) Adenovirus virus-associated RNA and translation control. *Journal of virology*, **65**, 5657-5662.
11. Thimmappaya, B., Weinberger, C., Schneider, R.J. and Shenk, T. (1982) Adenovirus VAI RNA is required for efficient translation of viral mRNAs at late times after infection. *Cell*, **31**, 543-551.
12. Bhat, R.A. and Thimmappaya, B. (1984) Adenovirus mutants with DNA sequence perturbations in the intragenic promoter of VAI RNA gene allow the enhanced transcription of VAII RNA gene in HeLa cells. *Nucleic acids research*, **12**, 7377-7388.
13. Kitajewski, J., Schneider, R.J., Safer, B., Munemitsu, S.M., Samuel, C.E., Thimmappaya, B. and Shenk, T. (1986) Adenovirus VAI RNA antagonizes the antiviral action of interferon by preventing activation of the interferon-induced eIF-2 alpha kinase. *Cell*, **45**, 195-200.
14. Desai, S.Y., Patel, R.C., Sen, G.C., Malhotra, P., Ghadge, G.D. and Thimmappaya, B. (1995) Activation of interferon-inducible 2'-5' oligoadenylate synthetase by adenoviral VAI RNA. *The Journal of biological chemistry*, **270**, 3454-3461.
15. Minamitani, T., Iwakiri, D. and Takada, K. (2011) Adenovirus virus-associated RNAs induce type I interferon expression through a RIG-I-mediated pathway. *Journal of virology*, **85**, 4035-4040.
16. Xu, N., Segerman, B., Zhou, X. and Akusjarvi, G. (2007) Adenovirus virus-associated RNAII-derived small RNAs are efficiently incorporated into the rna-induced silencing complex and associate with polyribosomes. *Journal of virology*, **81**, 10540-10549.

17. Andersson, M.G., Haasnoot, P.C., Xu, N., Berenjian, S., Berkhout, B. and Akusjarvi, G. (2005) Suppression of RNA interference by adenovirus virus-associated RNA. *Journal of virology*, **79**, 9556-9565.
18. Kondo, S., Yoshida, K., Suzuki, M., Saito, I. and Kanegae, Y. (2014) Adenovirus-encoding virus-associated RNAs suppress HDGF gene expression to support efficient viral replication. *PloS one*, **9**, e108627.
19. Fei, Z., Liu, Y., Yan, Z., Fan, D., Alexander, A. and Yang, J.H. (2011) Targeting viral dsRNA for antiviral prophylaxis. *FASEB journal : official publication of the Federation of American Societies for Experimental Biology*, **25**, 1767-1774.
20. Melchjorsen, J. (2013) Learning from the messengers: innate sensing of viruses and cytokine regulation of immunity - clues for treatments and vaccines. *Viruses*, **5**, 470-527.
21. Rider, T.H., Zook, C.E., Boettcher, T.L., Wick, S.T., Pancoast, J.S. and Zusman, B.D. (2011) Broad-spectrum antiviral therapeutics. *PloS one*, **6**, e22572.
22. Cirino, N.M., Li, G., Xiao, W., Torrence, P.F. and Silverman, R.H. (1997) Targeting RNA decay with 2',5' oligoadenylate-antisense in respiratory syncytial virus-infected cells. *Proceedings of the National Academy of Sciences of the United States of America*, **94**, 1937-1942.
23. Thakur, C.S., Jha, B.K., Dong, B., Das Gupta, J., Silverman, K.M., Mao, H., Sawai, H., Nakamura, A.O., Banerjee, A.K., Gudkov, A. *et al.* (2007) Small-molecule activators of RNase L with broad-spectrum antiviral activity. *Proceedings of the National Academy of Sciences of the United States of America*, **104**, 9585-9590.

24. Reich, P.R., Forget, B.G. and Weissman, S.M. (1966) RNA of low molecular weight in KB cells infected with adenovirus type 2. *Journal of molecular biology*, **17**, 428-439.
25. Soderlund, H., Pettersson, U., Vennstrom, B., Philipson, L. and Mathews, M.B. (1976) A new species of virus-coded low molecular weight RNA from cells infected with adenovirus type 2. *Cell*, **7**, 585-593.
26. Weinmann, R., Raskas, H.J. and Roeder, R.G. (1974) Role of DNA-dependent RNA polymerases II and III in transcription of the adenovirus genome late in productive infection. *Proceedings of the National Academy of Sciences of the United States of America*, **71**, 3426-3439.
27. Rohan, R.M. and Ketner, G. (1987) A comprehensive collection of point mutations in the internal promoter of the adenoviral VAI gene. *The Journal of biological chemistry*, **262**, 8500-8507.
28. Fowlkes, D.M. and Shenk, T. (1980) Transcriptional control regions of the adenovirus VAI RNA gene. *Cell*, **22**, 405-413.
29. Snouwaert, J., Bunick, D., Hutchison, C. and Fowlkes, D.M. (1987) Large numbers of random point and cluster mutations within the adenovirus VA I gene allow characterization of sequences required for efficient transcription. *Nucleic acids research*, **15**, 8293-8303.
30. Vennstrom, B., Pettersson, U. and Philipson, L. (1978) Two initiation sites for adenovirus 5.5S RNA. *Nucleic acids research*, **5**, 195-204.

31. Celma, M.L., Pan, J. and Weissman, S.M. (1977) Studies of low molecular weight RNA from cells infected with adenovirus 2. II. Heterogeneity at the 5' end of VA-RNA I. *The Journal of biological chemistry*, **252**, 9043-9046.
32. Xu, N., Gkountela, S., Saeed, K. and Akusjarvi, G. (2009) The 5'-end heterogeneity of adenovirus virus-associated RNAI contributes to the asymmetric guide strand incorporation into the RNA-induced silencing complex. *Nucleic acids research*, **37**, 6950-6959.
33. Weil, P.A., Segall, J., Harris, B., Ng, S.Y. and Roeder, R.G. (1979) Faithful transcription of eukaryotic genes by RNA polymerase III in systems reconstituted with purified DNA templates. *The Journal of biological chemistry*, **254**, 6163-6173.
34. Vennstrom, B., Pettersson, U. and Philipson, L. (1978) Initiation of transcription in nuclei isolated from adenovirus infected cells. *Nucleic acids research*, **5**, 205-219.
35. Kamel, W., Segerman, B., Punga, T. and Akusjarvi, G. (2014) Small RNA sequence analysis of adenovirus VA RNA-derived miRNAs reveals an unexpected serotype-specific difference in structure and abundance. *PloS one*, **9**, e105746.
36. Gunnery, S., Ma, Y. and Mathews, M.B. (1999) Termination sequence requirements vary among genes transcribed by RNA polymerase III. *Journal of molecular biology*, **286**, 745-757.
37. Wang, Z., Bai, L., Hsieh, Y.J. and Roeder, R.G. (2000) Nuclear factor 1 (NF1) affects accurate termination and multiple-round transcription by human RNA polymerase III. *The EMBO journal*, **19**, 6823-6832.

38. Celma, M.L., Pan, J. and Weissman, S.M. (1977) Studies of low molecular weight RNA from cells infected with adenovirus 2. I. The sequences at the 3' end of VA-RNA I. *The Journal of biological chemistry*, **252**, 9032-9042.
39. Akusjarvi, G., Mathews, M.B., Andersson, P., Vennstrom, B. and Pettersson, U. (1980) Structure of genes for virus-associated RNAI and RNAII of adenovirus type 2. *Proceedings of the National Academy of Sciences of the United States of America*, **77**, 2424-2428.
40. Weinmann, R., Brendler, T.G., Raskas, H.J. and Roeder, R.G. (1976) Low molecular weight viral RNAs transcribed by RNA polymerase III during adenovirus 2 infection. *Cell*, **7**, 557-566.
41. Orioli, A., Pascali, C., Quartararo, J., Diebel, K.W., Praz, V., Romascano, D., Percudani, R., van Dyk, L.F., Hernandez, N., Teichmann, M. *et al.* (2011) Widespread occurrence of non-canonical transcription termination by human RNA polymerase III. *Nucleic acids research*, **39**, 5499-5512.
42. Braglia, P., Percudani, R. and Dieci, G. (2005) Sequence context effects on oligo(dT) termination signal recognition by *Saccharomyces cerevisiae* RNA polymerase III. *The Journal of biological chemistry*, **280**, 19551-19562.
43. Hamada, M., Sakulich, A.L., Koduru, S.B. and Maraia, R.J. (2000) Transcription termination by RNA polymerase III in fission yeast. A genetic and biochemically tractable model system. *The Journal of biological chemistry*, **275**, 29076-29081.
44. Zuker, M. (2003) Mfold web server for nucleic acid folding and hybridization prediction. *Nucleic acids research*, **31**, 3406-3415.

45. Lerner, M.R., Boyle, J.A., Hardin, J.A. and Steitz, J.A. (1981) Two novel classes of small ribonucleoproteins detected by antibodies associated with lupus erythematosus. *Science*, **211**, 400-402.
46. Wolin, S.L. and Cedervall, T. (2002) The La protein. *Annual review of biochemistry*, **71**, 375-403.
47. Rinke, J. and Steitz, J.A. (1982) Precursor molecules of both human 5S ribosomal RNA and transfer RNAs are bound by a cellular protein reactive with anti-La lupus antibodies. *Cell*, **29**, 149-159.
48. Gaidamakov, S., Maximova, O.A., Chon, H., Blewett, N.H., Wang, H., Crawford, A.K., Day, A., Tulchin, N., Crouch, R.J., Morse, H.C., 3rd *et al.* (2014) Targeted deletion of the gene encoding the La autoantigen (Sjogren's syndrome antigen B) in B cells or the frontal brain causes extensive tissue loss. *Molecular and cellular biology*, **34**, 123-131.
49. Park, J.M., Kohn, M.J., Bruinsma, M.W., Vech, C., Intine, R.V., Fuhrmann, S., Grinberg, A., Mukherjee, I., Love, P.E., Ko, M.S. *et al.* (2006) The multifunctional RNA-binding protein La is required for mouse development and for the establishment of embryonic stem cells. *Molecular and cellular biology*, **26**, 1445-1451.
50. Fok, V., Friend, K. and Steitz, J.A. (2006) Epstein-Barr virus noncoding RNAs are confined to the nucleus, whereas their partner, the human La protein, undergoes nucleocytoplasmic shuttling. *The Journal of cell biology*, **173**, 319-325.

51. Coventry, V.K. and Conn, G.L. (2008) Analysis of adenovirus VA RNAI structure and stability using compensatory base pair modifications. *Nucleic acids research*, **36**, 1645-1653.
52. Ma, Y. and Mathews, M.B. (1993) Comparative analysis of the structure and function of adenovirus virus-associated RNAs. *Journal of virology*, **67**, 6605-6617.
53. Ma, Y. and Mathews, M.B. (1996) Secondary and tertiary structure in the central domain of adenovirus type 2 VA RNA I. *Rna*, **2**, 937-951.
54. Clarke, P.A., Pe'ery, T., Ma, Y. and Mathews, M.B. (1994) Structural features of adenovirus 2 virus-associated RNA required for binding to the protein kinase DAI. *Nucleic acids research*, **22**, 4364-4374.
55. Wahid, A.M., Coventry, V.K. and Conn, G.L. (2009) The PKR-binding domain of adenovirus VA RNAI exists as a mixture of two functionally non-equivalent structures. *Nucleic acids research*, **37**, 5830-5837.
56. Furtado, M.R., Subramanian, S., Bhat, R.A., Fowlkes, D.M., Safer, B. and Thimmappaya, B. (1989) Functional dissection of adenovirus VAI RNA. *Journal of virology*, **63**, 3423-3434.
57. Launer-Felty, K. and Cole, J.L. (2014) Domain interactions in adenovirus VAI RNA mediate high-affinity PKR binding. *Journal of molecular biology*, **426**, 1285-1295.
58. Wahid, A.M., Coventry, V.K. and Conn, G.L. (2008) Systematic deletion of the adenovirus-associated RNAI terminal stem reveals a surprisingly active RNA inhibitor of double-stranded RNA-activated protein kinase. *The Journal of biological chemistry*, **283**, 17485-17493.

59. Carnero, E., Sutherland, J.D. and Fortes, P. (2011) Adenovirus and miRNAs. *Biochimica et biophysica acta*, **1809**, 660-667.
60. Pe'ery, T., Mellits, K.H. and Mathews, M.B. (1993) Mutational analysis of the central domain of adenovirus virus-associated RNA mandates a revision of the proposed secondary structure. *Journal of virology*, **67**, 3534-3543.
61. Wilson, J.L., Vachon, V.K., Sunita, S., Schwartz, S.L. and Conn, G.L. (2014) Dissection of the adenoviral VA RNAI central domain structure reveals minimum requirements for RNA-mediated inhibition of PKR. *The Journal of biological chemistry*, **289**, 23233-23245.
62. Launer-Felty, K., Wong, C.J. and Cole, J.L. (2015) Structural analysis of adenovirus VAI RNA defines the mechanism of inhibition of PKR. *Biophysical journal*, **108**, 748-757.
63. Launer-Felty, K., Wong, C.J., Wahid, A.M., Conn, G.L. and Cole, J.L. (2010) Magnesium-dependent interaction of PKR with adenovirus VAI. *Journal of molecular biology*, **402**, 638-644.
64. Gwizdek, C., Ossareh-Nazari, B., Brownawell, A.M., Doglio, A., Bertrand, E., Macara, I.G. and Dargemont, C. (2003) Exportin-5 mediates nuclear export of minihelix-containing RNAs. *The Journal of biological chemistry*, **278**, 5505-5508.
65. Bohnsack, M.T., Czaplinski, K. and Gorlich, D. (2004) Exportin 5 is a RanGTP-dependent dsRNA-binding protein that mediates nuclear export of pre-miRNAs. *Rna*, **10**, 185-191.
66. Gwizdek, C., Bertrand, E., Dargemont, C., Lefebvre, J.C., Blanchard, J.M., Singer, R.H. and Doglio, A. (2001) Terminal minihelix, a novel RNA motif that directs

- polymerase III transcripts to the cell cytoplasm. Terminal minihelix and RNA export. *The Journal of biological chemistry*, **276**, 25910-25918.
67. Lu, S. and Cullen, B.R. (2004) Adenovirus VA1 noncoding RNA can inhibit small interfering RNA and MicroRNA biogenesis. *Journal of virology*, **78**, 12868-12876.
 68. Bennasser, Y., Chable-Bessia, C., Triboulet, R., Gibbings, D., Gwizdek, C., Dargemont, C., Kremer, E.J., Voinnet, O. and Benkirane, M. (2011) Competition for XPO5 binding between Dicer mRNA, pre-miRNA and viral RNA regulates human Dicer levels. *Nature structural & molecular biology*, **18**, 323-327.
 69. Lewis, B.P., Shih, I.H., Jones-Rhoades, M.W., Bartel, D.P. and Burge, C.B. (2003) Prediction of mammalian microRNA targets. *Cell*, **115**, 787-798.
 70. Kamel, W., Segerman, B., Oberg, D., Punga, T. and Akusjarvi, G. (2013) The adenovirus VA RNA-derived miRNAs are not essential for lytic virus growth in tissue culture cells. *Nucleic acids research*, **41**, 4802-4812.
 71. Aparicio, O., Razquin, N., Zaratiegui, M., Narvaiza, I. and Fortes, P. (2006) Adenovirus virus-associated RNA is processed to functional interfering RNAs involved in virus production. *Journal of virology*, **80**, 1376-1384.
 72. Sano, M., Kato, Y. and Taira, K. (2006) Sequence-specific interference by small RNAs derived from adenovirus VAI RNA. *FEBS letters*, **580**, 1553-1564.
 73. Bellutti, F., Kauer, M., Kneidinger, D., Lion, T. and Klein, R. (2014) Identification of RISC-associated adenoviral miRNAs, a subset of their direct targets, and global changes in the targetome upon lytic Ad5 infection. *Journal of virology*.

74. Harris, B. and Roeder, R.G. (1978) Structural relationships of low molecular weight viral RNAs synthesized by RNA polymerase III in nuclei from adenovirus 2-infected cells. *The Journal of biological chemistry*, **253**, 4120-4127.
75. Meister, G., Landthaler, M., Patkaniowska, A., Dorsett, Y., Teng, G. and Tuschl, T. (2004) Human Argonaute2 mediates RNA cleavage targeted by miRNAs and siRNAs. *Molecular cell*, **15**, 185-197.
76. Bhat, R.A., Domer, P.H. and Thimmappaya, B. (1985) Structural requirements of adenovirus VAI RNA for its translation enhancement function. *Molecular and cellular biology*, **5**, 187-196.
77. Aparicio, O., Carnero, E., Abad, X., Razquin, N., Guruceaga, E., Segura, V. and Fortes, P. (2010) Adenovirus VA RNA-derived miRNAs target cellular genes involved in cell growth, gene expression and DNA repair. *Nucleic acids research*, **38**, 750-763.
78. Tian, Q., Taupin, J., Elledge, S., Robertson, M. and Anderson, P. (1995) Fas-activated serine/threonine kinase (FAST) phosphorylates TIA-1 during Fas-mediated apoptosis. *The Journal of experimental medicine*, **182**, 865-874.
79. Lopez de Silanes, I., Galban, S., Martindale, J.L., Yang, X., Mazan-Mamczarz, K., Indig, F.E., Falco, G., Zhan, M. and Gorospe, M. (2005) Identification and functional outcome of mRNAs associated with RNA-binding protein TIA-1. *Molecular and cellular biology*, **25**, 9520-9531.
80. Kong, H.K., Yoon, S. and Park, J.H. (2012) The regulatory mechanism of the LY6K gene expression in human breast cancer cells. *The Journal of biological chemistry*, **287**, 38889-38900.

81. de Nooij-van Dalen, A.G., van Dongen, G.A., Smeets, S.J., Nieuwenhuis, E.J., Stigter-van Walsum, M., Snow, G.B. and Brakenhoff, R.H. (2003) Characterization of the human Ly-6 antigens, the newly annotated member Ly-6K included, as molecular markers for head-and-neck squamous cell carcinoma. *International journal of cancer. Journal international du cancer*, **103**, 768-774.
82. Furuse, Y., Ornelles, D.A. and Cullen, B.R. (2013) Persistently adenovirus-infected lymphoid cells express microRNAs derived from the viral VAI and especially VAI RNA. *Virology*, **447**, 140-145.
83. Samuel, C.E. (1991) Antiviral actions of interferon. Interferon-regulated cellular proteins and their surprisingly selective antiviral activities. *Virology*, **183**, 1-11.
84. Maran, A. and Mathews, M.B. (1988) Characterization of the double-stranded RNA implicated in the inhibition of protein synthesis in cells infected with a mutant adenovirus defective for VA RNA. *Virology*, **164**, 106-113.
85. Lee, J.Y., Marshall, J.A. and Bowden, D.S. (1994) Characterization of rubella virus replication complexes using antibodies to double-stranded RNA. *Virology*, **200**, 307-312.
86. Stollar, B.D. and Stollar, V. (1970) Immunofluorescent demonstration of double-stranded RNA in the cytoplasm of Sindbis virus-infected cells. *Virology*, **42**, 276-280.
87. Cole, J.L. (2007) Activation of PKR: an open and shut case? *Trends in biochemical sciences*, **32**, 57-62.
88. Hinnebusch, A.G. (1994) The eIF-2 alpha kinases: regulators of protein synthesis in starvation and stress. *Seminars in cell biology*, **5**, 417-426.

89. Krishnamoorthy, T., Pavitt, G.D., Zhang, F., Dever, T.E. and Hinnebusch, A.G. (2001) Tight binding of the phosphorylated alpha subunit of initiation factor 2 (eIF2alpha) to the regulatory subunits of guanine nucleotide exchange factor eIF2B is required for inhibition of translation initiation. *Molecular and cellular biology*, **21**, 5018-5030.
90. Rowlands, A.G., Panniers, R. and Henshaw, E.C. (1988) The catalytic mechanism of guanine nucleotide exchange factor action and competitive inhibition by phosphorylated eukaryotic initiation factor 2. *The Journal of biological chemistry*, **263**, 5526-5533.
91. O'Malley, R.P., Mariano, T.M., Siekierka, J. and Mathews, M.B. (1986) A mechanism for the control of protein synthesis by adenovirus VA RNAI. *Cell*, **44**, 391-400.
92. Davies, M.V., Furtado, M., Hershey, J.W., Thimmappaya, B. and Kaufman, R.J. (1989) Complementation of adenovirus virus-associated RNA I gene deletion by expression of a mutant eukaryotic translation initiation factor. *Proceedings of the National Academy of Sciences of the United States of America*, **86**, 9163-9167.
93. Wu, C., Bai, L., Li, Z., Samuel, C.E., Akusjarvi, G. and Svensson, C. (2015) Poor growth of human adenovirus-12 compared to adenovirus-2 correlates with a failure to impair PKR activation during the late phase of infection. *Virology*, **475**, 120-128.
94. Clarke, P.A. and Mathews, M.B. (1995) Interactions between the double-stranded RNA binding motif and RNA: definition of the binding site for the interferon-induced protein kinase DAI (PKR) on adenovirus VA RNA. *Rna*, **1**, 7-20.

95. Spangord, R.J., Vuyisich, M. and Beal, P.A. (2002) Identification of binding sites for both dsRBMs of PKR on kinase-activating and kinase-inhibiting RNA ligands. *Biochemistry*, **41**, 4511-4520.
96. Ghadge, G.D., Malhotra, P., Furtado, M.R., Dhar, R. and Thimmapaya, B. (1994) In vitro analysis of virus-associated RNA I (VAI RNA): inhibition of the double-stranded RNA-activated protein kinase PKR by VAI RNA mutants correlates with the in vivo phenotype and the structural integrity of the central domain. *Journal of virology*, **68**, 4137-4151.
97. Mellits, K.H., Kostura, M. and Mathews, M.B. (1990) Interaction of adenovirus VA RNAI with the protein kinase DAI: nonequivalence of binding and function. *Cell*, **61**, 843-852.
98. Rahman, A., Malhotra, P., Dhar, R., Kewalramani, T. and Thimmapaya, B. (1995) Effect of single-base substitutions in the central domain of virus-associated RNA I on its function. *Journal of virology*, **69**, 4299-4307.
99. Rosa, M.D., Gottlieb, E., Lerner, M.R. and Steitz, J.A. (1981) Striking similarities are exhibited by two small Epstein-Barr virus-encoded ribonucleic acids and the adenovirus-associated ribonucleic acids VAI and VAII. *Molecular and cellular biology*, **1**, 785-796.
100. Sharp, T.V., Schwemmle, M., Jeffrey, I., Laing, K., Mellor, H., Proud, C.G., Hilse, K. and Clemens, M.J. (1993) Comparative analysis of the regulation of the interferon-inducible protein kinase PKR by Epstein-Barr virus RNAs EBER-1 and EBER-2 and adenovirus VAI RNA. *Nucleic acids research*, **21**, 4483-4490.

101. Bhat, R.A. and Thimmappaya, B. (1983) Two small RNAs encoded by Epstein-Barr virus can functionally substitute for the virus-associated RNAs in the lytic growth of adenovirus 5. *Proceedings of the National Academy of Sciences of the United States of America*, **80**, 4789-4793.
102. Kerr, I.M., Brown, R.E. and Hovanessian, A.G. (1977) Nature of inhibitor of cell-free protein synthesis formed in response to interferon and double-stranded RNA. *Nature*, **268**, 540-542.
103. Hovanessian, A.G., Wood, J., Meurs, E. and Montagnier, L. (1979) Increased nuclease activity in cells treated with pppA2'p5'A2'p5' A. *Proceedings of the National Academy of Sciences of the United States of America*, **76**, 3261-3265.
104. Wreschner, D.H., McCauley, J.W., Skehel, J.J. and Kerr, I.M. (1981) Interferon action--sequence specificity of the ppp(A2'p)nA-dependent ribonuclease. *Nature*, **289**, 414-417.
105. Malathi, K., Saito, T., Crochet, N., Barton, D.J., Gale, M., Jr. and Silverman, R.H. (2010) RNase L releases a small RNA from HCV RNA that refolds into a potent PAMP. *Rna*, **16**, 2108-2119.
106. Nilsen, T.W. and Baglioni, C. (1979) Mechanism for discrimination between viral and host mRNA in interferon-treated cells. *Proceedings of the National Academy of Sciences of the United States of America*, **76**, 2600-2604.
107. Wreschner, D.H., James, T.C., Silverman, R.H. and Kerr, I.M. (1981) Ribosomal RNA cleavage, nuclease activation and 2-5A(ppp(A2'p)nA) in interferon-treated cells. *Nucleic acids research*, **9**, 1571-1581.

108. Li, X.L., Blackford, J.A. and Hassel, B.A. (1998) RNase L mediates the antiviral effect of interferon through a selective reduction in viral RNA during encephalomyocarditis virus infection. *Journal of virology*, **72**, 2752-2759.
109. Baglioni, C., De Benedetti, A. and Williams, G.J. (1984) Cleavage of nascent reovirus mRNA by localized activation of the 2'-5'-oligoadenylate-dependent endoribonuclease. *Journal of virology*, **52**, 865-871.
110. Andersen, J.B., Mazan-Mamczarz, K., Zhan, M., Gorospe, M. and Hassel, B.A. (2009) Ribosomal protein mRNAs are primary targets of regulation in RNase-L-induced senescence. *RNA biology*, **6**, 305-315.
111. Silverman, R.H. (2007) Viral encounters with 2',5'-oligoadenylate synthetase and RNase L during the interferon antiviral response. *Journal of virology*, **81**, 12720-12729.
112. Donovan, J., Dufner, M. and Korennykh, A. (2013) Structural basis for cytosolic double-stranded RNA surveillance by human oligoadenylate synthetase 1. *Proceedings of the National Academy of Sciences of the United States of America*, **110**, 1652-1657.
113. Kodym, R., Kodym, E. and Story, M.D. (2009) 2'-5'-Oligoadenylate synthetase is activated by a specific RNA sequence motif. *Biochemical and biophysical research communications*, **388**, 317-322.
114. Hartmann, R., Norby, P.L., Martensen, P.M., Jorgensen, P., James, M.C., Jacobsen, C., Moestrup, S.K., Clemens, M.J. and Justesen, J. (1998) Activation of 2'-5' oligoadenylate synthetase by single-stranded and double-stranded RNA aptamers. *The Journal of biological chemistry*, **273**, 3236-3246.

115. Meng, H., Deo, S., Xiong, S., Džananović, E., Donald, L.J., van Dijk, C.W. and McKenna, S.A. (2012) Regulation of the interferon-inducible 2'-5'-oligoadenylate synthetases by adenovirus VA(I) RNA. *Journal of molecular biology*, **422**, 635-649.
116. Vachon, V.K., Calderon, B.M. and Conn, G.L. (2015) A novel RNA molecular signature for activation of 2'-5' oligoadenylate synthetase-1. *Nucleic acids research*, **43**, 544-552.
117. Justesen, J., Ferbus, D. and Thang, M.N. (1980) Elongation mechanism and substrate specificity of 2',5'-oligoadenylate synthetase. *Proceedings of the National Academy of Sciences of the United States of America*, **77**, 4618-4622.
118. Sarkar, S.N., Pandey, M. and Sen, G.C. (2005) Assays for the interferon-induced enzyme 2',5' oligoadenylate synthetases. *Methods in molecular medicine*, **116**, 81-101.
119. Deo, S., Patel, T.R., Džananović, E., Booy, E.P., Zeid, K., McEleney, K., Harding, S.E. and McKenna, S.A. (2014) Activation of 2' 5'-oligoadenylate synthetase by stem loops at the 5'-end of the West Nile virus genome. *PLoS one*, **9**, e92545.
120. Zhao, L., Birdwell, L.D., Wu, A., Elliott, R., Rose, K.M., Phillips, J.M., Li, Y., Grinspan, J., Silverman, R.H. and Weiss, S.R. (2013) Cell-type-specific activation of the oligoadenylate synthetase-RNase L pathway by a murine coronavirus. *Journal of virology*, **87**, 8408-8418.
121. Nallagatla, S.R., Hwang, J., Toroney, R., Zheng, X., Cameron, C.E. and Bevilacqua, P.C. (2007) 5'-triphosphate-dependent activation of PKR by RNAs with short stem-loops. *Science*, **318**, 1455-1458.

122. Yamaguchi, T., Kawabata, K., Kouyama, E., Ishii, K.J., Katayama, K., Suzuki, T., Kurachi, S., Sakurai, F., Akira, S. and Mizuguchi, H. (2010) Induction of type I interferon by adenovirus-encoded small RNAs. *Proceedings of the National Academy of Sciences of the United States of America*, **107**, 17286-17291.
123. Yoneyama, M., Kikuchi, M., Natsukawa, T., Shinobu, N., Imaizumi, T., Miyagishi, M., Taira, K., Akira, S. and Fujita, T. (2004) The RNA helicase RIG-I has an essential function in double-stranded RNA-induced innate antiviral responses. *Nature immunology*, **5**, 730-737.
124. Hornung, V., Ellegast, J., Kim, S., Brzozka, K., Jung, A., Kato, H., Poeck, H., Akira, S., Conzelmann, K.K., Schlee, M. *et al.* (2006) 5'-Triphosphate RNA is the ligand for RIG-I. *Science*, **314**, 994-997.
125. Elbashir, S.M., Lendeckel, W. and Tuschl, T. (2001) RNA interference is mediated by 21- and 22-nucleotide RNAs. *Genes & development*, **15**, 188-200.
126. Marques, J.T., Devosse, T., Wang, D., Zamanian-Daryoush, M., Serbinowski, P., Hartmann, R., Fujita, T., Behlke, M.A. and Williams, B.R. (2006) A structural basis for discriminating between self and nonself double-stranded RNAs in mammalian cells. *Nature biotechnology*, **24**, 559-565.
127. Malathi, K., Dong, B., Gale, M., Jr. and Silverman, R.H. (2007) Small self-RNA generated by RNase L amplifies antiviral innate immunity. *Nature*, **448**, 816-819.
128. Machitani, M., Sakurai, F., Katayama, K., Tachibana, M., Suzuki, T., Matsui, H., Yamaguchi, T. and Mizuguchi, H. (2013) Improving adenovirus vector-mediated RNAi efficiency by lacking the expression of virus-associated RNAs. *Virus research*, **178**, 357-363.

129. Machitani, M., Katayama, K., Sakurai, F., Matsui, H., Yamaguchi, T., Suzuki, T., Miyoshi, H., Kawabata, K. and Mizuguchi, H. (2011) Development of an adenovirus vector lacking the expression of virus-associated RNAs. *Journal of controlled release : official journal of the Controlled Release Society*, **154**, 285-289.
130. Pei, Z., Shi, G., Kondo, S., Ito, M., Maekawa, A., Suzuki, M., Saito, I., Suzuki, T. and Kanegae, Y. (2013) Adenovirus vectors lacking virus-associated RNA expression enhance shRNA activity to suppress hepatitis C virus replication. *Scientific reports*, **3**, 3575.
131. Cascallo, M., Capella, G., Mazo, A. and Alemany, R. (2003) Ras-dependent oncolysis with an adenovirus VAI mutant. *Cancer research*, **63**, 5544-5550.

CHAPTER 3:

Plasmid template design and *in vitro* transcription of short RNAs within a ‘structure cassette’ for structure probing experiments

The following Chapter has been published:

Vachon, V.K. and Conn, G.L. (2012). Plasmid template design and *in vitro* transcription of short RNAs within a ‘structure cassette’ for structure probing experiments. *Methods. Mol. Biol.* 941:157-69.

I am responsible for the work presented in each of the figures within this chapter.

ABSTRACT

Chemical and enzymatic RNA structure probing methods are important tools for examining RNA secondary and tertiary structures and their interactions with proteins, small molecules, and ions. The recently developed ‘Selective- 2’-Hydroxyl Acylation Analyzed by *Primer Extension*’ (SHAPE) approach has proven especially useful for uncovering details of secondary structures, complex tertiary interactions, and RNA dynamics. Analysis of short RNAs using SHAPE or other probing methods that require reverse transcription to detect RNA modifications presents a technical hurdle in that intense bands corresponding to abortive transcription during primer extension and the full-length RT product may obscure information corresponding to the 3’ and 5’ ends of the molecule, respectively. This chapter describes the design and use of an RNA ‘structure cassette’ that addresses these issues. First, we describe methods by which any RNA of interest may be cloned into a new plasmid preloaded with sequences that encode a structure cassette surrounding the short internal target RNA. Next, we outline key considerations and analyses of the RNAs produced that should be performed prior to SHAPE or other structure probing experiments.

INTRODUCTION

The ability to thoroughly dissect RNA structures and how they govern interactions with other regulatory molecules is critical for understanding their varied biological roles and functions. Well-established approaches to RNA structure probing in solution include enzymatic (e.g., RNase V1, T1, and A) and chemical probing with reagents such as dimethyl sulfate (DMS), kethoxal, 1-cyclohexyl-3-(2-morpholinoethyl)-carbodiimide metho-*p*-toluene sulfonate (CMCT), Pb^{2+} , or hydroxyl radical. More recently, a new approach termed ‘Selective 2’-Hydroxyl Acylation Analyzed by Primers Extension’ (SHAPE), pioneered by Kevin Weeks’ laboratory (1), has added a new and powerful dimension to such analyses. Together these methods can interrogate RNA secondary and tertiary structures, solvent accessibility, and, in the case of SHAPE, flexibility of each individual nucleotide in an RNA molecule. The quantitative analysis of each nucleotide that is possible with SHAPE is especially useful for identifying the overall architecture of an RNA molecule, tertiary interactions, and changes in nucleotide flexibility upon protein or aptamer binding and is a valuable tool for exploring the nature of RNA folding (2-4). The purpose of this chapter is to provide a method by which short RNAs can be efficiently produced for SHAPE or any other structure probing method that exploits reverse transcriptase (RT) primer extension for analysis.

RNA for structure probing can be obtained in various ways. For SHAPE analysis of the entire the HIV-1 genome, the RNA was obtained by direct purification from virions (5). In many cases, however, the RNA must be produced *in vitro*. For structure probing of longer RNAs, primers may be designed to anneal to different regions along the RNA so

that primer extension products for the entire RNA can be visualized on a denaturing polyacrylamide sequencing gel or using capillary electrophoresis (6,7). In either case, a limitation for shorter RNAs arises because aborted RT DNA transcripts and full-length products obscure the results of primer extension at the 3' and 5' ends of the molecule, respectively. In order to obtain structural information for the entirety of a short RNA, a 'structure cassette' has been adopted (1,3,6,8) which introduces linker regions encoding short stable RNA hairpins to both the 5'- and 3'-end of the RNA of interest. The 3'-end extension additionally provides a conserved RT primer binding site (**Figure 1**), so only a single DNA RT primer needs to be synthesized and labeled for all samples. Finally, this approach also alleviates problems of 5'- and 3'-end heterogeneity. Although potentially still present, heterogeneity at the 3' end of the RNA is of no consequence to the data obtained via primer extension since the heterogeneity exists beyond the primer-annealing site. Similarly, heterogeneity at the RNA 5' end lies beyond the area of interest in the reverse transcription reaction analysis. The structure cassette's linker regions were designed with stable tetraloops intended to avoid interference with the folding and structure of the internal RNA of interest (8). Although initially intended for use in SHAPE probing experiments, its usefulness extends to any RNA probing experiment in which short RNAs are analyzed by RT primer extension.

Typically the structure cassette is incorporated into the DNA *in vitro* transcription template via the forward and reverse primers of a polymerase chain reaction (PCR). Although widely applicable, this approach has some drawbacks. For example, long

primers need to be synthesized for each new RNA to be studied and we have found that for some RNAs, PCR reactions require significant troubleshooting and optimization.

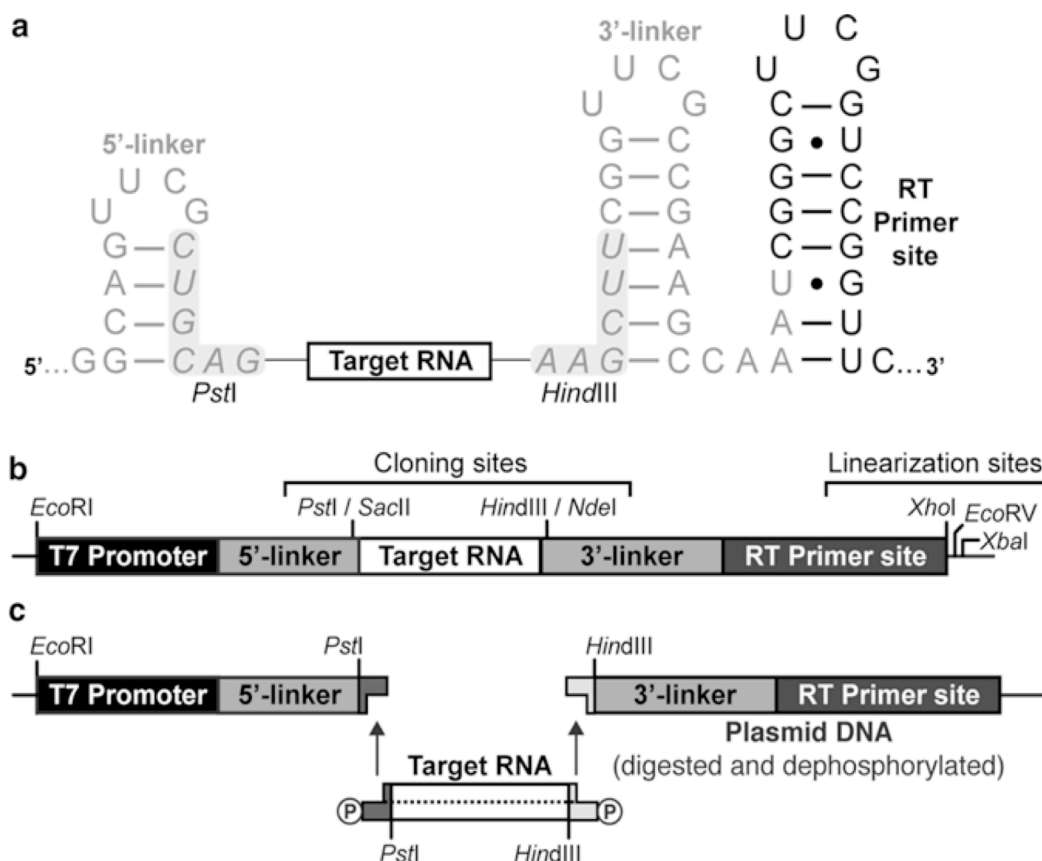


Figure 2 A plasmid system for in vitro transcription of RNAs within a “structure cassette.” (a)

Sequence and structure of the 5' and 3' hairpin linkers (grey) and 3'-end RT site (black). The structure cassette is shown with *PstI* and *HindIII* sequences (shaded regions); for the alternative cloning sites (*SacII* and *NdeI*) both strands of the hairpin stem are altered to maintain Watson-Crick base-pairing. (b) Organization of the structure cassette plasmid with all unique restriction enzyme sites for cloning and linearization for run-off transcription labeled. (c) Generation of new transcription templates by ligation of paired 5'-end phosphorylated DNA oligonucleotides synthesized with matching ‘sticky ends’ (shown here for *PstI* and *HindIII* double digested plasmid).

Generating templates for short or G-C-rich RNAs may be particularly challenging via PCR. PCR is also a potentially error-prone process which may lead to the production of fully altered or heterogeneous template DNA, and thus equivalent issues in the final transcribed RNA present in the structure probing reaction. Thus, an appealing alternative is a plasmid-based template system which can circumvent these issues. In such a system, the structure cassette elements may be pre-loaded onto the plasmid with suitable restriction enzyme sites built into the linker regions to allow simple cloning of only the RNA-encoding sequence. New constructs can be sequenced prior to use and protocols are well established that produce plasmid template of consistent yield and quality suitable for all structure probing applications.

We have created a structure cassette plasmid by modifying a general *in vitro* transcription system based on pUC19 that our laboratory previously developed (9). So that they may be utilized as internal restriction sites for the SHAPE plasmid, PstI and HindIII restriction sites were removed from the vector backbone by digesting with these enzymes, removal of 5' overhangs with T4 exonuclease and subsequent re-ligation of the plasmid.

Following these modifications, the first RNA of interest, the ~155 nt adenovirus VA RNAI, was amplified by PCR using primers encoding the structure cassette linkers and cloned into the plasmid at its EcoRI and XhoI restriction sites. This process was performed using each combination of forward and reverse primers containing one of the two unique internal restriction sites within the 5' and 3' linkers (PstI or SacII and HindIII or NcoI, respectively) to create a total of four structure cassette plasmids (Figure 1). These multiple options for cloning, in addition to three unique 3'-end run-off

transcription linearization sites (XhoI, EcoRV, and XbaI) derived from the original transcription plasmid (9), significantly reduce the likelihood that sequences within any new target RNA will make it incompatible with this plasmid based-structure cassette system. We have subsequently cloned and tested multiple VA RNA_I sequence variants and a second noncoding viral RNA, Epstein–Barr EBER1, into this system using the protocols described here.

First, this chapter describes approaches to cloning new RNA-encoding sequences into this structure cassette plasmid system using either PCR (Cloning Method 1) or direct ligation of pairs of complementary chemically synthesized DNA oligonucleotides (Cloning Method 2). Once sequence-verified clones are obtained, plasmid DNA can be purified and used in RNA *in vitro* transcription reactions using other established protocols (10). Both the chemical purity and conformational homogeneity of the RNA-structure cassette transcripts should be assessed before use in probing experiments, using denaturing and native polyacrylamide gel electrophoresis, respectively. The key steps involved are described in the final protocols of this chapter using both VA RNA_I and EBER1 RNA as examples.

MATERIALS

Generating a structure cassette plasmid containing a target RNA sequence.

1. Plasmid containing the structure cassette with the appropriate internal restriction sites (see **Figure 1** and **Note 1**).

2. Competent cells of an *Escherichia coli* strain suitable for plasmid propagation, such as DH5 α .
3. 50 mg/ml Ampicillin solution in water. This is a 1000 \times stock for 50 mg/ml final concentration.
4. LB-agar plates: 10 g peptone from casein, 5 g yeast extract, 10 g sodium chloride, and 12 g agar dissolved in water to a total volume of 1 L. Divide into media bottles and autoclave. LB-agar can be stored after autoclaving; melt solid LB-agar in a microwave on low power. After autoclaving or microwaving, allow to cool to <60 $^{\circ}$ C, add 50 mg/ml ampicillin to a suitable final concentration (e.g., 50 or 100 mg/ml), and pour into plates.
5. LB broth: 2.5 g peptone from casein, 1.25 g yeast extract, and 2.5 g sodium chloride dissolved in water to a total volume of 250 mL. Autoclave immediately after preparation.
6. Restriction enzymes and corresponding 10 \times buffer provided by the supplier. An appropriate combination of *Pst*I or *Hind*III and *Sac*II or *Nco*I is needed depending on the plasmid being used. For the example protocol here, we use *Pst*I and *Hind*III.
7. Calf intestinal alkaline phosphatase (CIAP).
8. Agarose gel DNA extraction kit.
9. DNA ligase with corresponding ligase buffer.

Cloning Method 1: PCR.

1. Forward and reverse DNA oligonucleotide PCR primers that contain a) regions complementary to the target RNA-encoding sequence to be amplified and b) the

desired restriction enzyme sites to be used for cloning into the structure cassette plasmid (see **Note 2**).

2. *Taq* and Vent DNA polymerases: Mix at 60:1 unit ratio (see **Note 3**).
3. 10 mM dNTPs (i.e., a mixture of 10 mM dATP, 10 mM dCTP, 10 mM dGTP, and 10 mM dTTP).
4. *Optional*: PCR cloning kit for use with *Taq* polymerase (see **Note 4**).
5. *Optional*: 20 mg/ml X-Gal for blue-white screening if using the cloning kit.

Cloning Method 2: Direct ligation of chemically synthesized DNA oligonucleotides.

1. Two chemically synthesized DNA oligos of sequence corresponding to the coding and complementary strands of the target RNA. The 5' and 3' ends of each DNA strand are designed to match the sticky ends produced by restriction enzyme digest of the desired target plasmid (see **Figure 1** and **Note 5**).
2. T4 polynucleotide kinase (T4 PNK).
3. DNA ligase buffer (see **Note 6**).

Analysis of transcribed RNA.

1. Purified product of *in vitro* transcription resuspended in TE buffer. For descriptions of RNA *in vitro* transcription and purification see **Chapters 4-6**. Generally, one 50-100 ml transcription reaction will yield sufficient RNA for approximately 50 structure probing reactions.
2. Tris-Boric acid-EDTA Buffer (TBE, 10×): 1 M Tris, 1 M boric acid and 10 mM EDTA.

3. Denaturing polyacrylamide gel solution: Acrylamide/ N,N'-methylene-bis-acrylamide (19:1 ratio) and 50% (w/v) urea dissolved in 1× TBE (see **Note 7**).
4. Native polyacrylamide gel solution: Acrylamide/ N,N'-methylene-bis-acrylamide (19:1 ratio) in 1× TBE.
5. 10% (w/v) Ammonium persulfate solution.
6. Tetramethylethylenediamine (TEMED).
7. Denaturing Gel Loading Dye (2×): 50% (w/v) urea, 0.25% (w/v) bromophenol blue, and 0.25% (w/v) xylene cyanol dissolved in 1× TE Buffer (10 mM Tris pH 7.5 and 1 mM EDTA pH 8).
8. Native Gel Loading Dye: 40% (w/v) sucrose, 0.17% (w/v) xylene cyanol, and 0.17% (w/v) bromophenol blue.

METHODS

Generating structure cassette plasmids with new target RNAs.

We have used two approaches to cloning target RNAs into the structure cassette plasmid: DNA amplification via a standard PCR and chemical synthesis of paired DNA oligonucleotides encoding the desired RNA target. PCR requires a DNA template corresponding to the target RNA and primers containing appropriate flanking restriction sites (e.g., *Pst*I and *Hind*III; see **Figure 1**). The resulting PCR product may either be digested and ligated directly into the structure cassette vector or cloned via an intermediate vector using a PCR cloning kit. The second method uses chemically synthesized DNA oligonucleotides that are 5'-phosphorylated with T4 PNK, annealed, and ligated directly into the structure cassette plasmid. This approach has proven to be

especially useful for the introduction of mutations that were difficult to obtain using site-directed mutagenesis and for creating templates for many RNA variants in parallel.

1. In a total volume of 20 ml, digest 1 mg of the structure cassette plasmid with *Pst*I and *Hind*III restriction enzymes (see **Note 8**).
2. Add 1 unit of CIAP and incubate for an additional hour at 37 °C.
3. Dilute to 100 ml final volume with water and then purify the digested plasmid DNA using an agarose gel DNA extraction kit following the manufacturer's instructions (see **Note 9**).
4. Measure the concentration of the plasmid at 260 nm using a Nanodrop or other spectrophotometer (if necessary, use the conversion 1 OD₂₆₀ = 50 mg/ml plasmid DNA). Ideally, the concentration should be > 25 ng/ml.
5. Prepare the insert DNA as described in section 3.1.1 or 3.1.2, below.
6. Calculate the amount of insert DNA required for ligation reactions containing 50 ng of vector DNA and with a molar ratio of vector to insert of 1:1 and 1:3. For example, for a 3,000 base pair plasmid and 150 base pair insert, 2.5 and 7.5 ng of insert is required, respectively.
7. Perform ligation reactions with vector:insert molar ratios of 1:0 (background control), 1:1, and 1:3, using a standard ligation with T4 ligase enzyme or a rapid ligation kit, according to the manufacturer's instructions.
8. Use 1-3 ml of ligation reaction to transform 30-50 ml aliquots of competent *E.coli* DH5α cells (see **Note 10**). Following incubation on ice for 30 minutes, heat shock at 42 °C for 90 s and then return to ice for 5-10 minutes. Add 500 ml of LB broth to

- each and incubate at 37 °C with gentle agitation for 45-60 minutes. Plate 100 µl of each transformation onto an LB-agar plate containing 100 mg/ml ampicillin.
9. Assess the efficiency of ligation by comparing the number of colonies on each plate. For a successful reaction expect to see at least twice as many colonies on one or both of the plates containing insert DNA compared to the background control.
 10. Miniprep plasmid DNA from 2-3 colonies grown overnight in LB medium with 100 mg/ml ampicillin and confirm the presence of the correct insert using an automated DNA sequencing service.

Cloning Method 1: PCR.

1. Perform a standard PCR reaction using the RNA-encoding template and primers incorporating the *Pst*I and *Hind*III restriction sites (see **Notes 8** and **11**).
2. Run the PCR reaction on a 1% agarose gel, cut out the band (DNA insert) using a clean blade, and recover the DNA using the agarose gel extraction kit.
3. Directly following purification of the DNA insert, double digest with *Pst*I and *Hind*III restriction enzymes (see **Note 8**).
4. Clean up the digested DNA using the agarose gel extraction kit (omitting the initial steps required to melt the gel slice) or a PCR reaction purification kit. Alternatively, heat deactivate the restriction enzymes following the enzyme supplier's instructions and use the digested DNA directly.
5. Determine the concentration of the insert using a Nanodrop spectrophotometer or by comparison of the purified insert to standards of known mass on an agarose gel.

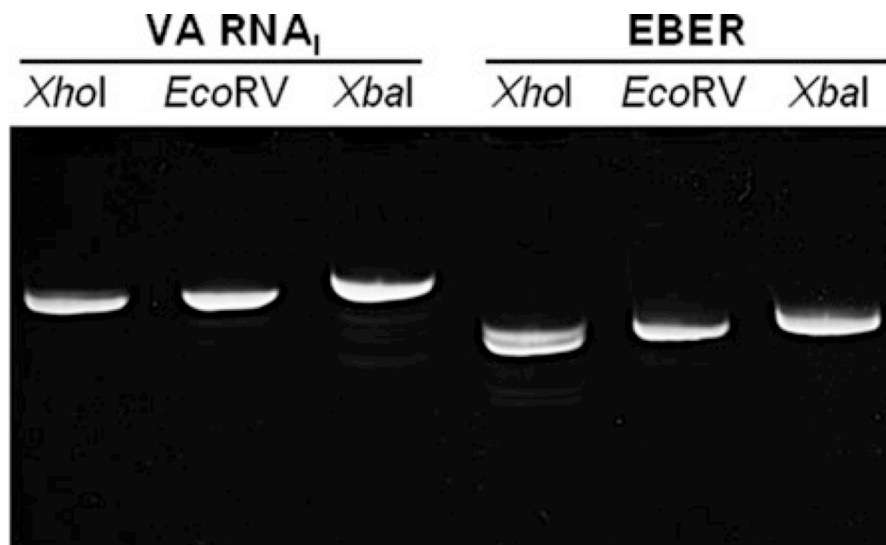


Figure 2 Denaturing polyacrylamide gel analysis of target RNAs within the structure cassette.

Purified samples of VA RNA₁ and EBER1 within the structure cassette prepared by run-off transcription from plasmid templates linearized with each of the three available restriction sites (*Xho*I, *Eco*RV, and *Xba*I). Note that transcription of EBER1 RNA from plasmid linearized with *Xho*I produces two closely spaced bands indicating the presence of n+1 transcript; this is absent in the equivalent VA RNA₁ sample and with the other linearization sites for EBER1 RNA.

Cloning Method 2: Direct ligation of chemically synthesized DNA oligonucleotides.

1. Using the estimate of DNA yield provided by the supplier, dissolve each DNA oligonucleotide in sterile water to a final concentration of 1 mg/ul (see **Note 12**).
2. Individually phosphorylate 1 mg of each DNA using T4 PNK in a 20 ml reaction (see **Note 6**).
3. Mix the phosphorylated DNA oligonucleotides, anneal by heating at 95 °C for 5 minutes, then turn off the heat block, and allow to cool to 30 °C.
4. Dilute the phosphorylated DNA oligos with 960 ml of water to make the final DNA duplex concentration 1 ng/ml (see **Note 13**).

Analysis and preparation of transcribed RNA for probing experiments.

After RNA has been transcribed and purified, it is important to verify that it is both chemically pure and that it exists in a single conformation prior to carrying out structure probing experiments. The purity and integrity of the RNA can be verified using denaturing gel electrophoresis, and its conformational homogeneity prior to and after annealing can be examined using native polyacrylamide gel electrophoresis.

1. Prepare a stock of the purified RNA at a concentration of 50 ng/ml.
2. Evaluate the purity of the isolated RNA by running 200 ng of each RNA on a 50% urea denaturing polyacrylamide gel of appropriate percentage for the RNA size. Stain the gel by adding 10 ml of 2 mg/ml of ethidium bromide to 20 ml of 1x TBE and soaking for 10 min. Visualize the bands using a UV gel imaging system; a single band corresponding to the full-length RNA within the structure cassette is expected (see **Note 14** and **Figure 2**).
3. Determine the optimal annealing temperature and conditions to ensure that the RNA is folded and conformationally homogeneous. These must be experimentally determined; a good starting point is to incubate 100 ng of RNA for 10 minutes at 25, 37, and 65 °C and allow the sample to cool slowly to room temperature on the bench top for 10 minutes before placing on ice (see **Note 15**). Compare each sample of RNA on a native polyacrylamide gel at 4 °C (see **Note 16**) and visualize by staining with ethidium bromide as described in step 2.

Many RNAs exist in multiple conformations, particularly after denaturing purification, and will appear as multiple bands on a native polyacrylamide gel (**Figure 3A and B**, left panels). However, typically some combination of annealing at an empirically determined

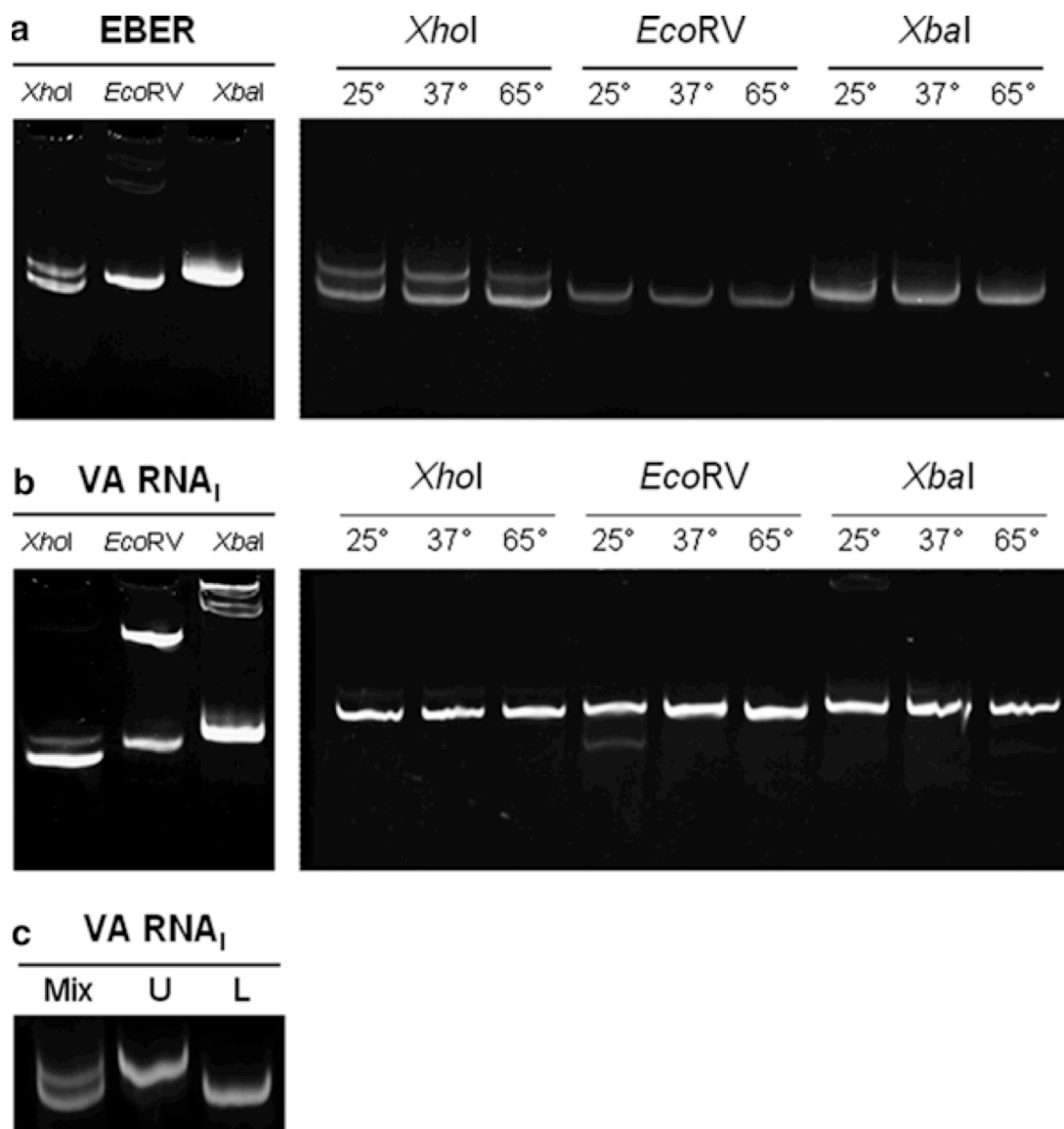


Figure 3 Native polyacrylamide gel analysis of RNAs within the structure cassette. **(a)** EBER1 RNA within the structure cassette produced using each possible run-off site, immediately after denaturing purification (left panel) and following annealing at the indicated temperatures (right panel). **(b)** As panel (A) but for VA RNA₁. **(c)** Separation of the two differently migrating conformations of VA RNA₁ within the structure cassette produced by run-off transcription at the *XhoI* site.

temperature in step 3 in the above protocol and solution conditions, e.g., varying monovalent salt or Mg^{2+} concentrations, will result in a homogeneous sample demonstrated by a single band on a native gel (see **Figure 3A** and **B**, right panels). Alternatively, if the different RNA conformers are sufficiently well resolved on the native gel, they may be separately excised and recovered (they should then be rerun on a native gel to ensure that they are conformationally unique and not two structures in equilibrium). In the example shown in **Figure 3C** for VA RNA_I, only the faster running form gave significant RT products after probing experiments, suggesting a misfolding that occluded the RT primer binding site. Once a homogeneous sample is obtained, it can be used for SHAPE or other RNA structure probing using detailed protocols provided elsewhere (6,9).

NOTES

1. Each SHAPE structure cassette plasmid contains a single internal restriction site on each side of the target RNA for cloning. Each possible combination of two different 5' and 3' sites has been generated, *Pst*I or *Sac*II and *Hind*III or *Nco*I respectively, to produce a collection of four plasmids designed to accommodate a wide range of target RNAs (see **Figure 1**). Plasmids are available from the authors upon request.
2. In the primer design, additional 5'-end nucleotides may be required for efficient direct restriction enzyme digestion of the PCR product (check the supplier's recommendation for each enzyme).
3. A 60:1 mixture of *Taq* and a proofreading polymerase, such as Vent, ensures high fidelity but still allows sufficient addition of 3'-end non-templated adenine onto the PCR product by *Taq* for initial cloning into a commercial 'TA Cloning' vector.

4. Although it adds an additional cloning step, using an intermediate commercial cloning kit can greatly simplify the process of sequence verification and propagation for purification of insert to transfer to the structure cassette plasmid.
5. It is also possible to exploit a unique internal restriction site within the RNA-encoding sequence if one is present. This can be useful, for example, to clone RNAs beyond the limit of economical DNA synthesis (>100 nts). In this case a set of four DNA oligonucleotides corresponding to the coding and complementary strands of the 5' and 3' halves of the RNA should be individually phosphorylated, annealed in pairs, and mixed together with vector in ligation reactions. Once the initial construct is prepared the internal site can also be used to generate RNA sequence variants.
6. When using PNK to phosphorylate the oligonucleotides, it is important to use a buffer containing 10 mM ATP. Supplied T4 PNK buffer typically does not contain ATP whereas the similar T4 DNA ligase buffer does, making it a convenient substitute.
7. Acrylamides can be purchased as powders or in a premixed solution. Acrylamide is a neurotoxin that is easily absorbed through the skin and is more dangerous when handled in powder form. For this reason, we use premixed solutions (30 or 40%). Here, we used denaturing (50% urea) gels with 8% acrylamide in 1× TBE buffer; the appropriate percent depends on the size of the RNA of interest.
8. *Pst*I and *Hind*III are used in this example protocol; when using structure cassette plasmids with the alternate restriction sites, simply substitute the appropriate restriction enzymes. Use an appropriate 10× buffer provided with the enzymes (at 1× final concentration) and incubate at 37 °C for one hour, unless otherwise directed by the enzyme supplier. During this incubation, preparation of the insert can be started in

- parallel (see section 3.1.1 or 3.1.2).
9. Running the plasmid over the column of a gel extraction kit will remove any CIAP and restriction enzymes present in the digest. Because the digested plasmid has not actually been cut from a gel, there is no need to heat the sample as one would for an actual gel extraction. Simply add the required volume of buffer for a 100 mg gel slice and then follow the manufacturer's instructions.
 10. As the resulting number of colonies on each plate will later be compared to gauge the success of the ligation reaction, it is critical that all three transformations are prepared and treated identically. Ideally, a single stock of competent cells is thawed on ice, gently resuspend, and divided into equal volumes in three separate prechilled tubes. Volumes of ligation reaction and cells used can be increased to obtain more colonies but do not add ligation reaction volume corresponding to more than 10% of the volume of competent cells used. If a low ligation efficiency is expected, it is also possible, after plating 100 μ l of each transformation, to microcentrifuge each aliquot of transformed cells, leaving <200 μ l of supernatant in which cells are gently resuspended for plating on a second set of LB-agar plates.
 11. A suitable starting point for the PCR is 25 cycles of denaturing (95 $^{\circ}$ C, 45 s), annealing (57 $^{\circ}$ C, 30 s), and extension (72 $^{\circ}$ C, 90 s). The annealing temperature and magnesium concentration can be optimized to get a single intense band as the product of the reaction.
 12. It is advisable to confirm the DNA oligonucleotide concentration using a spectrophotometer after redissolving in water.
 13. Heat inactivation of the phosphorylation reaction is not necessary as the subsequent

- large dilution of the annealed oligos eliminates any effect the enzyme might have on the ligation reaction.
14. Denaturing gels should be used to assess the products of initial transcription experiments used to determine the optimal restriction site for run-off transcription, each new RNA *in vitro* transcription reaction, and purified RNA after extended storage. This analysis should be done prior to use in probing experiments to ensure that degradation of the RNA sample has not occurred. Although of little consequence to probing experiments, this type of gel can also show if there is any tendency for T7 RNA polymerase to add non-templated nucleotides to the end of the RNA (e.g., see **Figure 2**, lane corresponding to EBER RNA prepared from *XhoI* linearized template).
 15. The annealing conditions suggested in the protocol are a convenient starting point; however the annealing temperature, time of incubation, and method/ speed of cooling can all be varied in addition to the buffer conditions to identify the optimal annealing protocol for a new RNA. Higher temperatures are possible but we have found that VA RNA₁ begins to degrade extensively at temperatures above 85 °C. Problems of degradation at higher temperatures or extended incubation times will be exacerbated if divalent ions such as Mg²⁺ are required in the buffer. We have also found that the protocol producing a single RNA species may depend on the restriction enzyme that was used to linearize the plasmid for *in vitro* transcription (and thus the sequence of the RNA at its 3'-end beyond the RT primer binding site). Because of this variability, we recommend that for each new RNA, test transcriptions using each of the three possible linearization enzymes are performed and the resulting RNA tested (as shown

for VA RNA₁ and EBER1 in **Figure 3**). It is worth noting that it is not always the run-off site producing the greatest RNA yield in the transcription reaction that produces the best RNA for structure probing.

16. For the best results, native gels should be run at 4 °C. Prechill the buffer, assembled electrophoresis apparatus, and gel prior to running.

ACKNOWLEDGEMENTS

This work was supported by laboratory start-up funds from the Department of Biochemistry, the University Research Council of Emory University (grant 2010050), and the Microbiology and Molecular Genetics (MMG) NIH Training Grant (T32-AI007470). We thank Dr. Christine Dunham for critical comments on the manuscript during its preparation.

REFERENCES

1. Merino, E.J., Wilkinson, K.A., Coughlan, J.L. and Weeks, K.M. (2005) RNA structure analysis at single nucleotide resolution by selective 2'-hydroxyl acylation and primer extension (SHAPE). *JACS*, **127**, 4223-4231.
2. Reymond, C., Levesque, D., Bisailon, M. and Perreault, J.P. (2010) Developing three-dimensional models of putative-folding intermediates of the HDV ribozyme. *Structure*, **18**, 1608-1616.
3. Wilkinson, K.A., Merino, E.J. and Weeks, K.M. (2005) RNA SHAPE chemistry reveals nonhierarchical interactions dominate equilibrium structural transitions in tRNA(Asp) transcripts. *J Am Chem Soc*, **127**, 4659-4667.

4. Mortimer, S.A. and Weeks, K.M. (2009) Time-resolved RNA SHAPE chemistry: quantitative RNA structure analysis in one-second snapshots and at single-nucleotide resolution. *Nat Protoc*, **4**, 1413-1421.
5. Watts, J.M., Dang, K.K., Gorelick, R.J., Leonard, C.W., Bess Jr, J.W., Swanstrom, R., Burch, C.L. and Weeks, K.M. (2009) Architecture and secondary structure of an entire HIV-1 RNA genome. *Nature*, **460**, 711-716.
6. Wilkinson, K.A., Merino, E.J. and Weeks, K.M. (2006) Selective 2'-hydroxyl acylation analyzed by primer extension (SHAPE): quantitative RNA structure analysis at single nucleotide resolution. *Nat. Protoc.*, **1**, 1610-1616.
7. Vasa, S.M., Guex, N., Wilkinson, K.A., Weeks, K.M. and Giddings, M.C. (2008) ShapeFinder: a software system for high-throughput quantitative analysis of nucleic acid reactivity information resolved by capillary electrophoresis. *RNA*, **14**, 1979-1990.
8. Badorrek, C.S. and Weeks, K.M. (2005) RNA flexibility in the dimerization domain of a gamma retrovirus. *Nat Chem Biol*, **1**, 104-111.
9. Walker, S.C., Avis, J.M. and Conn, G.L. (2003) General plasmids for producing RNA *in vitro* transcripts with homogeneous ends. *NAR Methods*, **31**, e82.
10. Linpinsel, J.L. and Conn, G.L. (2012) General protocols for preparation of plasmid DNA template, RNA *in vitro* transcription, and RNA purification by denaturing PAGE. *Methods Mol Biol*, **941**, 43-58.

CHAPTER 4:**Dissection of the adenoviral VA RNA_I Central Domain structure reveals minimal requirements for RNA-mediated inhibition of PKR**

The following Chapter has been published:

Linpinsel, J.L.*, **Vachon, V.K.***, Sunita S., Schwartz, S., and Conn, G.L. (2014).

Dissection of the adenoviral VA RNA_I Central Domain structure reveals minimal requirements for RNA-mediated inhibition of PKR. *J.Biol. Chem.* 289: 23233-45. *co-first authors

I am responsible for the SHAPE probing data presented in figures 2 and 5, and for a substantial portion of the writing of this manuscript.

ABSTRACT

Virus-associated RNA-I (VA RNA_I) is a short (~160 nt) non-coding RNA transcript employed by adenovirus to subvert the innate immune system protein double-stranded RNA-activated protein kinase (PKR). The Central Domain of VA RNA_I is proposed to contain a complex tertiary structure that contributes to its optimal inhibitory activity against PKR. Here, we use a combination of VA RNA_I mutagenesis, structural analyses, as well as PKR activity and binding assays to dissect this tertiary structure and assess its functional role. Our results support the existence of a pH- and Mg²⁺-dependent tertiary structure involving pseudoknot formation within the Central Domain. Unexpectedly, this structure appears to play no direct role in PKR inhibition. Deletion of Central Domain sequences within a minimal, but fully active construct, lacking the tertiary structure reveal a crucial role in PKR binding and inhibition for nucleotides in the 5'-half of the Central Domain. Deletion of the Central Domain 3'-half also significantly impacts activity, but appears to arise indirectly by reducing its capacity to assist in optimally presenting the 5'-half sequence. Collectively, our results identify regions of VA RNA_I critical for PKR inhibition and reveal that the requirements for an effective RNA inhibitor of PKR are simpler than previously appreciated.

INTRODUCTION

The double-stranded RNA-activated protein kinase (PKR) is a central component of innate cellular immunity. Upon binding double-stranded RNA (dsRNA) produced as a consequence of viral replication, PKR initiates the shut down of general translation, blocking synthesis of viral proteins. As a countermeasure to this activity, adenoviruses

produce copious quantities ($\sim 10^8$ per cell) of a ~ 160 nucleotide non-coding transcript VA RNA_I that binds to PKR, and prevents it from exerting its antiviral effect (1,2).

In addition to its well-established role as a proviral, non-coding RNA, VA RNA_I is a substrate of Dicer, and therefore an effective inhibitor of the RNAi system as its high cellular concentration results in saturation of the RISC complex (3,4). Specific regulation of host genes by VA RNA_I-derived microRNAs has been proposed (5,6), but a precise functional role in adenoviral replication is not yet established (7). The remaining portion of the Dicer-processed VA RNA_I is a truncated form of the transcript, lacking the viral microRNA sequences at both the 5'- and 3'-end, that retains full activity against PKR (8). Paradoxically, full length VA RNA_I activates a second protein of the innate immune response, 2'-5'-oligoadenylate synthetase 1 (OAS1), leading to downstream activation of RNaseL and degradation of viral and cellular RNAs (9). Recently, however, Dicer-processing was shown to largely reverse this stimulatory activity as the truncated form of VA RNA_I acts as a pseudoinhibitor of OAS1 (10). Thus, a single VA RNA_I transcript possesses multiple activities: it can inhibit two antiviral proteins (PKR and OAS1), potentially regulate gene expression via the cellular RNAi system, and saturate the RNA processing enzyme Dicer.

VA RNA_I molecules from different adenovirus serotypes vary considerably at the sequence level (11). While differences in the details of their secondary structures also likely exist, all possess three major structural domains: Apical Stem, Central Domain, and Terminal Stem (11,12). The Apical Stem serves as the primary binding site for the two N-terminal dsRNA binding domains of PKR, while the Central Domain is believed

to be responsible for inhibition of the kinase (13-20). However, identification of specific Central Domain sequence(s) or structure(s) that form the direct contacts with PKR required to impart this activity has remained elusive. Despite this, the notion persists that the Central Domain folds into a complex tertiary structure and its placement adjacent to the primary PKR binding site in the Apical Stem confers upon VA RNA_I its inhibitory activity against PKR.

Based on a wealth of prior mutagenesis, RNA structure probing, and functional analyses, a model for the Central Domain was proposed for adenovirus type 2 (Ad2) VA RNA_I in which the two loops within the Central Domain interact to form a pseudoknot structure (**Fig. 1A**, loops connected by a dashed line) (21). At the center of this pseudoknot structure in the Central Domain's helical junction are two highly conserved and base paired tetranucleotide sequences that appear critical in both their sequence and orientation for optimum VA RNA_I activity (**Fig. 1A**, nts in outline font) (11,12,21). We have shown that the stability of the Central Domain structure is also highly sensitive to solution pH, suggesting the involvement of a protonated base-base tertiary interaction (8). Finally, Mg²⁺ and PKR were shown to induce similar structural rearrangements in the Central Domain (14) and Mg²⁺ appears to fine-tune the mode and affinity of the PKR-VA RNA_I interaction (22). Together, these features lend strong support to the presence of a tertiary structure within the Central Domain.

Our initial objectives in the present study were to address two important remaining questions regarding the VA RNA_I Central Domain: what is the nature of its tertiary

structure and what role does it play in PKR inhibition? The analyses presented here reveal the defining features of the Central Domain tertiary structure, but demonstrate that it is not required for activity against PKR. Instead, inhibition requires only a subset of the Central Domain's secondary structural elements. Thus, the requirements for optimal inhibitory activity against PKR are far simpler than previously appreciated, offering a satisfying explanation for the consistently observed inhibition of PKR by VA RNA₁ molecules from different adenovirus serotypes despite their significant differences at the sequence and secondary structural levels.

EXPERIMENTAL PROCEDURES

RNA in vitro transcription—The RNA construct used as the starting point for these studies (**Fig. 1A**) possesses both a deleted terminal stem, previously termed TSΔ21 RNA (8), and a deletion in the Apical Stem (A2dl2) which removes conformational heterogeneity in this region (23). This RNA and its derivatives generated in this study are expected to form a 1:1 complex with PKR (8). All new RNAs prepared here contain the A2dl2 mutation, but for brevity are named only for their terminal deletion or point mutation(s) made within the TSΔ21-A2dl2 context.

New templates were created by direct ligation of 5'-end phosphorylated double-stranded DNA into a plasmid previously created for transcription of target RNAs with a 3'-end fused hepatitis delta virus (3'-HDV) ribozyme (24,25). RNAs were produced by run-off *in vitro* transcription using T7 RNA polymerase under optimal conditions for VA RNA₁ (26), purified by preparative denaturing PAGE, and recovered as described previously

(8,27). TSΔ21 RNA was also transcribed without the fused 3'-HDV ribozyme by insertion of an additional guanosine immediately after the VA RNA_I coding sequence, creating a new *NaeI* restriction enzyme site for plasmid linearization at the authentic 3'-end of the TSΔ21 encoding sequence (GCC↓GGC; inserted G is *underlined*). No difference in gel mobility, melting profile, or PKR-inhibitory activity was observed for RNA produced in this manner (data not shown). The A123U construct was made exclusively with the *NaeI* run-off site. RNAs for SHAPE and Tb³⁺ probing were generated by the same direct ligation approach, but using a modified plasmid pre-loaded with 5'- and 3'-flanking sequences encoding a 'structure cassette' (25,28).

PKR expression and purification—PKR was expressed from plasmid pET-PKR/PPase (29) as described previously (8). Protein was expressed in *E. coli* Rosetta 2 (DE3) and purified sequentially using heparin affinity, poly(I)•poly(C) RNA affinity, and gel filtration chromatographies on an ÄKTA Purifier10 system (GE Healthcare). Protein from the gel filtration column was obtained in 20 mM HEPES pH 7.5 buffer containing 150 mM NaCl, 0.1 mM EDTA, 10 mM β-mercaptoethanol, and 10% (v/v) glycerol.

RNA UV-melting analysis—UV melting curves at 260 and 280 nm were collected on a Cary 400 UV/Vis spectrophotometer (Varian) with a six-cell multichanger and in-cell temperature probe placed in a buffer-only sample. Samples contained 20-25 μg RNA in a solution of 50 mM KCl and 10 mM MOPS buffer pH 7.5, or 10 mM MES buffer pH 5.5. Experiments with Mg²⁺ were performed in the pH 7.5 buffer solution with addition of 0.01-5.0 mM MgCl₂. Experiments with PKR were performed using RNA in the pH 7.5

buffer solution mixed with an equal volume of PKR in gel filtration buffer (to give 0.5, 1, and 2 molar equivalents of protein). To facilitate comparison between different RNAs or solution conditions, the UV melting data are presented as ‘melting profiles’ corresponding to the first derivative of the UV absorbance curve.

Selective 2'-hydroxyl acylation analyzed by primer extension (SHAPE) probing—RNA was annealed in 0.5× Tris-EDTA (TE) buffer at 65 °C for 10 minutes, cooled to room temperature over 10 minutes, and then placed on ice. Samples were examined by 50 % (w/v) urea denaturing and native PAGE to evaluate their purity and conformational homogeneity, respectively. SHAPE RNA probing with N-methylisatoic anhydride (NMIA) was carried out as described previously (28), but with the following modifications. Reactions were initiated by addition of 1 µL of 10× NMIA (100 mM in DMSO) or 1 µL of DMSO for controls without NMIA, and allowed to proceed for five NMIA hydrolysis half lives, i.e. 0.5, 10, 30, and 240 minutes at 85, 50, 40, and 20 °C, respectively (28). Reverse transcription was performed with Superscript III reverse transcriptase (Invitrogen) using a 5'-end [$\gamma^{32}\text{P}$]-labeled DNA primer (0.12 µM final concentration) corresponding to the sequence of the 3'-flanking region of the structure cassette (25) in a total volume of 10 µL in 100 mM HEPES buffer pH 8.0 containing 100 mM NaCl. Reactions were stopped by addition of 35 µL of a 4:25 (v/v) mixture of 1 M unbuffered Tris-HCl and gel loading solution (85% formamide, 0.5× TBE pH 8.0, and 50 mM EDTA with trace bromophenol blue and xylene cyanol dyes) and heating to 95 °C for 5 minutes. A 3 µL aliquot of each RT reaction was resolved on an 8% acrylamide, 50% (w/v) urea, 1× TBE PAGE sequencing gel. Gels were imaged using a Typhoon Trio

phosphorimager (GE Healthcare) and analyzed using ImageQuant software. Background subtraction, band normalization, and generation of cut-off values for no (<5.5 %), low (5.5 – 11 %), medium (11 – 22 %), and high (>22 %) reactivity were done as previously described (30).

SHAPE probing reactions with PKR were performed in 30 μ L total volume and contained 1 μ L protein in gel filtration column buffer (giving a final PKR:RNA molar ratio of 2:1). Equivalent reactions without PKR were also performed in the same way, but using 1 μ L gel filtration column buffer with no protein. After initiation by addition of 3 μ L 10 \times NMIA (or DMSO for controls) and incubation at 20 $^{\circ}$ C, reactions were diluted by addition of 200 μ L of 0.5 \times TE and extracted twice with two volumes of premixed phenol:chloroform:isoamyl alcohol (25:24:1) and once with two volumes of chloroform. The RNA was recovered by ethanol precipitation in the presence of glycogen (20 μ g/mL) at -80 $^{\circ}$ C for 30 minutes, resuspended in 10 μ L of 0.5 \times TE, and subjected to RT analysis as described above.

Tb³⁺ RNA probing— Tb^{3+} probing reactions were performed in a total volume of 10 μ L in solution containing 100 mM HEPES buffer pH 8.0 and 100 mM NaCl. TS Δ 21 RNA (100 nM) was incubated with $TbCl_3$ (0-0.25 mM) at 37 $^{\circ}$ C for 15 minutes. RNA in each probing reaction was ethanol precipitated, recovered, and analyzed by RT as described for SHAPE probing.

PKR activity assays—Assays of PKR activation contained PKR (0.1 μ g), alone or with

eIF2 α (0.25 μ g), in 50 mM Tris buffer pH 7.8 containing poly(I)•poly(C) dsRNA (0-100 μ g/mL), 20 μ M ATP, 10 μ Ci [γ ³²P]-ATP (10 mCi/mL, 6000 Ci/mmol), 50 mM KCl, 2 mM MgCl₂, 2.5 mM DTT, and 10% glycerol in a total reaction volume of 10 μ L. Reactions were incubated at 25 °C for 10 minutes and then stopped by addition of gel loading dye (for SDS-PAGE analysis) or 400 μ L of ice-cold phosphate buffered saline containing 200 μ M ATP (for slot blot analysis). In the latter case, quenched samples were promptly applied to a Bio-Dot SF (BioRad) microfiltration system and proteins were bound to a nitrocellulose membrane under vacuum. The membrane was washed to remove unreacted [γ ³²P]-ATP and then air-dried for 15 minutes. For both membranes and dried SDS-PAGE gels, the extent of PKR and eIF2 α phosphorylation was determined by exposure to a phosphor storage screen and analysis using a Typhoon FLA 7000 phosphorimager and ImageQuant software (GE Healthcare).

PKR inhibition assays were performed in a similar manner, but included a 10 minute preincubation step at 25 °C with the VA RNA_I variant (0-10 μ M) and PKR (0.1 μ g), either alone or with eIF2 α (0.25 μ g), in 50 mM Tris buffer pH 7.8 containing 50 mM KCl, 2.5 mM DTT, and 10% glycerol. Reactions (10 μ L final volume) were initiated by addition of 0.04 μ g/mL poly(I)•poly(C) dsRNA, 20 μ M ATP, 10 μ Ci [γ ³²P]-ATP (10 mCi/mL, 6000 Ci/mmol), and 2 mM MgCl₂. After a 10 minute incubation at 25°C, the reactions were quenched and the products quantified as described above for the activation assays.

Isothermal Titration Calorimetry (ITC)—Binding affinities for mutant VA RNA_I-PKR

interaction were measured using an Auto-iTC₂₀₀ microcalorimeter (GE Healthcare). Protein and RNA samples were individually dialyzed against 50 mM Tris buffer pH 7.5 containing 100 mM NaCl. PKR (60 μ M, syringe) was titrated into RNA (6 μ M, sample cell) at 25 °C in 16 x 2.5 μ L injections with 150 s spacing. Titration curves were fit by a non-linear least-squares method in MicroCal Origin software using the single site binding model.

RESULTS AND DISCUSSION

A putative pH-dependent VA RNA_I Central Domain tertiary structure is stabilized by Mg²⁺ and PKR—A new VA RNA_I variant was created (**Fig. 1A**) that combines two previously characterized mutations: a 21 base pair truncation of the Terminal Stem (TS Δ 21) which mirrors that produced by Dicer processing *in vivo* (8) and a six nucleotide deletion in the Apical Stem (A2d12) (31). These independent mutations are within functionally separate domains and each retains the full inhibitory activity of wild-type VA RNA_I (8,18). The global folding of this new RNA was assessed by UV melting analysis (**Fig. 1B**) and the melting profiles obtained were found to be entirely consistent with previous studies of the individual deletions (8,23). First, the region of the melting profile corresponding to the Central Domain is essentially identical to that observed for VA RNA_I with only the TS Δ 21 deletion (8). Second, the A2d12 mutation stabilizes the Apical Stem, significantly increasing its apparent T_m (to >90 °C) relative to the wild-type sequence (apparent T_m ~86 °C). Third, the absence of any additional effects on other regions of the profile resulting from the A2d12 mutation corroborates our previous finding that the Apical Stem and Central Domain structures and stabilities are completely

independent (27). This new construct, henceforth termed TSA Δ 21 for brevity (see Experimental Procedures), is ideal for detailed analysis of the Central Domain structure as the stabilizing effect of the A2dl2 mutation fully resolves the apparent transitions corresponding to the Central Domain and Apical Stem (**Fig. 1B**).

Our previous analysis (8) showed the TSA Δ 21 Central Domain unfolds in at least two overlapping apparent transitions between 30 and 80 °C. Here, a low temperature starting point of ~15 °C allowed us to identify an additional broad apparent unfolding transition centered on ~30 °C that is present only at pH 7.5 (**Fig. 1B**). The dramatic stabilization of the Central Domain structure at low pH (8) shifts this apparent transition to significantly higher T_m at pH 5.5. We hypothesized that this newly identified apparent transition corresponds to the unfolding of the putative Central Domain tertiary structure. The dramatic rightward shift and coupling of this and the second apparent transition (centered on ~45 °C at pH 7.5) into a single apparent transition (centered on ~57 °C at pH 5.5) is consistent with a low-stability (apparent T_m ~30 °C) tertiary structure at pH 7.5 that is stabilized via a protonated tertiary contact. Through the largely hierarchical nature of RNA folding, this stabilized tertiary structure additionally stabilizes the Central Domain secondary structure components from which it is formed.

Previous VA RNA_I structure probing studies in the presence of Mg²⁺ or PKR have shown that both induce similar structural changes in the Central Domain (14). More recently, the interaction between PKR and VA RNA_I was shown to be sensitive to the presence of Mg²⁺ (22). Having identified a new apparent transition that potentially corresponds to the

RNA tertiary structure, we next examined the effect of Mg^{2+} and PKR on the RNA melting profile. As expected, addition of Mg^{2+} stabilizes all elements of the VA RNA_I structure, corresponding to a rightward shift in all apparent transitions (**Fig. 1C**). The first apparent transition is, however, especially sensitive to addition of Mg^{2+} with a significant shift in apparent T_m at only 10-25 μ M and complete coupling of the first and second apparent transitions at 0.1-0.2 mM and higher. Melting experiments with PKR are complicated by precipitation of the protein at ~ 50 °C, but again indicate that the putative tertiary structure, corresponding to the broad first apparent transition, is stabilized by PKR (**Fig. 1D**).

The behavior of this newly identified, first low-temperature apparent transition in the melting profile of T Δ 21 RNA at low pH and in the presence of Mg^{2+} is consistent with it representing the unfolding of an RNA tertiary structure. Thus, from these various lines of evidence, we conclude that the Central Domain does, as previously proposed, contain a set of tertiary interactions, including a protonated base, and that its stability is influenced by specific binding of one or more Mg^{2+} or PKR. This conclusion is further corroborated by the results of SHAPE and mutagenesis experiments described below.

SHAPE analysis of the VA RNA_I Central Domain tertiary structure—To identify the regions of the Central Domain involved in forming its tertiary structure, we used SHAPE to probe nucleotide flexibility in T Δ 21 RNA at two temperatures that define the lower (20 °C) and upper (40°C) boundaries of the tertiary structure unfolding transition identified in the melting experiments (indicated by the black arrowheads in **Fig. 1B**).

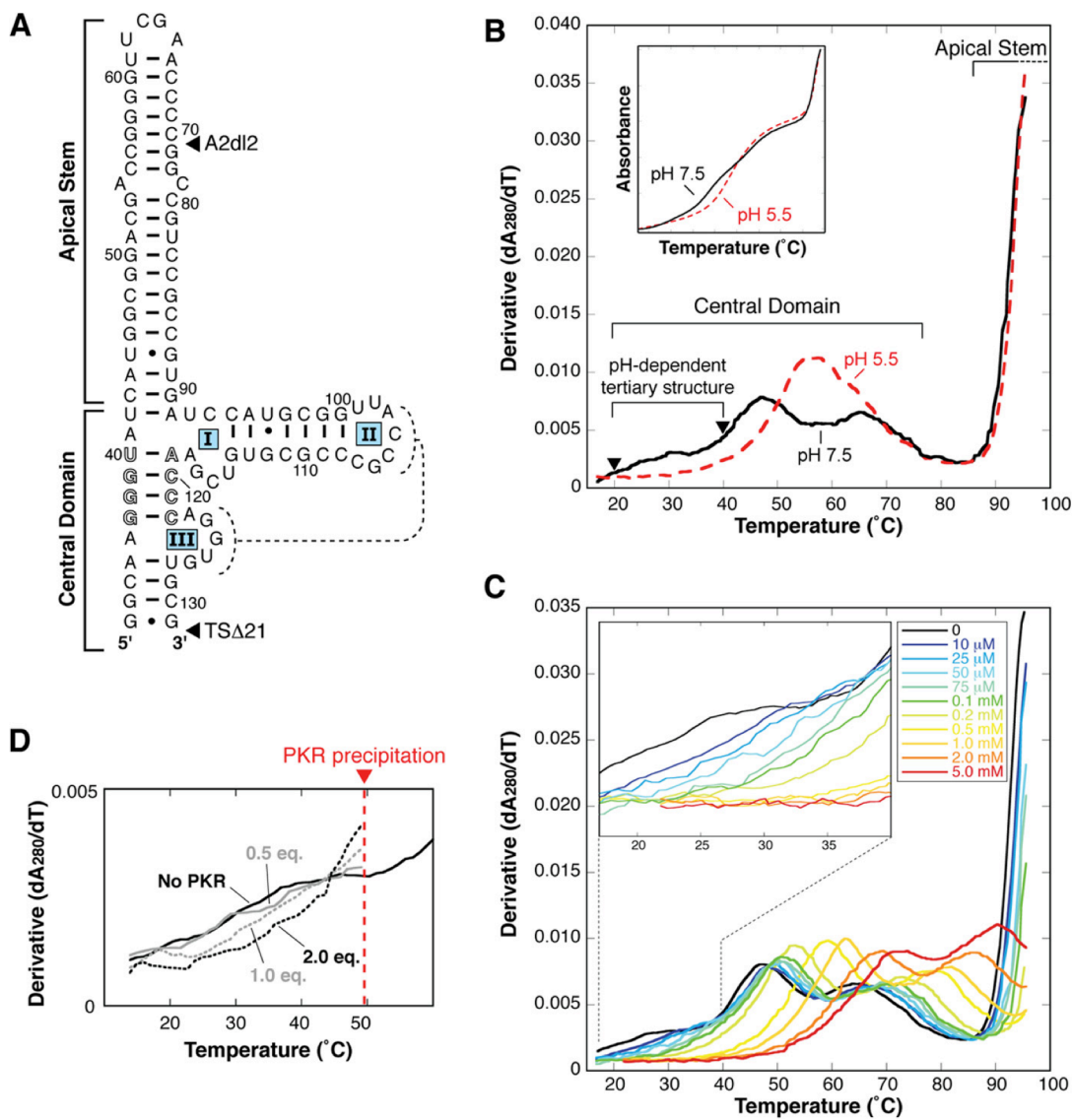


Figure 1 The VA RNA₁ Central Domain contains putative tertiary interactions that are stabilized by low pH, Mg²⁺ and PKR. *A*, TSΔ21, the truncated form of Ad2 VA RNA₁, used as the starting point in this study. This RNA construct lacks all Terminal Stem nucleotides (TSΔ21) and has a six nucleotide deletion in the Apical Stem (A2dl2). The proposed pseudoknot interaction between Loop II and Loop III (dashed lines) and conserved complementary tetranucleotide sequences (outline font) are highlighted. *B*, UV melting analysis of VA RNA₁ with combined TSΔ21 and A2dl2 deletions. Melting profiles depict the first derivative of the UV melting curve (*inset*), at pH 5.5 (red) and 7.5 (black). Apparent transitions ('peaks') in the melting profile correspond to unfolding of structures within the VA RNA₁ Apical Stem (partly visible at >90 °C) and Central Domain (three at pH 7.5 and two at pH 5.5 over the range 20-80 °C)

are indicated. Of the Central Domain transitions, the first is assigned to the putative RNA tertiary structure, and is dramatically stabilized at low pH (rightward shift of profile in red dashed line). Black arrowheads denote temperatures used for SHAPE probing of this RNA. The first apparent transition is also stabilized by both *C*, Mg^{2+} -ion and *D*, PKR. The concentration of divalent ion or molar equivalents of PKR included in the experiment are indicated.

These conditions should thus reflect nucleotide flexibility in the presence and absence of the folded tertiary structure, respectively.

At 20 °C, most nucleotides predicted to be base paired display low SHAPE reactivity as expected (**Fig. 2A,B**). The only exceptions are nucleotides bordering Loops I and III, and those at the 3' end (nts 129-131). Most notably, much lower reactivity than expected is observed for the majority of nucleotides in Loops II and III (nts 104-107 and 123-127), indicating lower nucleotide flexibility and therefore involvement in interactions beyond those depicted in the secondary structure model. In contrast, nts 115-117 of the 3'-side of Loop I display the high reactivity expected for non-base paired nucleotides. At 40 °C, reactivity of these Loop II and III nucleotides increases substantially along with a general increase in reactivity of paired and Loop I nucleotides in the 3'-half of the Central Domain (nts 111-131; **Fig. 2B inset**). The low reactivity of the Loop II and III nucleotides and their concomitant increase in reactivity at a temperature above the identified tertiary structure unfolding event support the conclusion that these partially complementary nucleotides directly base pair to form a pseudoknot structure within the Central Domain.

Role of Mg^{2+} and protonation in Central Domain tertiary structure formation—To

further explore the role of Mg^{2+} in the formation of the Central Domain tertiary structure, we used Tb^{3+} probing, a method previously applied to both the mapping of ion binding sites and monitoring RNA folding (32). TS Δ 21 RNA was incubated with a range of $TbCl_3$ concentrations and the induced strand cleavages were examined using reverse transcription. Two major sites of strand scission were identified, A123 and G97 (**Fig. 2B,C**). Each site was present at the lowest Tb^{3+} concentration used and increased consistently in intensity with increasing Tb^{3+} concentration. These results point to the presence of at least one Mg^{2+} binding site in the proximity of Loop III and, unexpectedly, a base paired nucleotide in the middle of the Central Domain stem-loop structure. A third weaker strand scission is also noted at A103 within Loop II which may indicate the presence of an additional Mg^{2+} site or that this nucleotide is in proximity to the ion located at G97/A123.

Next, we exploited the strong influence of solution pH on Central Domain stability to further dissect the features critical for formation of its tertiary structure. We hypothesized that pH dependence arises through specific protonation of at least one Central Domain nucleotide involved in a direct tertiary contact. Further, mutation of this nucleotide should result in loss of pH dependence, and therefore identical RNA melting profiles at pH 5.5 and 7.5. The pK_a of cytosine N3 is ~ 4.5 in the free nucleotide, making this site on one or more of the Central Domain's single stranded cytosine residues the most likely candidate for the origin of its pH sensitivity. Each of these residues, C104, C105, C107, and C116, was individually mutated to U and the effect on pH dependence in the RNA melting profile assessed (**Fig. 3A,B**). Notably, none of the individual mutations

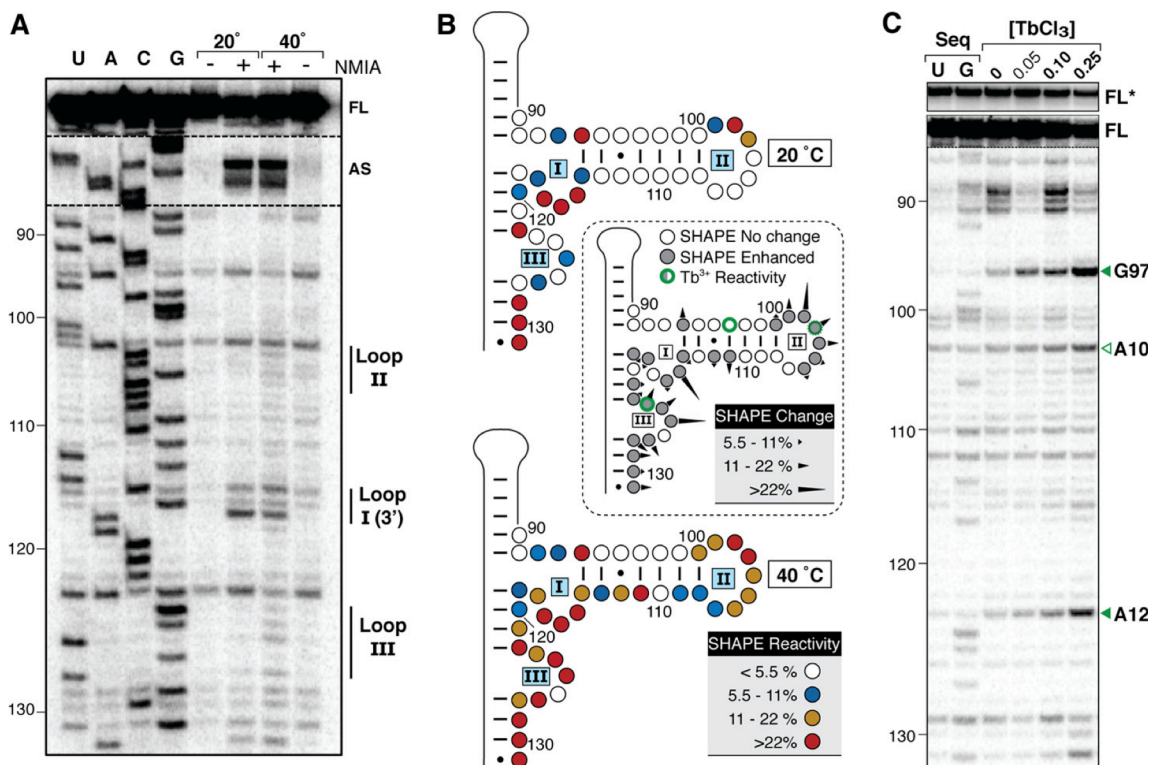


Figure 2 Identification of tertiary interactions and Mg²⁺ binding sites within the VA RNA_I Central Domain. *A*, Representative gel showing SHAPE probing of TSD21 RNA below (20 °C) and above (40 °C) the apparent transition corresponding to the Central Domain tertiary structure unfolding (marked with black arrowheads in Figure 1B). Lanes with (+) and without (-) SHAPE reagent (NMIA) and RT reactions with dideoxynucleotides (U, A, C, G) for RNA sequencing are indicated. VA RNA_I nucleotide numbering is shown on the *left*, and bands corresponding to Central Domain Loops I-III, the Apical Stem (AS) loop, and full-length product (FL) are indicated on the *right*. *B*, Quantification of SHAPE reactivity at 20 (*top*) and 40 °C (*bottom*), and changes between these temperatures (*center*). Normalized band intensities were averaged from three sets of reactions and categorized according to the reactivity keys shown. *C*, Tb³⁺ probing of the VA RNA_I Central Domain with sites of RNA cleavage enhanced by increasing concentrations of Tb³⁺ (0 to 0.25 mM) indicated (*right*), and shown on the secondary structure map in *panel B* (*center*). Sequencing lanes (*Seq*) contain the complementary dideoxynucleotide. *FL**, full-length product with contrast reduced 5 x.

eliminated the strong stabilization of the tertiary structure in the pH 5.5 melting profile, indicating that none of these residues harbors the putative site of protonation. However, the role of Loop II nucleotides in forming the Central Domain tertiary structure is further corroborated by these mutations. First, the broad low temperature apparent transition corresponding to the tertiary structure at pH 7.5 is absent in C104U, C105U, and C107U RNAs (compare black and blue solid line between 20-40 °C in **Fig. 3B**). Second, while folding of the Central Domain in each of these RNAs is driven by protonation at pH 5.5 (rightward shift of the first apparent transition), the melting profiles show some change in apparent T_m , transition shape, and/ or hypochromicity, indicative of additional subtle structural alterations. The C116U mutant is distinct in that it appears to retain the tertiary fold, but a component of the secondary structure is destabilized at pH 7.5. In contrast, at lower pH where Central Domain folding is driven by the base protonation, this mutant's melting profile is identical to that of the parent TS Δ 21 construct.

Nucleotide A123 was implicated by our Tb³⁺ probing experiments in Mg²⁺ binding and, like the adjacent nucleotides involved in the Central Domain pseudoknot structure, displays lower than expected SHAPE reactivity. We therefore mutated A123 to U (A123U RNA) to determine if it harbors the protonation site (adenine N1, pKa ~3.8). The melting profile for A123U RNA at pH 7.5 lacks the broad, low-temperature apparent transition corresponding to the tertiary structure (**Fig. 3C**), but was otherwise unchanged aside from a small increase in hypochromicity in the highest T_m (~65 °C) apparent transition. At pH 5.5, the profile was nearly identical to that observed at pH 7.5, with only small changes in hypochromicity of each apparent transition and a small decrease in

apparent T_m for the highest T_m (~65 °C) apparent transition (**Fig. 3C**). Critically, neither pH-dependent stabilization nor the reappearance of an apparent transition corresponding to the tertiary unfolding was observed. We conclude that A123 is the protonated base within the Central Domain critical for the formation of its tertiary structure.

Though none of the individual mutations in Loop II (C104U, C105U, and C107U) resulted in melting profiles indicative of the loss of tertiary structure, a result similar to that observed for A123U was obtained when all three cytosines of Loop II were mutated to uridines (3U RNA, **Fig. 3C**). We interpret this as being a more significant disruption of the Loop II-Loop III pseudoknot tertiary interaction, such that A123 protonation-driven tertiary folding cannot compensate as it does for an individual C to U mutation at each location.

Protonated adenine bases have been observed in non-Watson-Crick base pairs with either guanine or cytidine partners in RNA crystal structures. For the VA RNA_I Central Domain, the latter possibility is largely eliminated, as we have demonstrated the existence of a pseudoknot structure in which C104 and C105 are base paired with G124 and G125, and the mutation of each single-stranded C residue does not affect the structural pH dependence. Formation of the pseudoknot structure between Loops II and III potentially creates a G□A pair between G106 and A123. However, while the G106A mutation resulted in an expected loss of the broad tertiary structure unfolding at pH 7.5, it did not eliminate the Central Domain folding dependence upon pH (data not shown). This result does not exclude an interaction between G106 and A123 as part of the pseudoknot,

but shows that it is not dependent upon pH. Although G97 is base paired with C111 in the secondary model, our Tb^{3+} probing data implicate this guanine residue, together with A123, in coordinating a Mg^{2+} within the Central Domain. Of the known base pairings in RNA, we speculate that a parallel strand orientation, *cis* Watson-Crick/ Hoogsteen A123⁺□G97 base pair (family 3 (33); **Fig. 3D**) would meet the requirement for a protonated A123 interaction within the Central Domain structure without the need for strand reversal. This pairing would also leave open the Watson-Crick face of G97 for base pairing with C111, and the Hoogsteen face of A123 for (non-protonated) interaction with G106 as part of the Loop II-Loop III pseudoknot. While a high-resolution structure will be required to fully resolve the interactions of A123 in VA RNA_I, such A⁺□G base pairs are found within several RNA structures in the PDB (34), including both eukaryotic and prokaryotic ribosomal subunits (35,36) where they are engaged in complex tertiary structures stabilized by Mg^{2+} .

Minimum sequence requirements for Central Domain tertiary structure formation—

Having defined several critical features of the VA RNA_I Central Domain structure, including the formation of a pseudoknot interaction, we sought to determine the minimal sequence required to form the tertiary structure using additional deletion mutants. The first, TSΔ25 RNA, lacks nucleotides at both the 5'- and 3'-ends (nts 32-36, and 123-131, respectively) compared to the original TSΔ21 construct, corresponding to Loop III and the terminal base paired nucleotides (**Fig. 4**). As might be expected, this substantial deletion destabilizes the Central Domain folding, resulting in a profile for TSΔ25 RNA with significantly lowered hypochromicity and broad, flat features in which only the

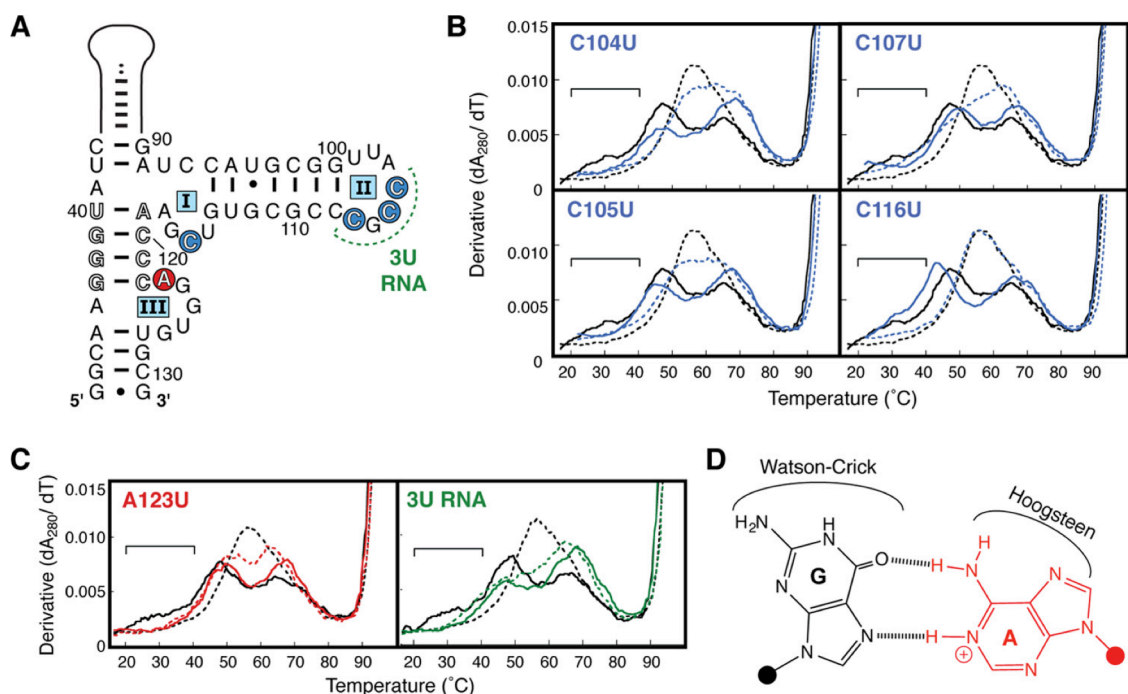


Figure 3 A123 is the protonated nucleotide within the VA RNA₁ Central Domain. *A*, Central Domain secondary structure highlighting the four individual single-stranded C to U mutants (blue circles), mutation of all three Loop II C nucleotides to U (3U RNA; green), and the A123 to U point mutant (red circle). *B,C*, UV melting profiles of C104U, C105U, C107U, C116U (blue), A123U (red), and 3U RNA (green). The melting profile for each RNA is shown at pH 7.5 (solid line) and pH 5.5 (dashed line) and compared to those of TSA21 RNA (black). The region corresponding to unfolding of the TSA21 RNA pH-dependent tertiary structure at pH 7.5 is marked with a horizontal bar. *D*, The *cis* Watson-Crick/ Hoogsteen A⁺•W base pair proposed for A123⁺•G97, highlighting the available base edges for potential additional interactions as discussed in the main text.

highest T_m apparent transition (~65 °C) of the Central Domain appears largely unaffected (**Fig. 4, top panel**). Critically, the TSA25 RNA melting profiles at pH 7.5 and 5.5 are identical, demonstrating that the Central Domain folding in this RNA is pH-independent and, therefore, that the tertiary structure interactions are absent. This was expected because the TSA25 mutation removes the protonated base A123 and all Loop III

nucleotides involved in forming the pseudoknot structure.

A second mutant, TS Δ 25+L RNA, was created which also lacks the terminal base paired nucleotides deleted in TS Δ 25 RNA, but retains the five residues of Loop III (nts 123-127) as a 3'-end single-stranded extension (**Fig. 4**). The melting profile of TS Δ 25+L RNA is similarly altered with broad, flat features. However, in sharp contrast to TS Δ 25, it retains a clear additional broad apparent transition centered on ~ 35 °C at pH 7.5. Further, TS Δ 25+L RNA also retains a strong dependence upon pH, with a profile at pH 5.5 identical to that of TS Δ 21 RNA, but with a lowered hypochromicity that correlates with its reduction in length and secondary structural content.

To verify that this apparent restoration of tertiary structure and its associated pH dependence is due to specific interaction between nucleotides of Loop II and III, we created a final mutant, TS Δ 25xL RNA. This RNA possesses an identical secondary structure to that of TS Δ 25+L, but with mutation of the 3'-single stranded nucleotides corresponding to Loop III to the sequence UUGCG. The melting profile of this RNA was identical to that observed for TS Δ 25 (data not shown), indicating that no interaction occurs between the Loop II and the mutated Loop III nucleotides. These results show that the terminal base paired nucleotides absent in TS Δ 25 RNA play no role in tertiary structure formation and that the specific sequence of Loop III is necessary and sufficient to form the Central Domain pseudoknot tertiary interaction.

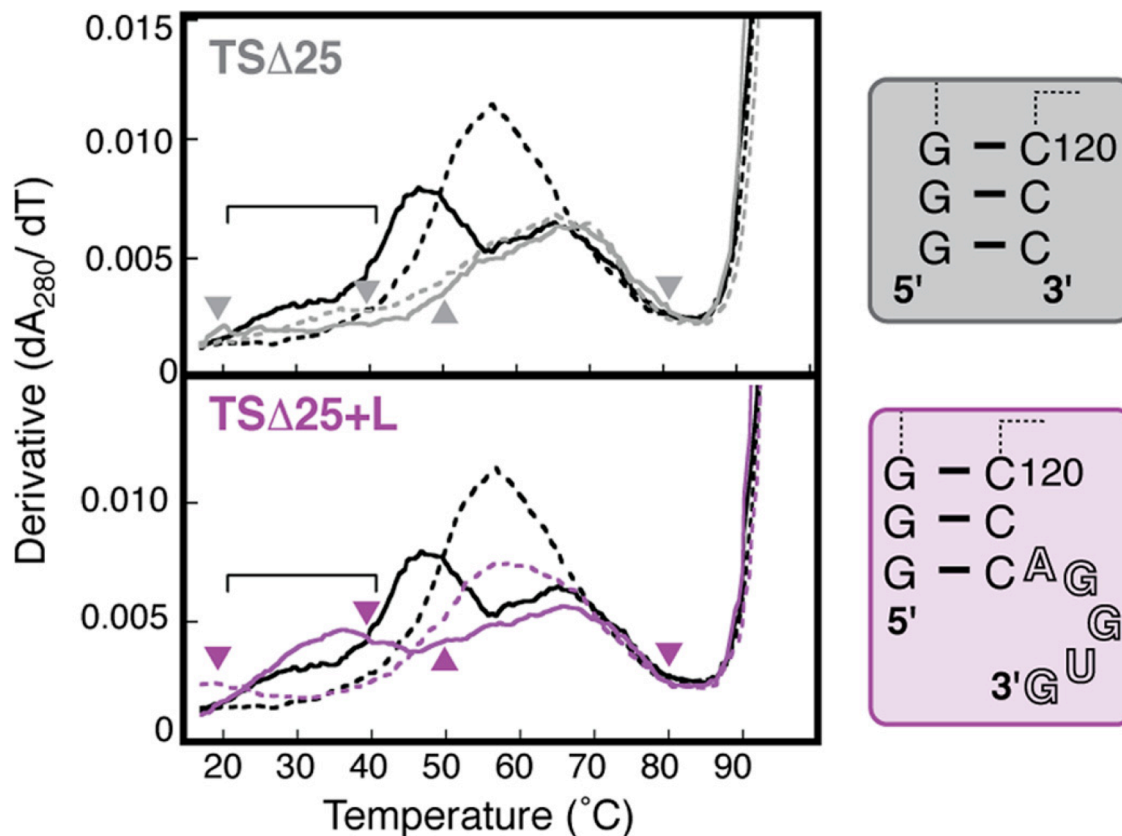


Figure 4 Loop III nucleotides 123-127 are sufficient to form the Central Domain pseudoknot structure. Melting profiles of TS Δ 25+L (purple) and TS Δ 25 (grey) RNAs shown at pH 7.5 (solid line) and pH 5.5 (dashed line) and compared to those of TS Δ 21 RNA (black). The region corresponding to unfolding of the pH-dependent tertiary structure present in TS Δ 25+L RNA, but absent in TS Δ 25 RNA is marked with a horizontal bar. Arrowheads on each profile denote temperatures used for SHAPE probing of the corresponding RNA. Loop III nucleotides are shown in outline font in the structure of TS Δ 25+L RNA (boxed, right).

Conformational heterogeneity within the mutant VA RNA_I Central Domain—The substantial changes in melting profile between TS Δ 21 and the TS Δ 25/ TS Δ 25+L constructs prompted us to explore the Central Domain secondary structures of these new RNAs using SHAPE. As before, each RNA structure was probed at pH 7.5 at

temperatures corresponding to boundaries of apparent transitions for Central Domain unfolding (marked with arrowheads in **Fig. 4**). Reactions were performed at 20 and 50 °C to identify changes corresponding to the broad lower temperature apparent transition, and at 85 °C to identify additional changes that occur upon complete Central Domain unfolding (**Fig. 5**). Each RNA was also probed at 40 °C, to allow direct comparison to the equivalent experiments with TSΔ21 RNA (probed at 20 and 40 °C; **Fig. 2**).

The temperature-dependent SHAPE reactivities of nucleotides in Loop II (nts 105-107) and the 3'-side of Loop III (nts 124-128) in TSΔ25+L RNA are very similar to those observed for TSΔ21 RNA. These two regions show lower than expected reactivity with NMIA at 20°C, and a concomitant increase in reactivity at 50 °C where the tertiary, but not secondary structures, are unfolded (**Fig. 5A,B**). This suggests that these nucleotides maintain tertiary pairing interactions that, in conjunction with a protonated A123, participate in the formation of the Central Domain tertiary structure of TSΔ25+L RNA. In further support of this, in TSΔ25 RNA where the 3'-end nucleotides of Loop III are deleted, the reactivity of Loop II nucleotides is high even at 20 °C (**Fig. 5D,E**). While the Loop II-Loop III pseudoknot interaction appears to be maintained in TSΔ25+L RNA, other substantial changes in nucleotide flexibility are observed. Both RNAs lack the exceptionally strong reactivity of Loop I (nts 115-117) in TSΔ21 RNA. Additionally, much higher than expected SHAPE reactivity is observed for the 3'-half of the Central Domain stem loop (nts 108-114) even at the lowest temperature. This implies that in both TSΔ25 and TSΔ25+L RNAs these nucleotides are not base paired with nts 94-99, suggesting that the changes in secondary structure of these RNAs are more complex than

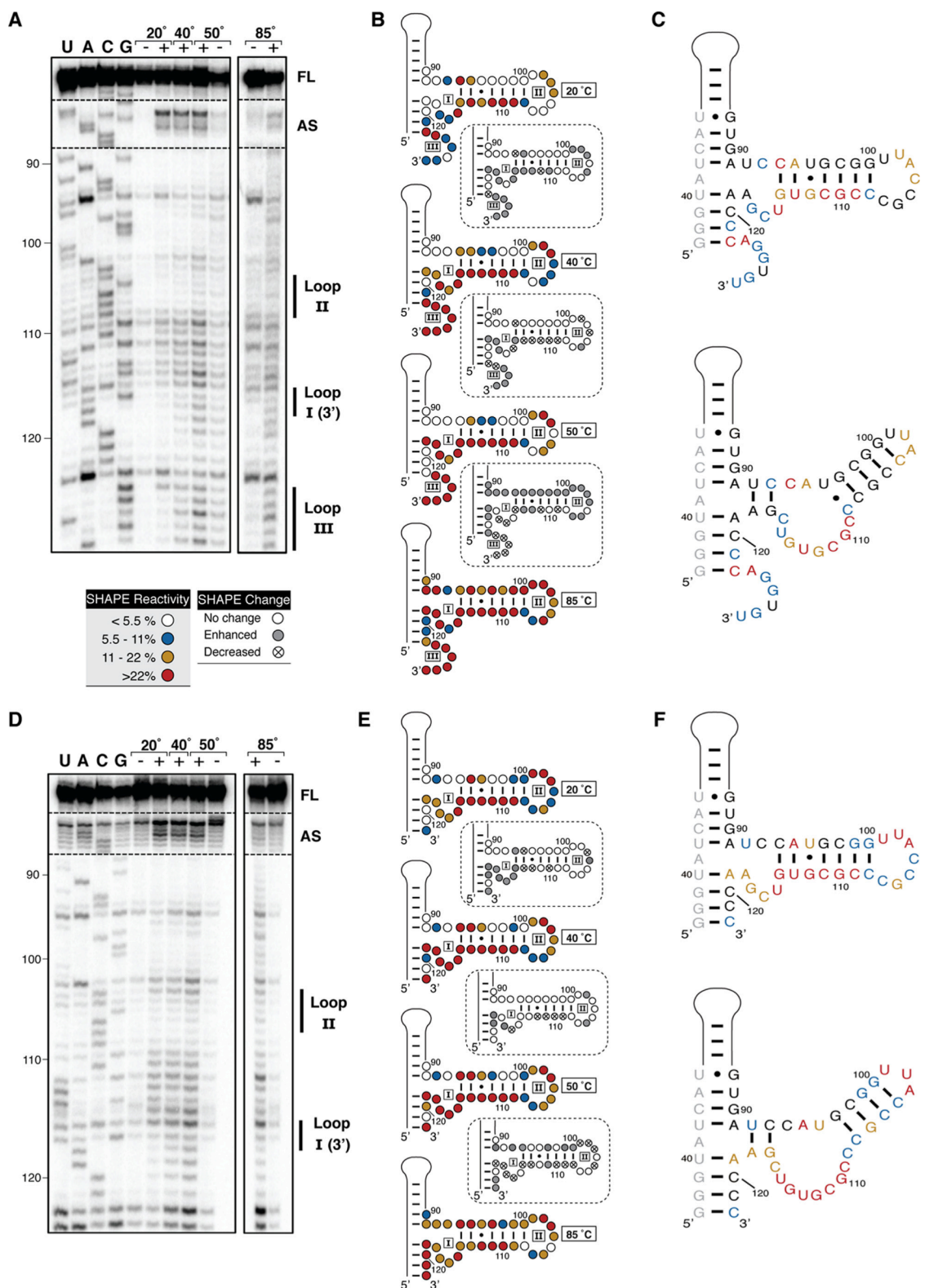


Figure 5 SHAPE analysis of TSΔ25+L and TSΔ25 RNAs. *A*, Representative gel showing SHAPE probing of TSΔ25+L RNA at temperatures below (20 °C), between (40 and 50 °C), and above (85 °C) the apparent transitions corresponding to the unfolding of the Central Domain structure. Lanes with (+) and without (-) SHAPE reagent (NMIA) and RT reactions with dideoxynucleotides (U, A, C, G) for RNA sequencing are indicated. VA RNA₁ nucleotide numbering is shown on the *left*, and bands corresponding to Central Domain Loops I-III, the Apical Stem (AS) loop, and full-length product (FL) are indicated on the *right*. *B*, Quantification of SHAPE reactivity from low to high temperature (*top* to *bottom*), with relative changes shown between each pair of temperatures (*dashed boxes*). Normalized band intensities were averaged from three sets of reactions and categorized according to the reactivity key shown. *C*, Nucleotide flexibility at 20 °C mapped on the nucleotide sequence of TSΔ25+L RNA in the currently established Central Domain secondary structure (*top*) and redrawn based on observed SHAPE reactivities. *D*, *E*, and *F*, As *panels A-C* for TSΔ25 RNA.

a simple erasure of nucleotides from the model of TSΔ21 (**Fig. 5C,F, top**). We therefore revised the secondary structure models of these RNAs to reflect our experimentally determined nucleotide flexibilities (**Fig. 5C,F, bottom**).

As TSΔ25+L RNA appears to retain only some elements of the Central Domain structure, we next asked whether PKR could directly influence its structure. We hypothesized that PKR binding to TSΔ25+L RNA might result in reorganization of the Central Domain to resemble that of TSΔ21 RNA such that both RNAs ultimately use the same structure to inhibit PKR. This, however, was not the case, as we found the structure of TSΔ25+L RNA determined by SHAPE to be identical in the absence or presence of PKR (data not shown). We conclude that TSΔ25+L and TSΔ25 RNAs adopt a Central Domain secondary structure, distinct from TSΔ21 RNA, that is maintained when bound by PKR,

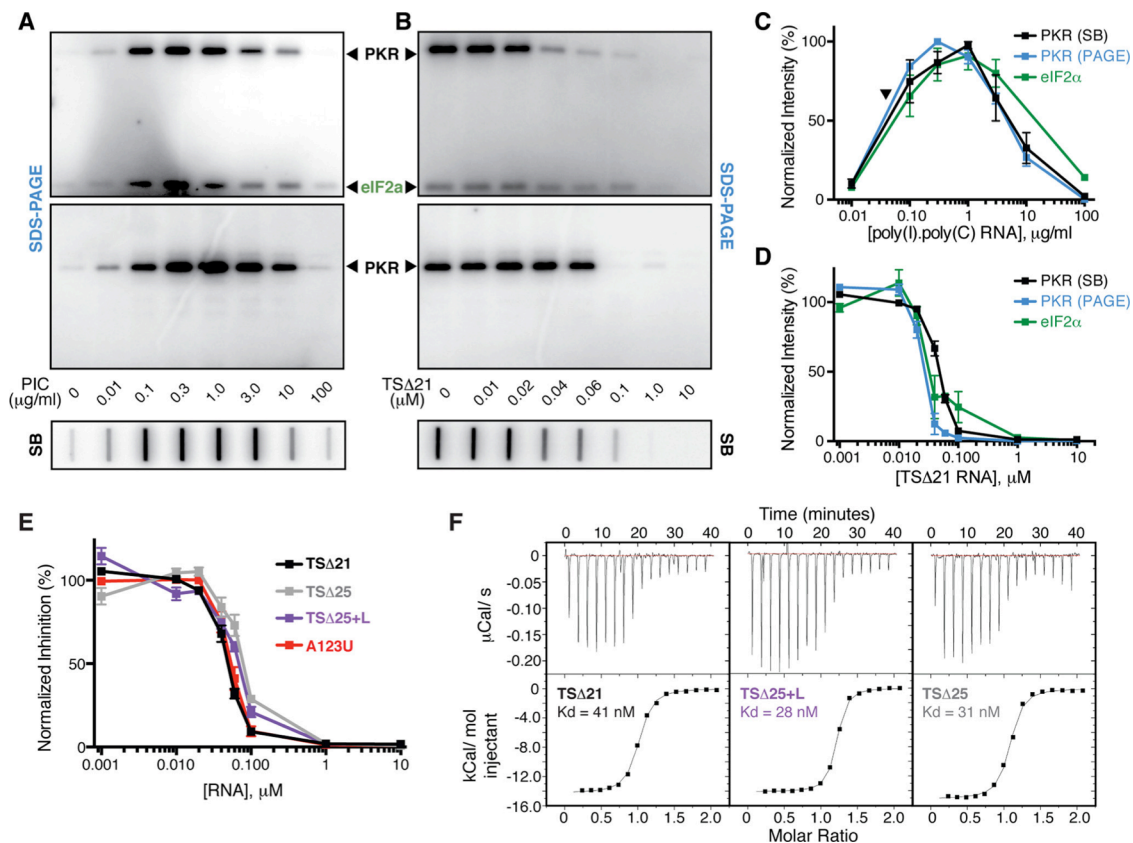


Figure 6 The intact VA RNA₁ Central Domain tertiary structure is not required for PKR

inhibition or binding. *A*, Comparison of representative assays of phosphorylation activation by poly(I)•poly(C) dsRNA in the presence of [γ^{32} P]-ATP with PKR/ eIF2 α (*top*) and PKR alone (*middle*) using SDS-PAGE, and with PKR alone (*bottom*) using the newly established slot blot method (SB). *B*, As *panel A*, but for inhibition of phosphorylation by TSA Δ 21 RNA. *C*, *D*, Quantification of replicate experiments shown in *panels A* and *B*, respectively, demonstrating the reproducibility of the approach and correlation between PKR autophosphorylation (blue, SDS-PAGE; black, slot blot) and phosphorylation of the substrate eIF2 α (green). The black arrowhead in *panel C* indicates the concentration of PKR used in all subsequent kinase inhibition assays. *E*, Quantification of [γ^{32} P]-ATP slot blot PKR autophosphorylation inhibition assays using the VA RNA₁ variants: TSA Δ 21, TSA Δ 25, TSA Δ 25+L, and A123U RNAs at a fixed concentration of poly(I)•poly(C) dsRNA activator. *F*,

The VA RNA₁ Central Domain tertiary structure is not required for PKR inhibition—
TSA Δ 21 RNA is an effective inhibitor of PKR despite lacking the entire terminal stem of

wild-type VA RNA_I (8). Additionally, recent evidence demonstrates that the Central Domain acts in concert with the Apical Stem to initiate Mg²⁺-dependent, high-affinity PKR binding (37), in addition to its established role in inhibition. Having established the minimal context in which the VA RNA_I Central Domain adopts a pH-dependent tertiary structure (TSA Δ 25+L RNA) and a small deletion that eliminates it (TSA Δ 25 RNA), we next used these RNAs to directly test the role of the Central Domain tertiary structure in PKR inhibition. To assess the activity of each RNA, we developed a PKR inhibition assay using a slot blot apparatus analogous to the established SDS-PAGE analysis, but allowing for higher throughput (see Experimental Procedures). This new assay was first validated by comparative analysis of PKR activation (autophosphorylation) by poly(I)•poly(C) dsRNA and inhibition by TSA Δ 21 RNA between SDS-PAGE and the slot blot apparatus (**Fig. 6A,B**). For both activation and inhibition, results obtained by each method were essentially identical (**Fig. 6C,D**). Additionally, we confirmed that inhibition of eIF2 α substrate phosphorylation by TSA Δ 21 RNA correlates well with PKR inhibition (**Fig. 6A-D**), solidifying our ability to link *in vitro* PKR activation to eIF2 α modification and shut-down of general translation. As expected, with its intact pH-dependent tertiary structure, TSA Δ 25+L RNA inhibited PKR almost as well as TSA Δ 21 (**Fig. 6E**). Surprisingly, however, TSA Δ 25 RNA, which lacks the pH-dependent tertiary structure, also inhibited PKR equally well. To test the possibility that the altered secondary structure of these two RNAs might be responsible for this unexpected activity, we tested the A123U mutant, which lacks the pH-dependent Central Domain tertiary structure within the TSA Δ 21 context. We found that A123U RNA also retains full inhibitory activity against PKR, comparable to TSA Δ 21 (**Fig. 6E**). This result excludes the Central Domain structural

rearrangements as the origin of the activity of these RNAs in the absence of tertiary structure. Correlating with the comparable activity of these RNAs against PKR, we found that PKR binding affinity was not significantly altered by the presence or absence of the tertiary structure (K_d 28-41 nM; **Fig. 6F**).

From these data, we conclude that the Central Domain tertiary structure does not contribute to PKR binding and is not required for full inhibition of PKR. Taken together, SHAPE probing and these functional analyses suggest that substantially different secondary structures can be appended to the VA RNA_I Apical Stem to produce potent PKR inhibitors. This observation is significant as it explains how activity against PKR is maintained despite extensive variation in the VA RNA_I Central Domain sequence and secondary structure among different adenovirus serotypes (11).

PKR inhibition requires only the VA RNA_I Apical Stem and three-helix junction— Collectively, the results presented above demonstrate that while the VA RNA_I Central Domain possesses a complex tertiary structure, it is not required for PKR inhibition. Given the Central Domain's well-established role in PKR inhibition, the critical question remains: what are the features of the VA RNA_I Central Domain that truly define it as an inhibitor and therefore an effective mechanism for circumventing innate cellular immunity? We made six further mutations in the TSΔ25 RNA context to dissect the contributions made to PKR inhibition by the pair of conserved tetranucleotide sequences within the Central Domain (21), as well as the structures within its 5'- and 3'-halves (**Fig. 7A**). 5'-mut and 5'/3'-bp RNAs contain mutations in the 5'-conserved tetranucleotide

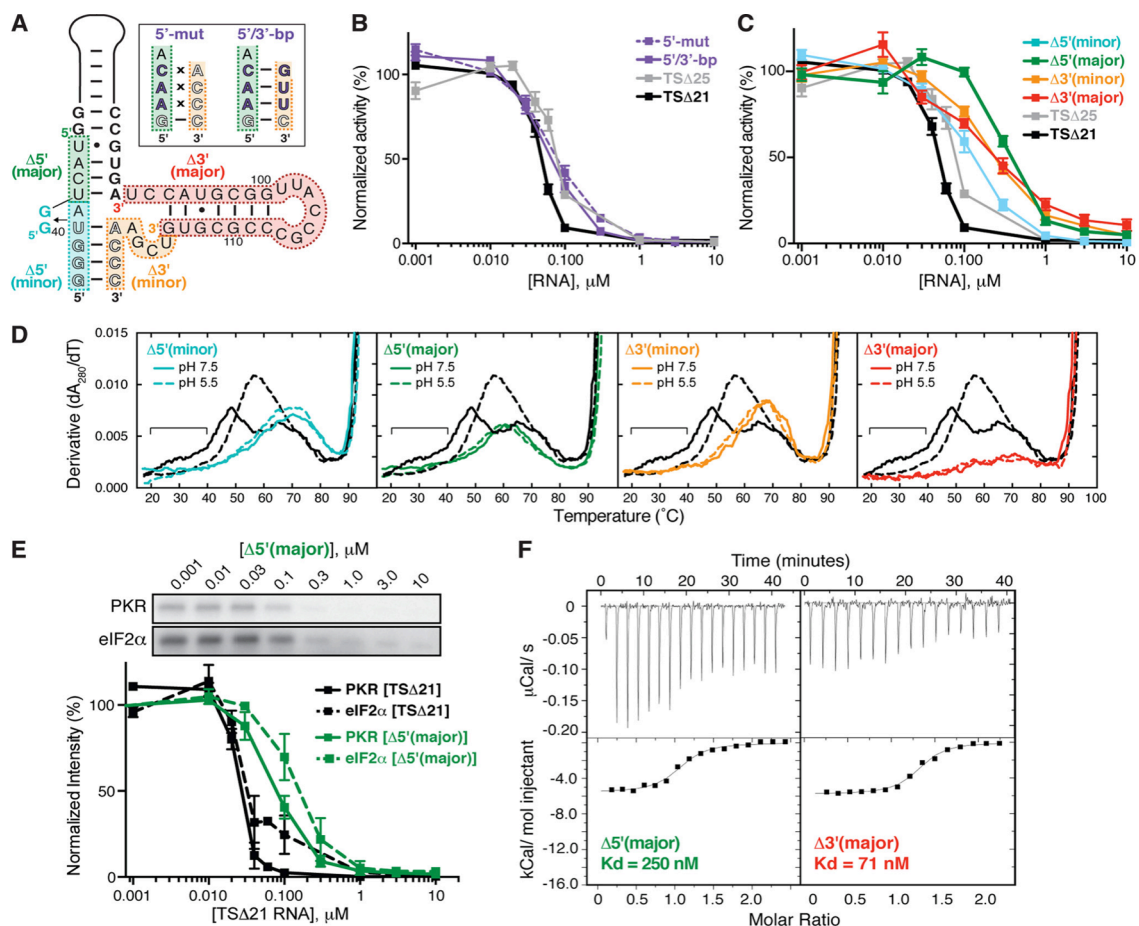


Figure 7 Role of the Central Domain 5'-strand nucleotides and three-helix junction in optimal

PKR inhibition. *A*, VA RNA₁ Central Domain mutants made in the TSΔ25 context: two terminus sequence variants, 5'-mut and 5'/3'-bp RNAs, and four deletion mutants, Δ5'(minor), Δ5'(major), Δ3'(minor), and Δ3'(major) RNAs. *B*, Quantification of slot blot PKR autophosphorylation inhibition assays for the 5'-mut (dashed purple line) and 5'/3'-bp (solid purple line) sequence variants in the presence of [γ ³²P]-ATP and poly(I)•poly(C) dsRNA activator. TSΔ21 (black) and TSΔ25 (gray) are shown for comparison. *C*, As *panel B*, but for the deletion mutants Δ5'(minor) RNA (cyan), Δ5'(major) RNA (green), Δ3'(minor) RNA (orange), and Δ3'(major) RNA (red). *D*, UV melting profiles of each deletion mutant (colored as in *panels A* and *C*). The melting profile for each RNA is shown at pH 7.5 (solid line) and pH 5.5 (dashed line) and compared to those of TSΔ21 RNA (black). The region corresponding to unfolding of the TSΔ21 RNA pH-dependent tertiary structure at pH 7.5 is marked with a horizontal bar. *E*, Representative SDS-PAGE analysis (*top*) and quantification of replicate (*bottom*)

PKR (solid line) and eIF2 α (dashed line) phosphorylation inhibition experiments with $\Delta 5'$ (major) RNA (green) in the presence of poly(I)•poly(C) dsRNA activator and [$\gamma^{32}\text{P}$]-ATP. Equivalent TSA21 RNA data shown for comparison are the same as shown in **Figure 6** (*panel D*). *F*, Representative ITC experiments for titration of PKR into $\Delta 5'$ (major) (*left*) and $\Delta 3'$ (major) (*right*) RNAs.

sequence, without and with compensatory changes on the 3'-side, respectively. Deletion mutants $\Delta 5'$ (minor), $\Delta 5'$ (major), $\Delta 3'$ (minor), and $\Delta 3'$ (major) RNAs lack part or all of one half of the Central Domain. We first assessed the ability of each RNA to inhibit PKR autophosphorylation using the slot blot apparatus as described above. Alteration of the 5'-half of the conserved tetranucleotide sequence with or without compensatory changes in the 3'-half, in 5'/3'-bp and 5'-mut RNAs respectively, had no effect on inhibitory activity compared to TSA25 RNA (**Fig. 7B**). This result was unexpected given the previous demonstration that in the context of the full-length RNA, mutation of these nucleotides caused loss of activity in a cell-based translational rescue assay that could be partially restored by compensatory mutations (21). Additionally, in this previous study these same mutations were found to cause major changes in the nuclease sensitivity of Loops II and III consistent with their role in tertiary structure formation. Despite this discrepancy, the activity of our mutated RNAs in the TSA25 RNA context is consistent with our finding that the tertiary structure plays no role in PKR inhibition and collectively these observations point to additional roles for the Central Domain tertiary structure in a cellular context.

In contrast, each of the Central Domain deletion mutants impacted PKR inhibitory capacity, ranging from a very modest effect with the smaller 5'-end deletion, $\Delta 5'$ (minor),

to the greatest decrease in activity with the larger 5'-end deletion in $\Delta 5'$ (major) (**Fig. 7C**). Both 3'-end deletions had an essentially identical intermediate impact on PKR inhibition. This latter observation suggests that the 3'-half of the Central Domain may contribute to inhibitory activity through its interaction with the critical region located at the base of the Apical Stem on its 5'-side.

Because short hairpin RNAs with single-stranded 5'- and 3'-extensions (ss-ds-RNAs) are dependent upon a 5'-end triphosphate for potent PKR activation (38), we considered the possibility that our $\Delta 5'$ and $\Delta 3'$ variants might resemble such RNAs and activate poorly because their terminal extensions are suboptimal for activation (absent, too short, or base paired). We reasoned that this might result in pseudo-inhibition as the poorer VA RNA₁ mutant activator out competes the more potent poly(I)•poly(C) dsRNA at higher concentrations. However, other than a modest change in the activity of $\Delta 3'$ (minor) RNA, no differences were observed between equivalent RNAs with a 5'-triphosphate or 5'-hydroxyl (generated by CIAP treatment; data not shown).

Each of the four deletions represents a substantial truncation of the Central Domain structure. To assess the global folding of each RNA for any unexpected effects on its structure, we examined the UV melting profile of each RNA (**Fig. 7D**). However, as expected, all four RNAs lack the first (pH-dependent) and second apparent transitions (as for TSA $\Delta 25$ RNA; **Fig. 4**) with further loss of hypochromicity in each of the larger deletions, corresponding to the greater reduction in structural content. With its almost complete deletion of the Central Domain, other than the short single-stranded 5'-end

sequence, $\Delta 3'$ (major) RNA has essentially no hypochromicity in the regions of the profile corresponding to Central Domain unfolding (**Fig. 7D**, *rightmost panel*).

Finally, we assessed the functional impacts of the largest Central Domain deletion mutants. As expected, the ability of $\Delta 5'$ (major) to inhibit downstream phosphorylation of eIF2 α by PKR was markedly decreased, directly correlating with its substantially reduced inhibition of PKR autophosphorylation (**Fig. 7E**). We also measured the binding affinity of $\Delta 5'$ (major) and $\Delta 3'$ (major) RNAs for PKR using ITC. Despite its substantial impact on PKR inhibition, deletion of the entire 3'-half of the Central Domain resulted in only a ~2-fold reduction in affinity while deletion of the 5'-end resulted in a more dramatic decrease in K_d (**Fig. 7F**).

These results, together with the kinase assays, indicate that the 5'-half of the Central Domain is most critical for mediating high affinity PKR binding and conferring full inhibitory activity. While the conserved 5'-side tetranucleotide sequence (nts 37-40) does not appear critical as we had anticipated, the larger deletion in $\Delta 5'$ (major) RNA partially overlaps with an unusually thermodynamically stable region at the base of the Apical Stem that is resistant to denaturation and results in aberrant migration of VA RNA_I in denaturing polyacrylamide gels (27). Whether this structure contributes to binding and/or inhibition will require additional detailed structural characterization of the PKR-VA RNA_I complex. The observation that disconnecting the 5'- and 3'-termini in $\Delta 3'$ (minor) RNA results in as great a reduction in activity as deletion of the entire 3'-half of the Central Domain suggests that the three-helix junction is required for full inhibitory

activity. Whether this is due to direct interactions at the junction or indirectly via optimal positioning of the 5'-strand of the Central Domain also remains to be determined.

Conclusions– The results presented here provide strong evidence for the formation of a pH- and Mg^{2+} -dependent tertiary structure within the adenovirus type 2 VA RNA_I Central Domain. In sharp contrast to our expectation, however, this structure is entirely dispensable for inhibition of PKR. Instead, the Central Domain's overall organization as a three-helix junction, in concert with the 5'-strand at the base of the Apical Stem, is critical for activity. During preparation of this manuscript, two reports were published describing PKR interactions with VA RNA_I using analytical ultracentrifugation and small angle X-ray scattering with molecular modeling (37,39). The observation that the Central Domain contributes to high-affinity PKR binding (37), potentially through placement of dsRBM2 at the helical junction (39), is entirely compatible with our finding of the direct and critical role for the 5'-half of this domain.

Collectively, our results reveal that requirements for RNA-mediated inhibition of PKR are substantially simpler than previously appreciated and highlight the need for an expanded view of RNA features required for PKR inhibition. Our findings offer a satisfying explanation for the ability of VA RNA_I from different serotypes with varying sequences and structures to effectively inhibit PKR and thereby ensure successful viral replication (11). Relaxed criteria in this sense reconcile the inclusion of seemingly disparate non-coding RNAs, such as the Epstein-Barr virus RNA EBER-1 (40) and the cellular RNA nc886 (41), with VA RNA_I in a collection of non-coding RNAs that exert

an inhibitory effect against PKR. In light of our finding that the highly conserved Central Domain structure previously reported as necessary for optimal VA RNA_I-mediated translational rescue (21) has a minimal impact on PKR inhibition, speculation on alternative roles for the VA RNA_I Central Domain raises several intriguing possibilities. For example, the Central Domain tertiary structure might protect the critical region of the helical junction from degradation, could influence Dicer processing of the Terminal Stem (3,4), or may mask structures or sequences that might cause unwanted regulation of other dsRNA binding proteins.

Proteins of the innate immune system must maintain features that render them sufficiently promiscuous for detection of a range of invading viruses, and yet not so much so that they elicit an autoimmune response. That an even wider range of structures than anticipated can fulfill an inhibitory role is in agreement with multiple lines of evidence pointing to the functional flexibility of PKR in its interactions with activating and inhibitory RNAs.

REFERENCES

1. Mathews, M. B., and Shenk, T. (1991) Adenovirus virus-associated RNA and translation control. *J. Virol.* **65**, 5657-5662
2. Garcia, M. A., Gil, J., Ventoso, I., Guerra, S., Domingo, E., Rivas, C., and Esteban, M. (2006) Impact of protein kinase PKR in cell biology: from antiviral to antiproliferative action. *Microbiol. Mol. Biol. Rev.* **70**, 1032-1060
3. Andersson, M. G., Haasnoot, P. C. J., Xu, N., Berenjian, S., Berkhout, B., and Akusjarvi, G. (2005) Suppression of RNA interference by adenovirus virus-associated RNA. *J. Virol.* **79**, 9556-9565
4. Lu, S. H., and Cullen, B. R. (2004) Adenovirus VA1 noncoding RNA can inhibit small interfering RNA and microRNA biogenesis. *J. Virol.* **78**, 12868-12876
5. Aparicio, O., Carnero, E., Abad, X., Razquin, N., Guruceaga, E., Segura, V., and Fortes, P. (2010) Adenovirus VA RNA-derived miRNAs target cellular genes involved in cell growth, gene expression and DNA repair. *Nucleic Acids Res.* **38**, 750-763
6. Aparicio, O., Razquin, N., Zaratiegui, M., Narvaiza, I., and Fortes, P. (2006) Adenovirus virus-associated RNA is processed to functional interfering RNAs involved in virus production. *J. Virol.* **80**, 1376-1384
7. Kamel, W., Segerman, B., Oberg, D., Punga, T., and Akusjarvi, G. (2013) The adenovirus VA RNA-derived miRNAs are not essential for lytic virus growth in tissue culture cells. *Nucleic Acids Res.* **41**, 4802-4812
8. Wahid, A. M., Coventry, V. K., and Conn, G. L. (2008) Systematic deletion of the Adenovirus-associated RNAI terminal stem reveals a surprisingly active RNA

- inhibitor of double-stranded RNA-activated protein kinase. *J. Biol. Chem.* **283**, 17485-17493
9. Desai, S. Y., Patel, R. C., Sen, G. C., Malhotra, P., Ghadge, G. D., and Thimmappaya, B. (1995) Activation of interferon-inducible 2'-5' oligoadenylate synthetase by adenoviral VAI RNA. *J. Biol. Chem.* **270**, 3454-3461
 10. Meng, H., Deo, S., Xiong, S., Dzananovic, E., Donald, L. J., van Dijk, C. W., and McKenna, S. A. (2012) Regulation of the interferon-inducible 2'-5'-oligoadenylate synthetases by adenovirus VA(I) RNA. *J. Mol. Biol.* **422**, 635-649
 11. Ma, Y. L., and Mathews, M. B. (1996) Structure, function, and evolution of adenovirus-associated RNA: A phylogenetic approach. *J. Virol.* **70**, 5083-5099
 12. Ma, Y. L., and Mathews, M. B. (1993) Comparative analysis of the structure and function of Adenovirus virus associated RNAs. *J. Virol.* **67**, 6605-6617
 13. Furtado, M. R., Subramanian, S., Bhat, R. A., Fowlkes, D. M., Safer, B., and Thimmappaya, B. (1989) Functional dissection of Adenovirus VAI RNA. *J. Virol.* **63**, 3423-3434
 14. Clarke, P. A., and Mathews, M. B. (1995) Interactions between the double stranded RNA binding motif and RNA - definition of the binding site for the interferon-induced protein kinase DAI (PKR) on Adenovirus VA RNA. *RNA* **1**, 7-20
 15. Clarke, P. A., Pe'ery, T., Ma, Y. L., and Mathews, M. B. (1994) Structural features of adenovirus 2 virus-associated RNA required for binding to the protein kinase DAI. *Nucleic Acids Res.* **22**, 4364-4374
 16. Ghadge, G. D., Malhotra, P., Furtado, M. R., Dhar, R., and Thimmappaya, B. (1994) In vitro analysis of Virus Associated RNA-I (VAI RNA) - Inhibition of the double

- stranded RNA activated protein kinase PKR by VAI RNA mutants correlates with the in vivo phenotype and the structural integrity of the central domain. *J. Virol.* **68**, 4137-4151
17. Ghadge, G. D., Swaminathan, S., Katze, M. G., and Thimmapaya, B. (1991) Binding of the Adenovirus VAI RNA to the interferon induced 68 kDa protein kinase correlates with function. *Proc. Natl. Acad. Sci. U. S. A.* **88**, 7140-7144
 18. Mellits, K. H., and Mathews, M. B. (1988) Effects of mutations in stem and loop regions on the structure and function of Adenovirus VA RNA1. *EMBO J.* **7**, 2849-2859
 19. Spanggard, R. J., and Beal, P. A. (2001) Selective binding by the RNA binding domain of PKR revealed by affinity cleavage. *Biochemistry* **40**, 4272-4280
 20. Spanggard, R. J., Vuyisich, M., and Beal, P. A. (2002) Identification of binding sites for both dsRBMs of PKR on kinase-activating and kinase-inhibiting RNA ligands. *Biochemistry* **41**, 4511-4520
 21. Ma, Y. L., and Mathews, M. B. (1996) Secondary and tertiary structure in the central domain of adenovirus type 2 VA RNA(I). *RNA* **2**, 937-951
 22. Launer-Felty, K., Wong, C. J., Wahid, A. M., Conn, G. L., and Cole, J. L. (2010) Magnesium-Dependent Interaction of PKR with Adenovirus VAI. *J. Mol. Biol.* **402**, 638-644
 23. Wahid, A. M., Coventry, V. K., and Conn, G. L. (2009) The PKR-binding domain of adenovirus VA RNAI exists as a mixture of two functionally non-equivalent structures. *Nucleic Acids Res.* **37**, 5830-5837

24. Walker, S. C., Avis, J. M., and Conn, G. L. (2003) General plasmids for producing RNA *in vitro* transcripts with homogeneous ends. *Nucleic Acids Res.* **31**, e82
25. Vachon, V. K., and Conn, G. L. (2012) Plasmid template design and *in vitro* transcription of short RNAs within a 'structure cassette' for structure probing experiments. *Methods Mol. Biol.* **941**, 157-169
26. Pe'ery, T., and Mathews, M. B. (1997) Synthesis and purification of single-stranded RNA for use in experiments with PKR and in cell-free translation systems. *Methods-a Companion to Methods in Enzymology* **11**, 371-381
27. Coventry, V. K., and Conn, G. L. (2008) Analysis of adenovirus VA RNA(I) structure and stability using compensatory base pair modifications. *Nucleic Acids Res.* **36**, 1645-1653
28. Wilkinson, K. A., Merino, E. J., and Weeks, K. M. (2006) Selective 2'-hydroxyl acylation analyzed by primer extension (SHAPE): quantitative RNA structure analysis at single nucleotide resolution. *Nat. Protoc.* **1**, 1610-1616
29. Lemaire, P. A., Lary, J., and Cole, J. L. (2005) Mechanism of PKR activation: Dimerization and kinase activation in the absence of double-stranded RNA. *J. Mol. Biol.* **345**, 81-90
30. Merino, E. J., Wilkinson, K. A., Coughlan, J. L., and Weeks, K. M. (2005) RNA structure analysis at single nucleotide resolution by selective 2'-hydroxyl acylation and primer extension (SHAPE). *J. Am. Chem. Soc.* **127**, 4223-4231
31. Fowlkes, D. M., and Shenk, T. (1980) Transcriptional control regions of the adenovirus VAI RNA gene. *Cell* **22**, 405-413

32. Hargittai, M. R., and Musier-Forsyth, K. (2000) Use of terbium as a probe of tRNA tertiary structure and folding. *RNA* **6**, 1672-1680
33. Leontis, N. B., and Westhof, E. (2001) Geometric nomenclature and classification of RNA base pairs. *RNA* **7**, 499-512
34. Petrov, A. I., Zirbel, C. L., and Leontis, N. B. (2011) WebFR3D--a server for finding, aligning and analyzing recurrent RNA 3D motifs. *Nucleic Acids Res.* **39**, W50-55
35. Ben-Shem, A., Garreau de Loubresse, N., Melnikov, S., Jenner, L., Yusupova, G., and Yusupov, M. (2011) The structure of the eukaryotic ribosome at 3.0 Å resolution. *Science* **334**, 1524-1529
36. Klein, D. J., Moore, P. B., and Steitz, T. A. (2004) The roles of ribosomal proteins in the structure assembly, and evolution of the large ribosomal subunit. *J. Mol. Biol.* **340**, 141-177
37. Launer-Felty, K., and Cole, J. L. (2014) Domain interactions in adenovirus VAI RNA mediate high-affinity PKR binding. *J. Mol. Biol.* **426**, 1285-1295
38. Nallagatla, S. R., Hwang, J., Toroney, R., Zheng, X., Cameron, C. E., and Bevilacqua, P. C. (2007) 5'-triphosphate-dependent activation of PKR by RNAs with short stem-loops. *Science* **318**, 1455-1458
39. Dzananovic, E., Patel, T. R., Chojnowski, G., Boniecki, M. J., Deo, S., McEleney, K., Harding, S. E., Bujnicki, J. M., and McKenna, S. A. (2014) Solution conformation of adenovirus virus associated RNA-I and its interaction with PKR. *J. Struct. Biol.* **185**, 48-57
40. Sharp, T. V., Schwemmler, M., Jeffrey, I., Laing, K., Mellor, H., Proud, C. G., Hilse, K., and Clemens, M. J. (1993) Comparative analysis of the regulation of the

- interferon-inducible protein kinase PKR by Epstein Barr virus RNAs EBER-1 and EBER-2 and Adenovirus VA(I) RNA. *Nucleic Acids Res.* **21**, 4483-4490
41. Jeon, S. H., Lee, K., Lee, K. S., Kunkeaw, N., Johnson, B. H., Holthausen, L. M., Gong, B., Leelayuwat, C., and Lee, Y. S. (2012) Characterization of the direct physical interaction of nc886, a cellular non-coding RNA, and PKR. *FEBS Lett.* **586**, 3477-3484

ACKNOWLEDGEMENTS

We thank Dr. Christine M. Dunham for critical reading of the manuscript and discussions and members of the Conn and Dunham laboratories for discussions.

FUNDING

*This work was supported by NIH grant R21-AI097803 and a grant from the Emory University Research Council (URC 2010050). The Auto-iTC₂₀₀ instrument was purchased with support from the NSF MRI program (grant 104177), the Winship Cancer Institute's shared resource program and the Biochemistry Department of Emory University.

²To whom correspondence should be addressed: Graeme L. Conn, Department of Biochemistry, Emory University School of Medicine, 1510 Clifton Road NE, Atlanta GA 30322, USA., Tel.: (404) 727-5965; Fax: (404) 727-2738; E-mail: gconn@emory.edu.

³The abbreviations used are: PKR, double-stranded RNA-activated protein kinase; Ad2, adenovirus type 2; VA RNA_I, 'virus-associated RNA I'; TS, terminal stem; CIAP, Calf intestinal alkaline phosphatase; *NMIA*, N-methylisatoic anhydride.

CHAPTER 5:

A novel RNA molecular signature for activation of 2'-5' oligoadenylate synthetase-1.

The following Chapter has been published:

Vachon, V.K., Calderon, B.M. and Conn, G.L. (2015). A novel RNA molecular signature for activation of 2'-5' oligoadenylate synthetase. *Nucleic Acids Res.* 43(1):544-552

I am responsible for generating the data presented all figures. nc886 RNA for use in assays was prepared by Brenda M. Calderon.

ABSTRACT

Human 2'-5' oligoadenylate synthetase-1 (OAS1) is central in innate immune system detection of cytoplasmic double-stranded RNA (dsRNA) and promotion of host antiviral responses. However, the molecular signatures that promote OAS1 activation are currently poorly defined. We show that the 3'-end polyuridine sequence of viral and cellular RNA polymerase III non-coding transcripts is critical for their optimal activation of OAS1. Potentiation of OAS1 activity was also observed with a model dsRNA duplex containing an OAS1 activation consensus sequence. We determined that the effect is attributable to a single appended 3'-end residue, is dependent upon its single-stranded nature with strong preference for pyrimidine residues, and is mediated by a highly conserved OAS1 residue adjacent to the dsRNA binding surface. These findings represent discovery of a novel signature for OAS1 activation, the 3'-single-stranded pyrimidine (3'-ssPy) motif, with potential functional implications for OAS1 activity in its antiviral and other anti-proliferative roles.

INTRODUCTION

The cellular innate immune system is the first line of defense against invading pathogens. Innate immunity proteins must detect pathogen-associated molecular patterns (PAMPS) indicative of infection, while still maintaining the stringency required to avoid inadvertent self activation. One potent PAMP is cytosolic double-stranded RNA (dsRNA), produced as a consequence of viral replication (1). This foreign nucleic acid is detected by cellular dsRNA sensors, such as the 2'-5' oligoadenylate synthetase (OAS) family of enzymes, each with distinct but overlapping specificities, which elicit host

antiviral responses (2-6). Activated OAS1 synthesizes 2'-5'-linked oligoadenylate (A(2'-5'A)_n) second messengers which then activate their only known target, the latent cellular ribonuclease RNase L, to shut down synthesis of host and viral proteins, thereby preventing viral replication.

The molecular evolution of this host system for efficient detection of viruses is countered by co-evolution of viral strategies to thwart the effects of these antiviral proteins. In the case of OAS, these viral strategies include direct inhibition, sequestration of dsRNA, 2'-5' phosphodiesterases, and production of 2'-5' analogs (7-10). This variety and abundance of viral countermeasures highlights the central importance of the OAS/ RNase L antiviral pathway. Indeed, viral mRNA susceptibility to RNase L cleavage is correlated with virus fitness (11), and susceptibility to viruses such as West Nile Virus and Dengue Virus can be mapped to polymorphisms in OAS isoform 1 (OAS1) (12,13). In spite of this growing body of evidence that viral evasion of OAS is important for effective replication of a range of viruses, many details of molecular control of this enzyme family remain unknown.

OAS1 is activated by cytosolic dsRNA with a minimum length of 17 base pairs (bp) and is strongly dependent on direct interaction with a single guanosine residue near the 3'-end of a previously reported activation consensus motif (WWN₉WG; where W is A or U) (14,15). The recent X-ray crystal structure of human OAS1 bound to a model 18 bp dsRNA duplex revealed that dsRNA binding allosterically drives a functionally essential structural reorganization within OAS1 that narrows the ATP-binding cleft and repositions

a catalytic residue to complete its active site (14). Although this structure allowed for some rationalization of RNA features currently known to activate OAS1 (15,16), the range of RNA structural and sequence motifs that drive OAS1 activation and the contexts in which such sequences function are not well defined.

The non-coding adenoviral associated RNA-I (VA RNA_I) accumulates to high levels in late stages of infection, and is critical for efficient adenoviral replication (17). In contrast to its established potent inhibition of double-stranded RNA-activated kinase (PKR) (18), VA RNA_I activates OAS1 but may be transformed into a pseudoinhibitor by the action of the cellular RNase Dicer (19-21). We therefore selected VA RNA_I as a model system to expand our understanding of the RNA sequences and disparate structural features that regulate OAS1 activity. Our initial analyses of VA RNA_I-mediated activation of OAS1 uncovered an unexpected RNA molecular signature for OAS1 activation, which we term "3'-ssPy." Here, we describe the discovery and mechanistic characterization of this novel potential PAMP recognized by OAS1. Our findings suggest a potential mechanism for innate immune signal amplification by RNase L products, and offer new insight into host-pathogen interaction and the emerging anti-proliferative cellular roles of the OAS/ RNase L pathway.

MATERIAL AND METHODS

RNA *in vitro* transcription

VA RNA_I, EBER-1 RNA and nc886 RNA were *in vitro* transcribed from linearized plasmid DNA templates using T7 RNA polymerase as described previously (22-24). All

in vitro transcribed RNAs, except nc886 RNA, were purified by denaturing PAGE, and recovered as previously described (25). nc886 RNA was annealed in 0.5xTBE buffer containing 10 mM KCl and purified by preparative native PAGE. nc886 bands were identified by UV shadowing, excised from the gel, eluted by ‘crush and soak’ and recovered by ethanol precipitation.

To generate 18 bp dsRNA duplexes, unmodified reverse strand and each forward strand were synthesized using established procedures. Unmodified reverse strand and each forward strand with 0, 1, 2, 4, or 8 uridines at the 3'-end were chemically synthesized (Integrated DNA Technologies) and used without further purification. Forward strands with modified 3'-end uridine residues were chemically synthesized and High Performance Liquid Chromatography (HPLC) purified (Dharmacon). Reverse strand with 5'-triphosphate was *in vitro* transcribed using chemically synthesized DNA template and primer under conditions optimized for short transcripts (26), and purified by denaturing PAGE. To generate duplexes, individual strands were mixed in equimolar concentration and annealed by heating to 85 °C and slowly cooling to 20 °C.

OAS1 expression and purification

Human OAS1 (p41/ E16 isoform) was expressed in *E. coli* BL21(DE3) as a SUMO-OAS1 fusion protein from vector pE-SUMOpro (LifeSensors). Cells for OAS1 expression were grown in Lysogeny Broth (LB) medium at 37 °C to an OD₆₀₀ of 0.4, protein expression induced with 0.1 mM isopropyl β-D-1-thiogalactopyranoside (IPTG) and growth continued overnight at 20 °C. Cells were lysed by sonication in 50 mM Tris-

HCl buffer (pH 8.0) containing 150 mM NaCl, 10 mM imidazole, 1 mM DTT and 10% (v/v) glycerol. Fusion protein was purified by sequential Ni²⁺-affinity and heparin-affinity chromatographies on an ÄKTA Purifier10 system (GE Healthcare). The fusion protein was then dialyzed overnight against SUMO cleavage buffer and cleaved with SUMO protease according to the manufacturer's instructions. Cleavage with SUMO protease leaves a native N-terminus, an important feature of the system as amino acid additions to the N-terminus of OAS1 have been reported to interfere with activity (27).

OAS1 activity assay using radiolabeled ATP

Polymerization of ATP was observed using α -³²P-ATP and resolution of 2',5'-oligoadenylate products by denaturing PAGE. Reactions (10 μ L) contained 1 μ L of 10 μ g/mL OAS1 in 100 mM Tris-HCl, pH7.0, 200 mM NaCl, and 10% glycerol; 5 μ L of 2 \times reaction buffer (40 mM Tris-HCl, pH 7.4, 40 mM magnesium acetate, and 5 mM DTT); 1 μ L of 100 μ M ATP (unless otherwise noted); 0.5 μ Ci of α -³²P-ATP (800 Ci/mmol); and either 18 bp dsRNA at final concentrations of 2, 5, or 10 μ M, or 50 μ g/ μ L poly(I):poly(C) as activating RNA. Reactions were incubated at 30 °C for 3 hours then stopped by addition of 3.5 volumes of a 4:25 (v/v) mixture of 1 M Tris-HCl and gel loading solution (85% formamide, 0.5 \times TBE pH 8.0 and 50 mM EDTA) and heating to 95 °C for 5 minutes. Reaction products were resolved on a 20% polyacrylamide, 50% (w/v) urea, 1 \times TBE PAGE sequencing gel run at 55 W for 1.5 hours. Gels were soaked (water; 10 minutes), fixed (40:10:10% methanol:acetic acid:glycerol; 15 minutes), dried, and then imaged using a Typhoon Trio phosphorimager (GE Healthcare). Band intensities were quantified using ImageQuant software, normalized to the 2'-5' oligoadenylate product of

highest intensity on the gel, and measured values plotted for comparison using Prism 6 (GraphPad).

Chromogenic assay of OAS1 activity

PPi produced as a result of 2',5'-oligoadenylate synthesis was monitored in triplicate using a chromogenic assay adapted from previously established methods for measurement of OAS1 activity (28). OAS1 (300 nM) was incubated with 20 µg/mL poly(I):poly(C), 300 nM non-coding RNA (VA RNA_I, EBER-1, or nc886 RNA), or 1 µM 18 bp dsRNA (unless otherwise stated). These established optimal conditions for OAS1 allowed direct comparisons of activity for RNA and protein sequence variants. Detailed kinetic experiments (measurement of V_{\max} and RNA K_{app}) were performed similarly but using RNA in the range 0.1-3 µM, and OAS1 at 300 nM.

OAS1 (300 nM) was incubated with RNA in the presence of 20 mM Tris-HCl, 7 mM MgCl₂, 1 mM DTT, and 1.5 mM ATP in 150 µL total volume at 37 °C. Aliquots (10 µL) were removed and immediately quenched by adding to 250 mM EDTA (2.5 µL), pre-loaded into the wells of a 96-well plate. At completion of the time course, molybdate reagent (10 µL, 2.5% ammonium molybdate in 2.5 M H₂SO₄), β-mercaptoethanol (10 µL, 0.5 M) and Eikonogen reagent (4 µL, 13 mM 1-amino-2-naphthol-4-sulfonic acid, 25 mM sodium sulfite, and 963 mM sodium meta-bisulfite dissolved in hot water and filter sterilized) were added to each well and the final volume brought to 100 µL with water. Absorbance at 580 nm was measured using a Synergy4 plate reader (BioTek) and readings converted to PPi produced determined by comparison with PPi standards (28).

While our OAS1 protein showed minimal prep-to-prep variability (**Supplementary Fig. S1B**), we did observe a time-dependent decrease in activity after purification. Because this time-dependent decrease in activity resulted in a proportional change in OAS1 activity for all test RNAs and poly(I):(C), comparisons between experimental sets were made after normalizing to the activity of OAS1 in response to an appropriate control RNA used in each set of experiments. Where data are presented as nmols PPi produced, these data were collected in triplicate using a single OAS1 prep.

For kinetic analyses of OAS1 activation, measurements were made at 5, 10 and 20 minute time points as described above, and linear regression analysis used to obtain the nmols PPi produced/ minute for each RNA concentration. Values were plotted using Prism 6 (GraphPad), and curves fit using non-linear regression to obtain V_{\max} and K_{app} values using the Michaelis-Menten model equation $Y = (V_{\max}X)/(K_{\text{app}} + X)$. For data comparing the effect of the 3'-ssPy motif on wild-type versus mutant OAS1 proteins, statistical analysis was by one-way ANOVA with significance assessed by Sidak's multiple comparisons test in Prism 6 (GraphPad).

RESULTS

OAS1 activation is strongly potentiated by the single-stranded 3'-end of VA RNA_I

We created a bacterial expression system to produce recombinant human OAS1 as an N-terminal SUMO protein fusion. Cleavage of the fusion protein with SUMO protease yielded the authentic OAS1 N-terminus and protein which displayed robust activation by

poly(I).poly(C) dsRNA in two complementary assays with low prep-to-prep variability (**Supplementary Fig. S1**). In contrast, our initial experiments failed to recapitulate previous observations of OAS1 activation by VA RNA_I (19,21). Our VA RNA_I *in vitro* transcript differed from those used previously only by the absence of a single-stranded four nucleotide sequence appended to the 3'-end of VA RNA_I (denoted CUUU-3'; **Fig. 1A** and **Supplementary Fig. S2A**) as a consequence of RNA Polymerase III (RNA Pol III) transcription termination *in vivo* (29). This 3'-end single-stranded sequence has no effect on PKR inhibition by VA RNA_I and was removed in our construct as we found this simplified purification of the *in vitro*-transcribed RNA (25,30). Remarkably, restoration of the complete wild-type sequence to include the CUUU-3' sequence dramatically enhanced OAS1 activation (**Fig. 1B** and **Supplementary Fig. S1**).

To understand the unexpected contribution of this sequence to OAS1 activation, we first asked whether the sequence of the single-stranded 3'-end is critical. Three VA RNA_I variants were generated in which the single-stranded CUUU-3' sequence was mutated to alternative pyrimidine-rich (UCCC-3') or purine-rich sequences (GAAA-3' or AGGG-3'). VA RNA_I containing the alternative pyrimidine-rich sequence (UCCC-3') activated OAS1 as effectively as wild-type (**Fig. 1C**). In contrast, each of the two purine-rich 3'-end sequences enhanced activation of OAS1 equally, but not to the same extent as either pyrimidine-rich sequence.

To confirm that the stimulatory effect of the 3'-end sequence is dependent upon it being single stranded, we created a further variant of the UCCC-3' construct with a fully

complementary sequence also appended to the 5' end (5'-GGGA; **Fig. 1C**). The UCCC-3' sequence was selected, rather than the wild-type 3'-end, as its complement retains the necessary 5'-end nucleotides for initiation of T7 RNA polymerase *in vitro* transcription. The ability of this extended base paired VA RNA_I (5'-GGGA/UCCC-3') to activate OAS1 was attenuated to the same extent as when the 3'-single stranded sequence was absent (**Fig. 1C**). Thus, the stimulatory effect of the additional 3'-end sequence does not simply arise through extension of the dsRNA length. Collectively, these results demonstrate that maximal activation of OAS1 by VA RNA_I is dependent upon its 3'-end being both pyrimidine-rich and single-stranded in nature. This is particularly striking given that OAS1 is a tightly controlled enzyme activated exclusively by dsRNA. We term this novel potentiator of OAS1 activation the 3'-single-stranded pyrimidine (3'-ssPy) motif.

The 3'-ssPy motif enhances OAS1 activation by other structured non-coding RNAs and a short dsRNA duplex

To determine whether the enhancement of OAS1 activation by the 3'-ssPy motif is a general phenomenon, we examined the requirement for similar sequences in two other structured RNA Pol III transcripts: the non-coding Epstein-Barr Virus encoded RNA 1 (EBER-1) and the cellular non-coding RNA 886 (nc886) (**Supplementary Fig. S2B and S2C**). Like VA RNA_I, EBER-1 inhibits PKR but activates OAS1 (31). We found that full length EBER-1 activated OAS1 to the same degree as VA RNA_I, and deletion of its single-stranded 3'-end RNA Pol III termination signal (UUUU-3') also dampened its

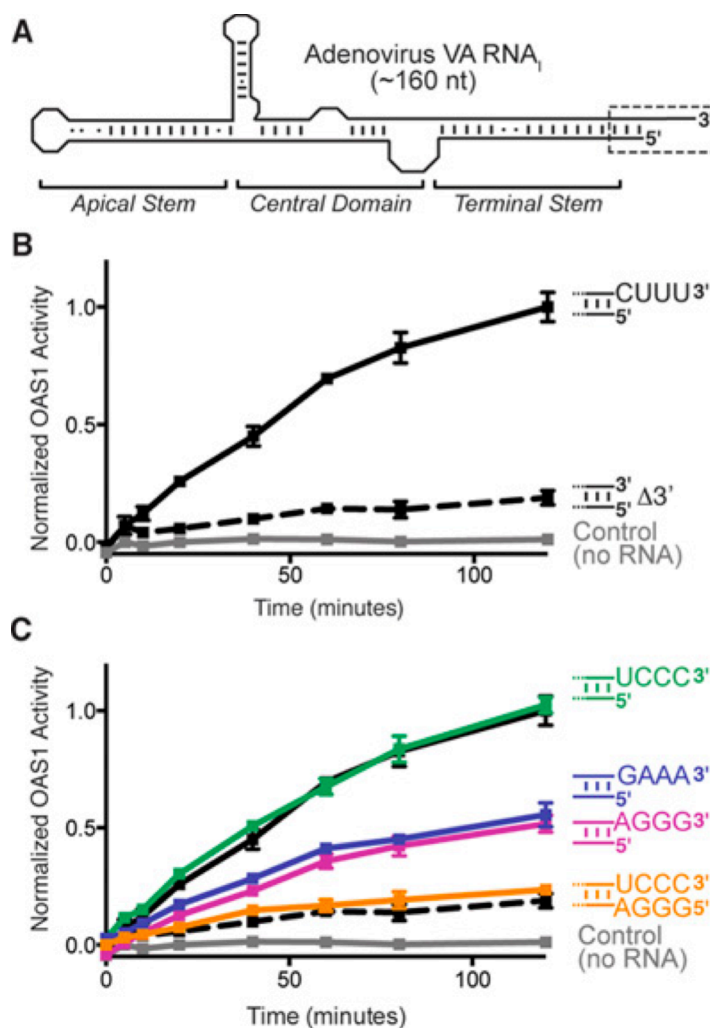


Figure 1 Activation of OAS1 by adenovirus VA RNA₁ requires its single-stranded pyrimidine-rich 3'-end. *(A)* VA RNA₁ secondary structure and domain organization. The Terminal Stem 3'-end contains a single-stranded sequence (CUUU-3'; dashed box and shown as sequence in subsequent panels). *(B)* Chromogenic assay of OAS1 activity shows that deletion of the wild-type 3'-end single-stranded sequence (Δ3'; dashed line) dramatically reduces OAS activation by full-length VA RNA₁ (CUUU-3'; solid line). *(C)* Alternate pyrimidine-rich (UCCC-3') or purine-rich (AGGG-3' or GAAA-3') single-stranded 3'-ends promote full and partial activation of OAS1, respectively. Addition of a complementary 5'-end extension to fully base pair the UCCC-3' sequence (5'-AGGG/UCCC-3') attenuates OAS1 activation to the same extent as when the 3'-end single-stranded sequence is absent. The data in panels B and C are normalized to wild-type VA RNA₁ (CUUU-3').

activity (**Supplementary Fig. S3A**). The cellular transcript nc886 is another potent inhibitor of PKR (32), but its activity against OAS1 was not previously tested. We found that nc886 demonstrates a remarkable ability to activate OAS1 that is again attenuated upon deletion of its UUUU-3' sequence (**Supplementary Fig. S3B**). Together, these results demonstrate that the effect of the 3'-ssPy motif in potentiating OAS1 activity is general among these structurally complex non-coding RNAs.

We next asked whether the 3'-ssPy motif could potentiate OAS1 activation by a simple dsRNA using the model 18 bp duplex cocrystallized with OAS1 (14). In this context, addition of a single-stranded UUUU-3' sequence enhanced OAS1 activation (**Fig. 2**). This pronounced potentiation of OAS1 activity is particularly surprising as the model dsRNA contains a potent activation consensus sequence (15). Thus, the 3'-ssPy motif is effective in potentiating the activity of both non-coding RNAs with complex secondary structures and simple dsRNAs.

Having established that the 3'-ssPy motif is effective in the 18 bp dsRNA duplex, we used this model system to determine the length requirement of the 3'-end single-stranded region for optimal OAS1 activation. We tested activity of the 18 bp dsRNA duplex with 1, 2, 4, or 8 single-stranded uridine residues (**Fig. 2B**) and found that a single uridine residue appended to the 3' end of the dsRNA was sufficient to confer the maximum potentiation of OAS1 activity. No further enhancement of OAS1 activation was observed upon extension of the 3'-end single-stranded sequence. Further, the 3'-ssPy motif cannot exert an effect unless it is appended to a double-stranded helical structure, as neither

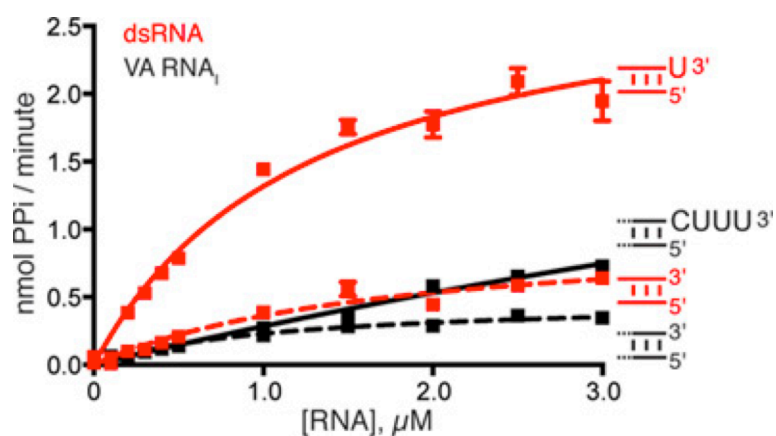


Figure 3 Kinetic analysis of OAS1 activation by RNAs with and without a 3'-ssPy motif. OAS1 activity over a range of VA RNA₁ and 18 bp dsRNA duplex concentrations both with (solid lines) and without (dashed lines) the 3'-ssPy motif (3'-CUUU and 3'-U, respectively). Data were fit using non-linear regression to obtain the kinetic parameters (V_{\max} and K_{app}) shown in **Table 1**.

TABLE 1. Influence of 3'-ssPy on OAS1 activity

RNA	V_{\max} (nmol PPI/min)	K_{app} (RNA) μM
18 bp dsRNA	1.0 ± 0.2	1.8 ± 0.5
18 bp dsRNA(3'-U)	3.0 ± 0.3	1.3 ± 0.3
VA RNA ₁ (Δ CUUU)	0.48 ± 0.05	1.1 ± 0.2
VA RNA ₁	4.0 ± 1.7	13.1 ± 6.6

The 3'-ssPy motif increases OAS1 activity but does not specifically alter A(2'-5'A)_n product lengths

To determine the effect of the 3'-ssPy motif on catalysis of A(2'-5'A)_n synthesis, we performed enzyme kinetic analyses of OAS1 activity with respect to activator RNA concentration. This analysis was performed for both the 18 bp dsRNA duplex and VA RNA_I with and without a 3'-ssPy motif (U-3' and CUUU-3', respectively; **Fig. 3** and **Table 1**). For the 18 bp dsRNA duplex, the presence of the 3'-ssPy motif increased OAS1 V_{\max} by 3-fold but had no apparent effect on RNA affinity (K_{app}). For VA RNA_I, both V_{\max} and K_{app} are increased by the presence of the CUUU-3' sequence by approximately 8- and 12-fold, respectively. The 3'-ssPy-mediated increase in OAS1 V_{\max} with both RNAs suggests that the effect of 3'-ssPy is similar in each context and arises, at least in part, by promoting OAS1 catalytic activity. However, the context specific influence of the 3'-ssPy motif on OAS1-RNA interaction (K_{app}) reflects an apparent decrease in RNA affinity that may be due to the fact that the dsRNA duplex has a single optimal binding orientation whereas VA RNA_I contains multiple potential binding sites of differing affinity and capacity to activate OAS1 (see Discussion).

Relative abundance of A(2'-5'A)_n product length can have significant functional consequences. For example, A(2'-5'A) dimers promote RNase L-mediated ribosomal stop codon readthrough, whereas A(2'-5'A)_{n≥2} oligomers induce its ribonuclease activity (33). The chromogenic assay effectively measures differences in overall OAS1 activity but cannot distinguish inorganic pyrophosphate (PP_i) produced through synthesis of oligoadenyates of specific lengths. Therefore, to determine whether 3'-ssPy influences

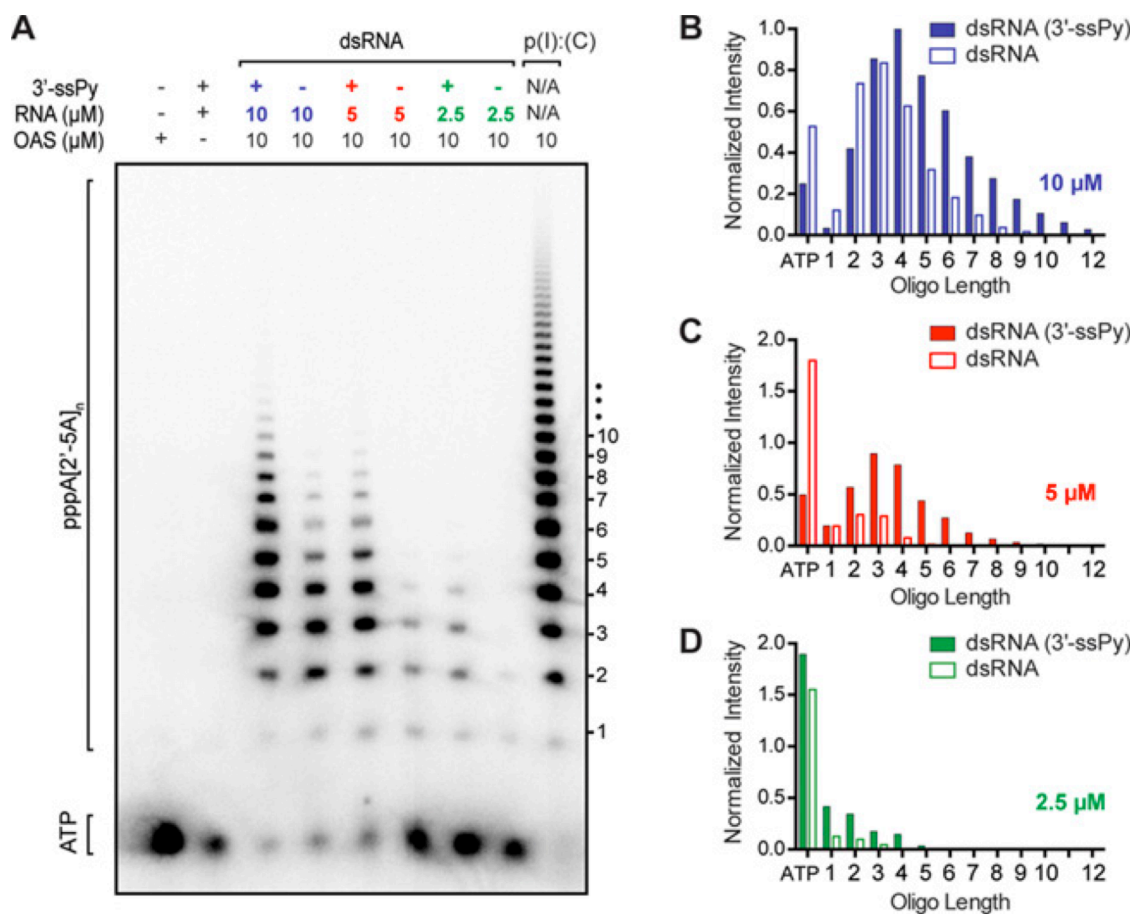


Figure 4 The 3'-ssPy motif causes an increase in OAS1 activity but not an altered accumulation of specific product lengths. *(A)* Phosphorimager analysis of denaturing PAGE showing OAS1 synthesis of 2'-5' oligoadenylates in the presence of 18 bp dsRNA activator with and without the 3'-ssPy motif at three different concentrations (10, 5 and 2.5 μM). OAS1 activation at a single concentration of the known activator poly(I).poly(C) RNA is shown for comparison. *(B-D)* Quantification of 2'-5' oligoadenylate product band intensities in the presence of *(B)* 10 μM , *(C)* 5 μM and *(D)* 2.5 μM 18 bp dsRNA activator with (solid bars) or without (open bars) the 3'-ssPy motif. All bands were normalized to the most intense product band produced (*i.e.*, $n=4$ oligoadenylate in the lane third from left, corresponding to 10 μM dsRNA with a 3'-ssPy). Remaining $\alpha\text{-}^{32}\text{P}\text{-ATP}$ is shown on the far-left of the x-axis.

the distribution of oligoadenylate products, we used denaturing polyacrylamide electrophoresis (PAGE) to separate the products of OAS1 incubated with three different concentrations of 18 bp dsRNA duplex both with and without a 3'-ssPy motif (**Fig. 4**). We found that the stimulatory effect of the 3'-ssPy motif did not result in accumulation of products of specific length. Instead, similar to the general stimulatory effect of increasing the dsRNA activator concentration, at each individual dsRNA concentration the 3'-ssPy motif resulted in higher overall activity and thus production of more oligoadenylate of greater length. Thus, from the two complementary assays of OAS1 activity, the difference between RNAs with and without 3'-ssPy appears to arise through an overall increase in OAS1 activity.

Modifications of the 3'-ssPy ribose distinguish chemical features responsible for mediating OAS1 interactions

Innate immune proteins that sense dsRNA often depend on interactions with the ribose 2'-OH within the structurally open dsRNA minor groove. For example, 2'-OH mediated binding is the primary determinant of dsRNA specificity for PKR (34) and introduction of 2'-O-methyl groups into the 18 bp dsRNA duplex attenuate OAS1 activation (15). To determine whether the 3'-ssPy motif 2'-OH or other feature of ribose is critical for its activity, we prepared 18 bp dsRNA duplexes with one of three chemical modifications in a single 3'-end single-stranded uridine residue: 2'-O-methyl, 2'-deoxyribose, and 3'-phosphate. We compared the ability of the unmodified and modified dsRNAs to activate OAS1 and found that the effect of the 3'-ssPy motif was increased to a small degree by the 2'-O-methyl group, and only minimally attenuated by 2'-deoxyribose (**Fig. 5A**).

However, none of the modifications reduced activity to the level of the duplex lacking the 3'-ssPy.

The presence of a 5'-triphosphate group may also enhance OAS1 activation in some contexts (21). Therefore, each dsRNA duplex was additionally tested with a 5'-end triphosphate group on the complementary strand. The 5'-triphosphate group had no effect on OAS1 activation by the 18 bp dsRNA duplex with or without a 3'-ssPy motif and also did not alter the relative effects of the 3'-ssPy modifications (**Fig. 5B** and **Supplementary Fig. S5**). However, the modest enhancement of OAS1 activation mediated by the 2'-O-methyl modified 3'-ssPy motif was more pronounced in the

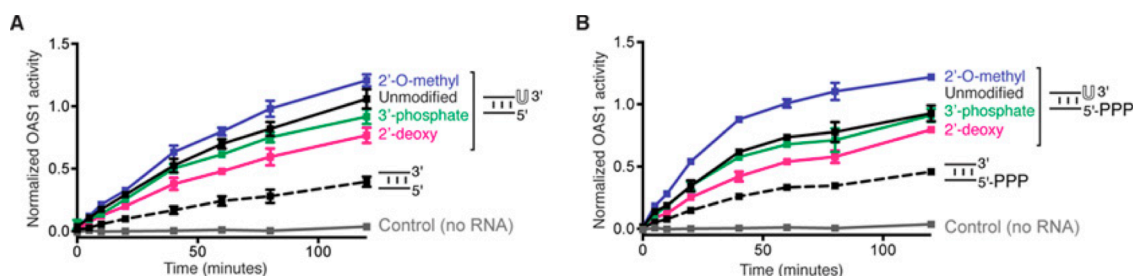


Figure 5 3'-end modifications have minor effects on 3'-ssPy activity, and are relatively unaltered by 5'-ppp on the reverse strand of 18 bp RNA. (A) Assays of OAS1 activation by dsRNA duplexes with chemical modifications to the 3'-ssPy motif ribose group: 2'-O-methyl, 2'-deoxyribose, and 3'-phosphate. dsRNA with unmodified 3'-ssPy (one single-stranded 3'-end uridine) and without a 3'-ssPy motif are shown for comparison. None of the modifications reduced activity to the level of the dsRNA lacking a 3'-ssPy motif but subtle changes in activation suggest an influence of the ribose sugar pucker on 3'-ssPy motif activity. (B) As panel A but for dsRNA duplexes with a 5'-triphosphate group on the complementary strand. The 5'-triphosphate group did not alter relative effects of the modifications on 3'-ssPy motif potency but does appear to modestly enhance activation by the 3'-ssPy motif with 2'-O-methyl ribose modification. In all panels data are normalized to the 18 bp dsRNA with the unmodified 3'-ssPy motif.

presence of a 5'-triphosphate on the complementary strand. Collectively, these results suggest that 3'-ssPy action is not mediated by direct interaction of OAS1 with its ribose 2'-OH group nor is the 3'-phosphate group required. Instead, 3'-ssPy action appears to be more subtly influenced by the ribose conformation as modifications likely to promote A-form (C3'-*endo*; 2'-methyl) or B-form (C2'-*endo*; 2'-deoxy) ribose sugar pucker modestly enhance or attenuate 3'-ssPy motif potency, respectively. Additionally, these results indicate that while viral RNAs are not known to be extensively 2'-O-methylated, such modification of viral or cellular RNAs would not impact activation of OAS1 by the 3'-ssPy motif.

Mutagenesis of OAS1 identifies a critical residue that mediates the effect of the 3'ssPy motif.

Our results show that enhancement of OAS1 activation by the 3'-ssPy motif has preference for a C3'-*endo* sugar pucker and a pyrimidine base but is insensitive to the specific base identity, indicating that the Watson-Crick base edge is not a key determinant of recognition by OAS1. These observations suggested to us that strong shape complementarity between the 3'-ssPy motif and the adjacent OAS1 surface might be most critical, with recognition driven primarily by base stacking and/ or packing of the ribose against the protein surface. We therefore sought to identify OAS1 residues to target for mutagenesis with the goal of revealing protein surface changes that render OAS1 insensitive to the 3'-ssPy motif, while maintaining its response to dsRNA.

To identify candidate residues for mutational analysis, we used ConSurf (35) to examine amino acid conservation among the 30 closest homologs of human OAS1. Two highly conserved regions on opposite sides of OAS1 were identified that correspond to the functionally critical dsRNA-binding surface and OAS1 catalytic center (**Supplementary Fig. S6**). We modeled the likely location of the 3'-ssPy motif by manually appending an additional 3'-end uridine residue and thus identified two smaller conserved patches, residues C54 and D154/G157, in close proximity (**Fig. 6A** and **6B**). Each of these residues was individually mutated to specifically alter the protein surface, and thus potential shape complementarity with the 3'-ssPy motif, by incorporating bulkier (C54Q, D154Q, or G157Q) and smaller side chains (C54A or D154A) at these locations.

We tested the ability of the 18 bp dsRNA duplex with and without the 3' ssPy motif to activate each mutant protein using the chromogenic assay, and compared the initial rate of reaction under the conditions used (**Fig. 6C** and **6D**). Unexpectedly, we found that both mutations at residue C54 enhanced overall OAS1 activity, whereas mutations at D154 had no measurable effect. Critically, however, in each case no effect on the enhancement of OAS1 activation by the 3'-ssPy motif was observed (**Fig. 6D**, compare solid and striped bars for each mutant). In contrast, G157Q reduced overall activation and in addition completely abrogated potentiation of OAS1 activation by the 3'-ssPy motif (**Fig. 6C** and **6D**). We conclude that G157 is critical and that the 3'-ssPy motif may exert its effect via direct contact with the protein surface containing this residue. That the effect of the 3'-ssPy motif may be governed by specific interaction with a short loop containing

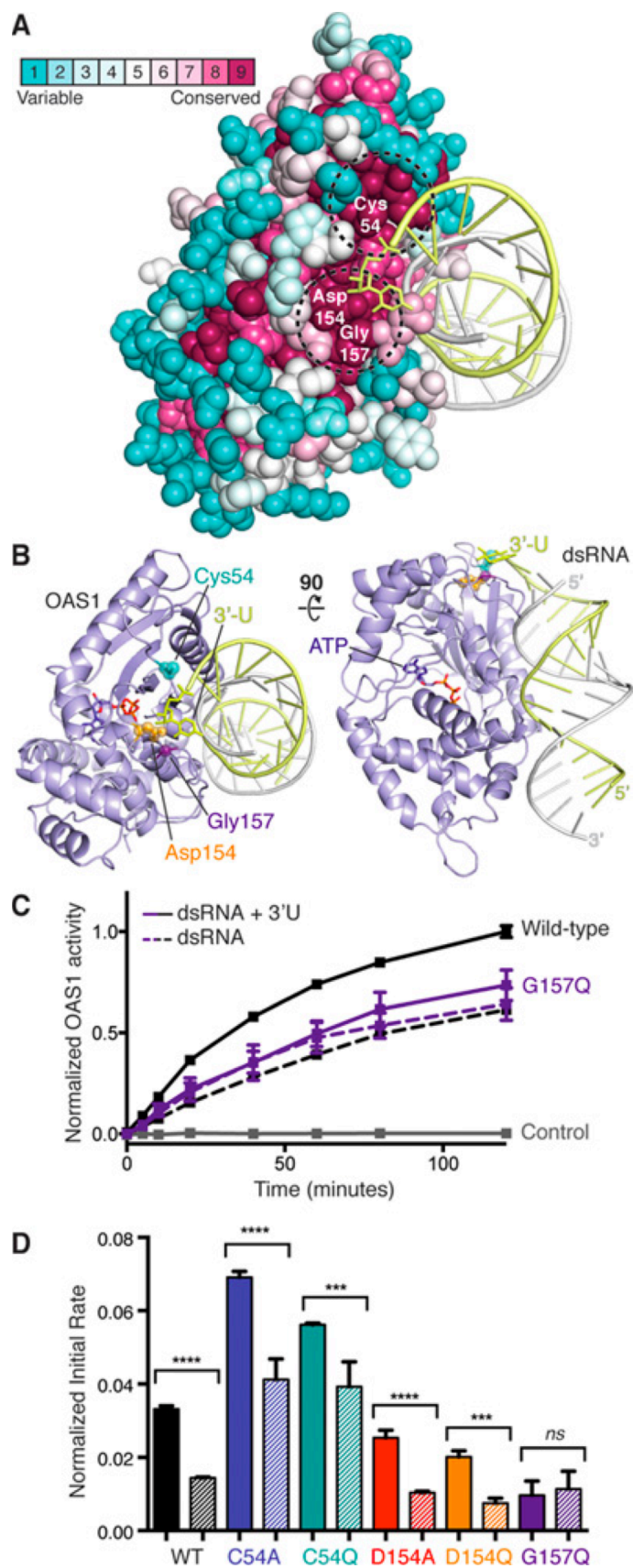


Figure 6 OAS1 G157 is a critical mediator of 3'-ssPy motif action. (A) ConSurf analysis of OAS1 run using the X-ray crystal structure of the human protein (PDB ID: 4IG8) determined in complex with the 18 bp dsRNA duplex. Two highly conserved patches (dashed circles) are located adjacent to the approximate position of the modeled 3'-ssPy motif. (B) Two orthogonal views of the OAS1-dsRNA structure with mutated protein residues and modeled 3'-ssPy motif highlighted. (C) Chromogenic assay showing the effect of the 3'-ssPy on wild-type and G157Q mutant OAS1 activity. (D) Comparison of initial rate of reaction for wild-type and mutant OAS1 proteins activated by the 18 bp dsRNA duplex with (solid bar) or without (striped bar) an additional 3'-end single-stranded uridine residue (3'-ssPy motif). One-way ANOVA: $p \leq 0.0001$ (****), p between 0.0001 and 0.001 (***), and not significant (ns; $p \geq 0.05$). In panels C-D, data are normalized to wild-type OAS1 activation by 18 bp dsRNA with the 3'-ssPy motif.

a single, highly conserved residue reveals a potentially powerful target for manipulation of OAS1 activity.

DISCUSSION

Detection of the molecular hallmarks of invading pathogens and potent activation of the innate immune system are critical for survival of infection. The present work has revealed a novel molecular signature, the 3'-ssPy motif, required for optimal activation of OAS1 by both simple duplex RNAs and highly structured viral or cellular non-coding RNAs. Our results demonstrate that optimal activation of OAS1 by dsRNAs with a 3'-ssPy motif is critically dependent on the single-stranded nature of the motif with strong preference for pyrimidine base. While further studies are necessary to define the impact of the novel 3'-ssPy motif in a cellular context, our findings suggest a previously unappreciated mechanism by which the sensitivity of the OAS1/ RNase L pathway is fine-tuned. Once activated by the products of OAS1, RNase L degrades single-stranded RNAs and single-

stranded regions present within loops or bulges in structured RNAs, preferentially following UA or UU dinucleotide sequences (36). RNase L action thus increases the pool of dsRNA with a 3'-ssPy motif and may sensitize the cell to viral invaders through rapid amplification of OAS1 activity and RNase L-mediated RNA degradation. 3'-ssPy motif action may also underpin the RNase L-dependent amplification observed by others (37). Thus, the present work provides a valuable starting point for future cell-based experiments to define the role of the 3'-ssPy motif in infection.

Our analysis of OAS1 activity promoted by the simple 18 bp dsRNA or the structured non-coding adenoviral transcript VA RNA₁ revealed a significant difference in the effect of the 3'-ssPy motif on apparent OAS1-RNA affinity (K_{app}). The 18 bp dsRNA duplex is optimal in length to span the dsRNA binding surface of OAS1 and also contains an

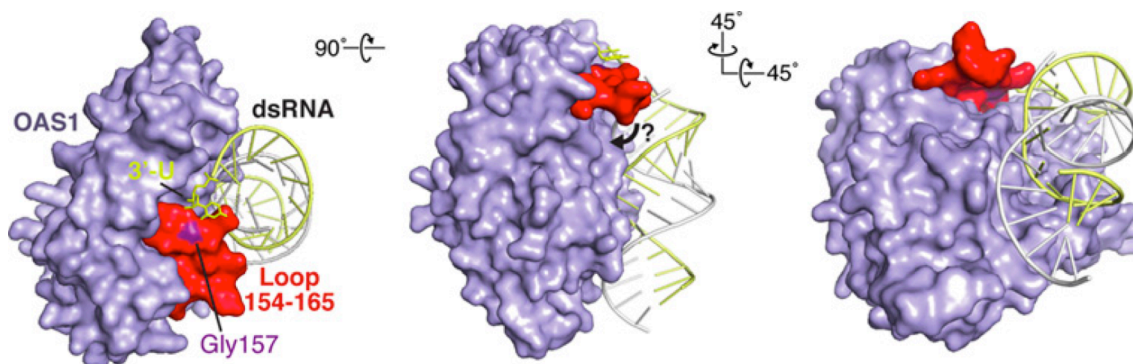


Figure 7 Model for 3'-ssPy motif action. Surface representations of the OAS1-dsRNA complex with modeled 3'-ssPy motif (3'-U). The OAS1 loop comprising residues 154 to 165 and the mutated residue which ablates dependence on the 3'-ssPy motif (Gly157) are highlighted. The three views are related by the rotations shown and the *left* image corresponds to the orientation shown in **Figure 6**. A potential 'closure' of the 154-165 loop mediated by 3'-ssPy interaction at the surface comprising G157 is denoted with an arrow (center image).

activation consensus sequence which likely directs the specific orientation adopted by this RNA (14). Our results show that, in this minimal context, the 3'-ssPy motif does not alter affinity but nonetheless directly promotes enzyme turnover (increased V_{\max}). Such enhancement could arise through a number of mechanisms but we hypothesize that the 3'-ssPy motif enhances promotion of the necessary dsRNA-driven conformational change for catalysis by OAS1 or directly stabilizes the reorganized active structure. This scenario would further fine tune this system, making OAS1 a powerful sensor of the continued presence of cytoplasmic dsRNA. In contrast to the simple dsRNA duplex, for VA RNA_I the 3'-ssPy motif significantly decreased RNA affinity (K_{app}) while increasing OAS1 enzyme activity. RNA binding affinity and potency of OAS1 activation do not necessarily correlate (16). Thus, our observation of the effect of 3'-ssPy on OAS1 activation by VA RNA_I may reflect the fact that larger structured RNAs may possess multiple, potentially overlapping OAS1 sites, each with a distinct capacity to activate OAS1. The presence of the 3'-ssPy motif may direct OAS1 to the double-stranded terminal region of VA RNA_I over otherwise preferred binding sites with a lower potential for OAS1 activation. Further studies of OAS1-RNA interaction are needed to complete our understanding of OAS1 binding and activation by dsRNA. Such studies of structured RNAs may also be a useful tool in the search for additional RNA sequences or structures that can potently activate or inhibit OAS1.

Mutagenesis of OAS1 identified a single residue change, G157Q, that specifically ablated the effect of the 3'-ssPy motif. G157 is located in a short loop structure adjacent to the dsRNA binding surface which makes limited contact with the surrounding protein surface

(14) (**Fig. 7**). We suggest that the 3'-ssPy motif promotes interaction of this surface loop with other structural elements of OAS1 to promote the active state and that this loop may represent a potential novel target for therapeutic manipulation of OAS1 activity. OAS1 serum levels have been correlated with positive responses of HCV patients to interferon treatment (38), suggesting that further augmenting the OAS1 response may be beneficial. Additionally, activation of innate immune proteins such as OAS1 concomitant with chemotherapy could bolster patient response and increase survival rates (39).

Discovery of this novel signature for OAS1 activation presents the question of when, other than through viral replication or RNase L action, might dsRNA with the 3'-ssPy motif be present and accessible to OAS1? We found that the cellular nc886 RNA is a remarkably potent activator of OAS1. nc886 is proposed to prevent inadvertent PKR activation but to be displaced from PKR by viral RNA in the infected cell (32). Thus free nc886 may serve to sensitize the antiviral response through potent activation of OAS1. Further, the comparative potency of nc886 may reflect a role in OAS1/ RNase L-mediated cell death in situations when infection has passed the "point of no return." Additionally, aberrant accumulation in the cytoplasm of unprocessed RNA Pol III transcripts, Dicer products with 3'-overhangs or of miRNAs tagged for degradation by 3'-polyuridylation (40,41) could promote OAS1-mediated translational regulation and represent other contexts in which the 3'-ssPy might be important outside of infection. Thus, OAS1 activation may serve as a measure of a cell's suitability for active translation of proteins. In support of this concept is a recent and growing appreciation for OAS1-mediated translational control in cell cycle control, adipocyte differentiation and the role

of RNase L in certain types of cancers (42-44). These diverse roles for OAS further highlight the importance of understanding the specific sequences or structural hallmarks that define an activating RNA as such.

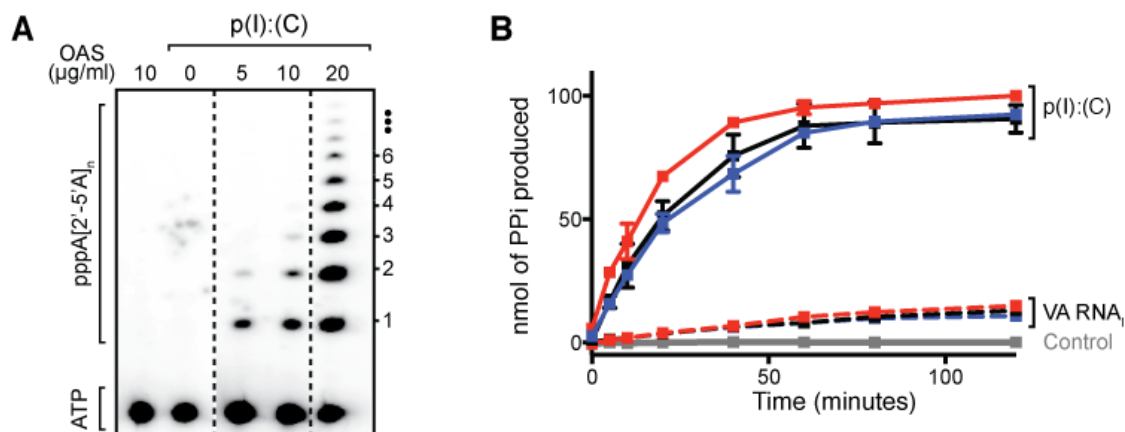
ACKNOWLEDGEMENT

We thank Dr. C. M. Dunham for critical reading of the manuscript and members of the Conn and Dunham groups for useful discussions during the course of this work.

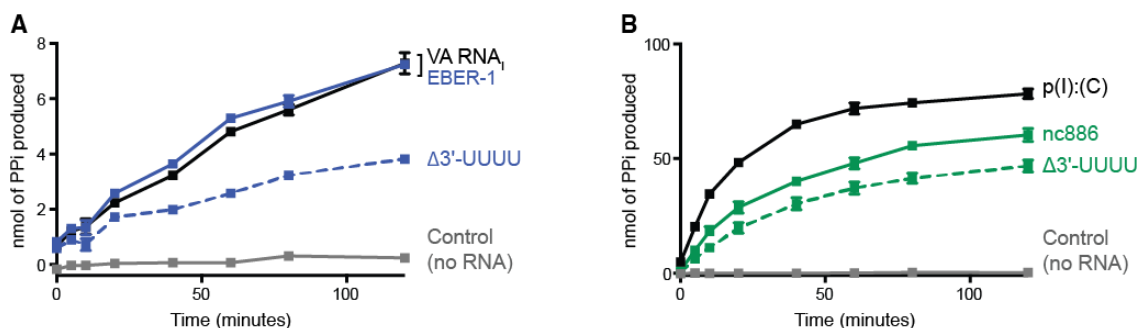
FUNDING

This work was supported by the National Institutes of Health-National Institute of Allergy and Infectious Diseases (R21-AI097803), National Institutes of Health-National Institute of General Medical Science (T32-GM008367) and Emory University Research Council (URC 2010050). Funding for open access charge: Department of Biochemistry, Emory University.

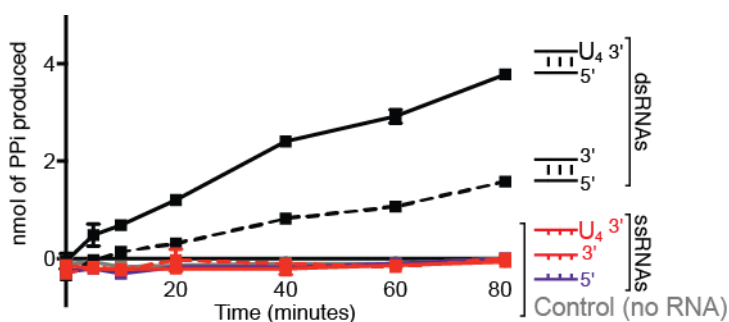
SUPPLEMENTAL FIGURES



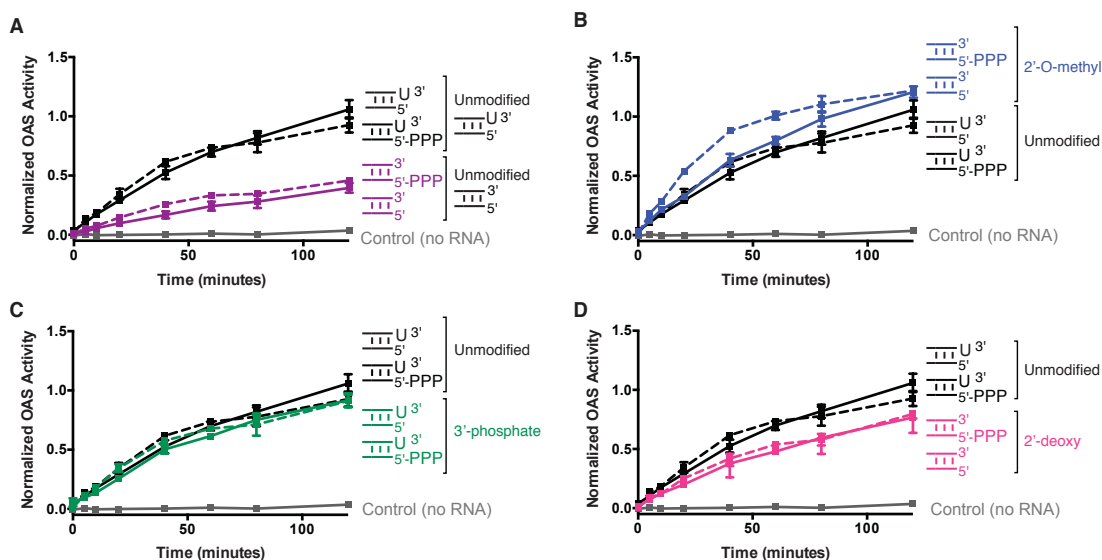
Supplementary Figure S1. Human OAS1 produced by cleavage of the SUMO-OAS1 fusion is active and shows only minimal prep-to-prep variation. (A) Phosphorimager analysis of denaturing PAGE demonstrating that OAS1 produced using the SUMO fusion system responds as expected to the known activator poly(I):poly(C) in the presence α -³²P-ATP. (B) As panel A but using chromogenic detection of PP_i produced as a by-product of oligoadenylate synthesis by OAS1 in response to poly(I):poly(C) RNA or full-length VA RNA₁. OAS1 prep-to-prep variability is minimal (compare red, blue and black lines for each RNA) and relative activation by each RNA for a given prep is maintained (compare solid and dashed lines).



Supplementary Figure S3. Full activation of OAS1 by structured viral and cellular non-coding RNAs requires their 3'-end single-stranded pyrimidine-rich sequence (3'-ssPy motif). (A) Chromogenic assays showing optimal activation of OAS1 by EBER-1 RNA is dependent upon the presence of its 3'-end single stranded sequence. OAS1 activity is shown in the presence of wild-type EBER-1 (solid blue line), EBER-1 lacking the UUUU-3' sequence ($\Delta 3'$ -UUUU; dashed blue line) and wild-type VA RNA₁ (black). (B) As *panel A* for the cellular nc886 RNA with and without the UUUU-3' sequence (green solid and dashed lines, respectively). Poly(I):poly(C) activator RNA (black) is shown for comparison as nc886 is an unusually potent activator of OAS1.



Supplementary Figure S4. ssRNA sequences corresponding to the 18 bp dsRNA do not activate OAS1. Chromogenic assays are shown of OAS1 activation by each forward and reverse ssRNA (0.3 μ M; red and purple, respectively) or dsRNA duplex (0.3 μ M) with and without the 3'-ssPy motif (black solid and dashed lines, respectively). OAS1 activity is tightly controlled with no activity observed in the presence of ssRNAs. Activation by the equivalent dsRNA sequences is optimal with the additional 3'-end single-stranded sequence. These data demonstrate that the 3'-ssPy motif must be part of a dsRNA in order to exert its effect.



Supplementary Figure S5. A 5'-triphosphate group on the reverse strand of the model 18 bp dsRNA

has little effect on 3'-ssPy motif activity. (A) Chromogenic assays of OAS1 activation by the 18 bp

dsRNA without (purple) and with (black) a 3'-ssPy motif, in the absence (solid lines) or presence (dashed lines) of a 5'-end triphosphate (5'-PPP) on the complementary strand. Data in this and other panels are

normalized to the final PPi produced in the presence of the 18 bp dsRNA with a 3'-ssPy motif but without a 5'-triphosphate on the complementary strand (solid black line).

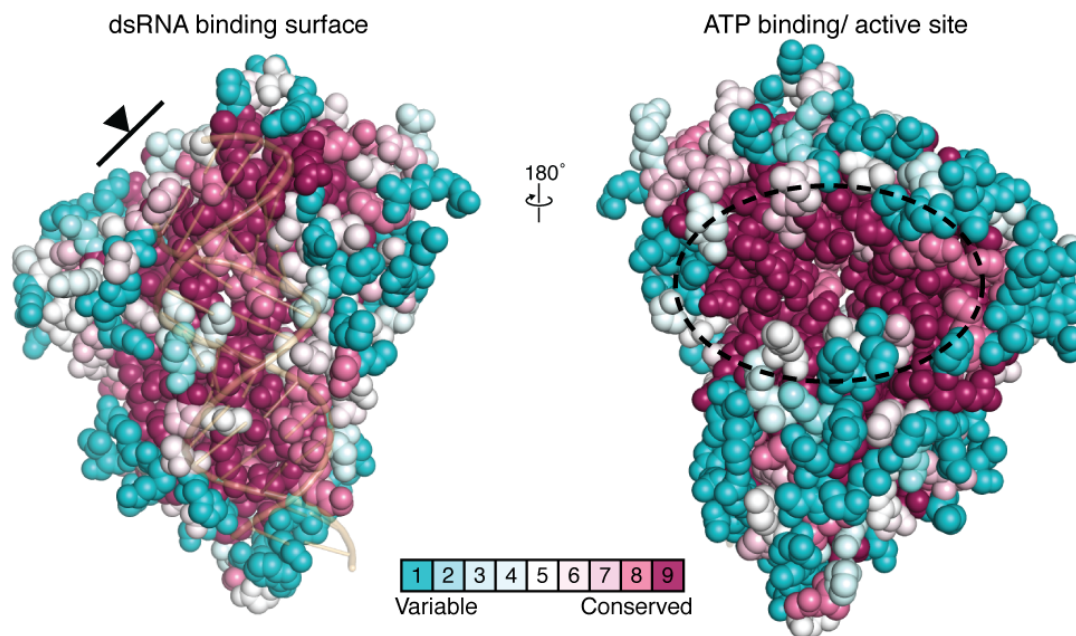
(B-D) The effect of the complementary strand 5'-triphosphate group on dsRNA duplexes with chemical modifications to the 3'-ssPy motif ribose group: (B) 2'-O-methyl (blue), (C) 3'-phosphate (green), and (D) 2'-deoxyribose (magenta).

Reaction curves for the 18 bp dsRNA with an unmodified 3'-ssPy, with and without a 5'-triphosphate on the complementary strand (dashed and solid black lines, respectively), shown for comparison in each panel are

the same as in *panel A*. The ability of the 3'-ssPy motif with chemical modifications to activate OAS1 was unaltered in the presence of a 5'-triphosphate group on the complementary strand, except for the 2'-O-

methyl ribose modification for the initial rate of PPi production was modestly enhanced (compare dashed and solid blue lines in *panel B*). The data presented in this figure are the same as those shown with a

different organization in **Figure 5** in the main text.



Supplementary Figure S6. Consurf analysis of OAS1. Consurf analysis (35) mapped onto the X-ray crystal structure of human OAS1 (PDB ID: 4IG8) determined in complex with the 18 bp dsRNA duplex (shown as transparent orange strands, *left*) highlighting the highly conserved dsRNA binding region (*left*) and ATP binding pocket (*right*, dashed circle). Regions predicted to interact with 3'-ssPy are located adjacent to the dsRNA binding surface (the plane and black arrow depict the orientation shown in **Figure 6**).

REFERENCES

1. Takeuchi, O. and Akira, S. (2010) Pattern recognition receptors and inflammation. *Cell*, **140**, 805-820.
2. Zust, R., Cervantes-Barragan, L., Habjan, M., Maier, R., Neuman, B.W., Ziebuhr, J., Szretter, K.J., Baker, S.C., Barchet, W., Diamond, M.S. *et al.* (2011) Ribose 2'-O-methylation provides a molecular signature for the distinction of self and non-self mRNA dependent on the RNA sensor Mda5. *Nat Immunol*, **12**, 137-143.
3. Kowalinski, E., Lunardi, T., McCarthy, A.A., Louber, J., Brunel, J., Grigorov, B., Gerlier, D. and Cusack, S. (2011) Structural basis for the activation of innate immune pattern-recognition receptor RIG-I by viral RNA. *Cell*, **147**, 423-435.
4. Cole, J.L. (2007) Activation of PKR: an open and shut case? *Trends Biochem Sci*, **32**, 57-62.
5. Yoneyama, M., Kikuchi, M., Natsukawa, T., Shinobu, N., Imaizumi, T., Miyagishi, M., Taira, K., Akira, S. and Fujita, T. (2004) The RNA helicase RIG-I has an essential function in double-stranded RNA-induced innate antiviral responses. *Nat Immunol*, **5**, 730-737.
6. Silverman, R.H. (2007) Viral encounters with 2',5'-oligoadenylate synthetase and RNase L during the interferon antiviral response. *J Virol*, **81**, 12720-12729.
7. Taguchi, T., Nagano-Fujii, M., Akutsu, M., Kadoya, H., Ohgimoto, S., Ishido, S. and Hotta, H. (2004) Hepatitis C virus NS5A protein interacts with 2',5'-oligoadenylate synthetase and inhibits antiviral activity of IFN in an IFN sensitivity-determining region-independent manner. *J Gen Virol*, **85**, 959-969.

8. Short, J.A.L. (2009) Viral evasion of interferon stimulated genes. *Bioscience Horizons*, **2**, 212-224.
9. Zhang, R., Jha, B.K., Ogden, K.M., Dong, B., Zhao, L., Elliott, R., Patton, J.T., Silverman, R.H. and Weiss, S.R. (2013) Homologous 2',5'-phosphodiesterases from disparate RNA viruses antagonize antiviral innate immunity. *Proc Natl Acad Sci U S A*, **110**, 13114-13119.
10. Cayley, P.J., Davies, J.A., McCullagh, K.G. and Kerr, I.M. (1984) Activation of the ppp(A2'p)nA system in interferon-treated, herpes simplex virus-infected cells and evidence for novel inhibitors of the ppp(A2'p)nA-dependent RNase. *Eur J Biochem*, **143**, 165-174.
11. Washenberger, C.L., Han, J.Q., Kechris, K.J., Jha, B.K., Silverman, R.H. and Barton, D.J. (2007) Hepatitis C virus RNA: dinucleotide frequencies and cleavage by RNase L. *Virus Res*, **130**, 85-95.
12. Alagarasu, K., Honap, T., Damle, I.M., Mulay, A.P., Shah, P.S. and Cecilia, D. (2013) Polymorphisms in the oligoadenylate synthetase gene cluster and its association with clinical outcomes of dengue virus infection. *Infect Genet Evol*, **14**, 390-395.
13. Lim, J.K., Lisco, A., McDermott, D.H., Huynh, L., Ward, J.M., Johnson, B., Johnson, H., Pape, J., Foster, G.A., Krysztof, D. *et al.* (2009) Genetic variation in OAS1 is a risk factor for initial infection with West Nile virus in man. *PLoS Pathog*, **5**, e1000321.

14. Donovan, J., Dufner, M. and Korennykh, A. (2013) Structural basis for cytosolic double-stranded RNA surveillance by human oligoadenylate synthetase 1. *Proc Natl Acad Sci U S A*, **110**, 1652-1657.
15. Kodym, R., Kodym, E. and Story, M.D. (2009) 2'-5'-Oligoadenylate synthetase is activated by a specific RNA sequence motif. *Biochem Biophys Res Commun*, **388**, 317-322.
16. Hartmann, R., Norby, P.L., Martensen, P.M., Jorgensen, P., James, M.C., Jacobsen, C., Moestrup, S.K., Clemens, M.J. and Justesen, J. (1998) Activation of 2'-5' oligoadenylate synthetase by single-stranded and double-stranded RNA aptamers. *J Biol Chem*, **273**, 3236-3246.
17. O'Malley, R.P., Mariano, T.M., Siekierka, J. and Mathews, M.B. (1986) A mechanism for the control of protein synthesis by adenovirus VA RNAI. *Cell*, **44**, 391-400.
18. Kitajewski, J., Schneider, R.J., Safer, B., Munemitsu, S.M., Samuel, C.E., Thimmappaya, B. and Shenk, T. (1986) Adenovirus VAI RNA antagonizes the antiviral action of interferon by preventing activation of the interferon-induced eIF-2 alpha kinase. *Cell*, **45**, 195-200.
19. Desai, S.Y., Patel, R.C., Sen, G.C., Malhotra, P., Ghadge, G.D. and Thimmappaya, B. (1995) Activation of interferon-inducible 2'-5' oligoadenylate synthetase by adenoviral VAI RNA. *J Biol Chem*, **270**, 3454-3461.
20. Andersson, M.G., Haasnoot, P.C., Xu, N., Berenjian, S., Berkhout, B. and Akusjarvi, G. (2005) Suppression of RNA interference by adenovirus virus-associated RNA. *J Virol*, **79**, 9556-9565.

21. Meng, H., Deo, S., Xiong, S., Džananović, E., Donald, L.J., van Dijk, C.W. and McKenna, S.A. (2012) Regulation of the interferon-inducible 2'-5'-oligoadenylate synthetases by adenovirus VA(I) RNA. *J Mol Biol*, **422**, 635-649.
22. Pe'ery, T. and Mathews, M.B. (1997) Synthesis and purification of single-stranded RNA for use in experiments with PKR and in cell-free translation systems. *Methods*, **11**, 371-381.
23. Linpinsel, J.L. and Conn, G.L. (2012) General protocols for preparation of plasmid DNA template, RNA in vitro transcription, and RNA purification by denaturing PAGE. *Methods Mol Biol*, **941**, 43-58.
24. Walker, S.C., Avis, J.M. and Conn, G.L. (2003) General plasmids for producing RNA in vitro transcripts with homogeneous ends. *Nucleic Acids Res*, **31**, e82.
25. Wahid, A.M., Coventry, V.K. and Conn, G.L. (2008) Systematic deletion of the adenovirus-associated RNAI terminal stem reveals a surprisingly active RNA inhibitor of double-stranded RNA-activated protein kinase. *J Biol Chem*, **283**, 17485-17493.
26. Lu, C. and Li, P. (2012) Preparation of short RNA by in vitro transcription. *Methods Mol Biol*, **941**, 59-68.
27. Sarkar, S.N., Pandey, M. and Sen, G.C. (2005) Assays for the interferon-induced enzyme 2',5' oligoadenylate synthetases. *Methods Mol Med*, **116**, 81-101.
28. Justesen, J. and Kjeldgaard, N.O. (1992) Spectrophotometric pyrophosphate assay of 2',5'-oligoadenylate synthetase. *Anal Biochem*, **207**, 90-93.
29. Nielsen, S., Yuzenkova, Y. and Zenkin, N. (2013) Mechanism of eukaryotic RNA polymerase III transcription termination. *Science*, **340**, 1577-1580.

30. Coventry, V.K. and Conn, G.L. (2008) Analysis of adenovirus VA RNAI structure and stability using compensatory base pair modifications. *Nucleic Acids Res*, **36**, 1645-1653.
31. Sharp, T.V., Raine, D.A., Gewert, D.R., Joshi, B., Jagus, R. and Clemens, M.J. (1999) Activation of the interferon-inducible (2'-5') oligoadenylate synthetase by the Epstein-Barr virus RNA, EBER-1. *Virology*, **257**, 303-313.
32. Jeon, S.H., Lee, K., Lee, K.S., Kunkeaw, N., Johnson, B.H., Holthauzen, L.M., Gong, B., Leelayuwat, C. and Lee, Y.S. (2012) Characterization of the direct physical interaction of nc886, a cellular non-coding RNA, and PKR. *FEBS Lett*, **586**, 3477-3484.
33. Le Roy, F., Salehzada, T., Bisbal, C., Dougherty, J.P. and Peltz, S.W. (2005) A newly discovered function for RNase L in regulating translation termination. *Nat Struct Mol Biol*, **12**, 505-512.
34. Bevilacqua, P.C. and Cech, T.R. (1996) Minor-groove recognition of double-stranded RNA by the double-stranded RNA-binding domain from the RNA-activated protein kinase PKR. *Biochemistry*, **35**, 9983-9994.
35. Ashkenazy, H., Erez, E., Martz, E., Pupko, T. and Ben-Tal, N. (2010) ConSurf 2010: calculating evolutionary conservation in sequence and structure of proteins and nucleic acids. *Nucleic Acids Res*, **38**, W529-533.
36. Wreschner, D.H., McCauley, J.W., Skehel, J.J. and Kerr, I.M. (1981) Interferon action--sequence specificity of the ppp(A2'p)nA-dependent ribonuclease. *Nature*, **289**, 414-417.

37. Malathi, K., Dong, B., Gale, M., Jr. and Silverman, R.H. (2007) Small self-RNA generated by RNase L amplifies antiviral innate immunity. *Nature*, **448**, 816-819.
38. Giannelli, G., Antonelli, G., Fera, G., Dianzani, F. and Schiraldi, O. (1993) 2',5'-Oligoadenylate synthetase activity as a responsive marker during interferon therapy for chronic hepatitis C. *J Interferon Res*, **13**, 57-60.
39. Jin, B., Cheng, L.F., Wu, K., Yu, X.H. and Yeo, A.E. (2014) Application of dsRNA in cancer immunotherapy: current status and future trends. *Anticancer Agents Med Chem*, **14**, 241-255.
40. Rissland, O.S. and Norbury, C.J. (2009) Decapping is preceded by 3' uridylation in a novel pathway of bulk mRNA turnover. *Nat Struct Mol Biol*, **16**, 616-623.
41. Choi, Y.S., Patena, W., Leavitt, A.D. and McManus, M.T. (2012) Widespread RNA 3'-end oligouridylation in mammals. *RNA*, **18**, 394-401.
42. Fabre, O., Salehzada, T., Lambert, K., Boo Seok, Y., Zhou, A., Mercier, J. and Bisbal, C. (2012) RNase L controls terminal adipocyte differentiation, lipids storage and insulin sensitivity via CHOP10 mRNA regulation. *Cell Death Differ*, **19**, 1470-1481.
43. Yu, L., Yan, K., Liu, P., Li, N., Liu, Z., Zhu, W., Chen, Y. and Han, D. (2014) Pattern recognition receptor-initiated innate antiviral response in mouse adipose cells. *Immunol Cell Biol*, **92**, 105-115.
44. Schoenfeld, J.D., Margalit, D.N., Kasperzyk, J.L., Shui, I.M., Rider, J.R., Epstein, M.M., Meisner, A., Kenfield, S.A., Martin, N.E., Nguyen, P.L. *et al.* (2013) A single nucleotide polymorphism in inflammatory gene RNASEL predicts outcome after radiation therapy for localized prostate cancer. *Clin Cancer Res*, **19**, 1612-1619.

CHAPTER 6:**Conclusions**

The preceding works have deepened our understanding of VA RNA_I interactions with innate immune proteins PKR and OAS1, and now serve as a platform for the formation of novel hypotheses for the mechanisms that control these proteins' activity (Figure 1). In the case of OAS1 in particular, many of the open questions call for validation in cells and exploration of the impacts of activation by specific RNAs on downstream innate immune proteins, specifically RNase L. In the following sections, the most immediate open questions are outlined, followed by more general discussion of the remaining gaps in our knowledge.

VA RNA_I INHIBITION OF PKR: OPEN QUESTIONS

Is VA RNA_I's inhibition of PKR defined by the three-helix junction?

Based upon the findings presented in Chapter 4, the primary requirement for VA RNA_I inhibition of PKR is a three-helix junction, an RNA feature far simpler than those previously hypothesized to govern VA RNA's ability to inhibit PKR (1-3). In addition to explaining how VA RNA_Is from a range of AdV serotypes are capable of inhibiting PKR, this finding also explains prior observations that large scale deletions and substitutions within VA RNA_I are tolerated by the virus (4): As long as the junction within VA RNA_I is maintained, PKR can still be effectively inhibited. In direct opposition to this observation of flexibility, however, are point mutations that are reported to significantly hamper VA RNA_I inhibition of PKR *in vitro* (5). It is difficult to reconcile the significant effects of single point mutations within the Central Domain with the more basic

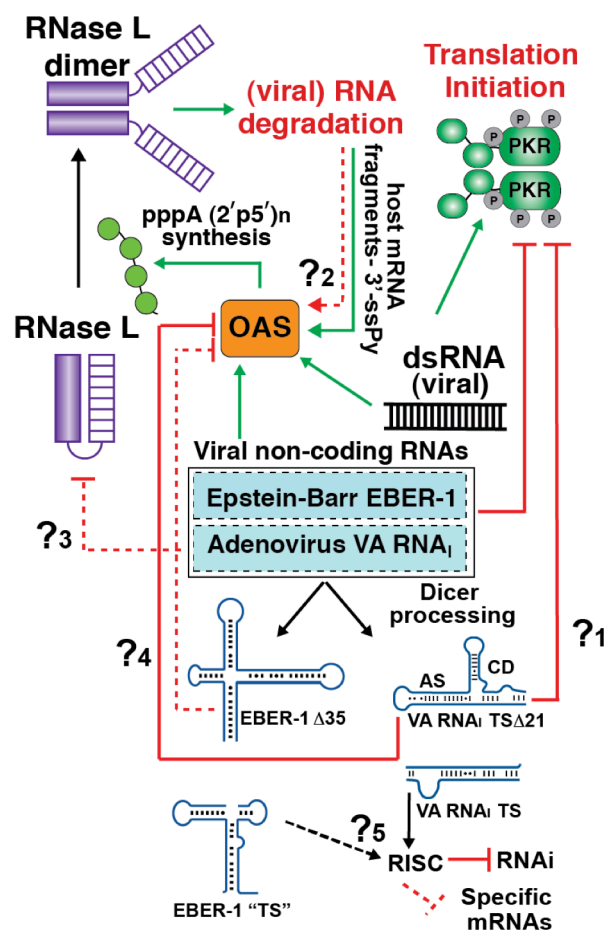


Figure 1. Updated model of interactions of viral non-coding VA RNA₁ and EBER-1 with dsRNA-activated innate immune proteins PKR (green) and OAS1 (orange). Remaining open questions arising from this work are highlighted: **1.** While the TSΔ21 fragment of VA RNA₁ retains its activity against PKR and possesses pseudoinhibitory activity against OAS1, this truncation is not identical to the Dicer-processed RNA. The question remains, are the activities of the authentic product of Dicer processing *in vivo* identical to those of the model RNA TSA21? **2.** Does amplification of the innate immune signal by RNase L degradation extend beyond host mRNA degradation and include viral mRNAs? Further, the 3'-ssPy motif may be an important part of this signal amplification. **3.** Does VA RNA₁ escape the consequences of OAS1 activation through direct inhibition of RNase L? **4.** EBER-1 is processed by Dicer *in vitro*, but do the activities of the truncated fragment mirror that of VA RNA₁? **5.** Are Dicer-processed EBER-1 fragments incorporated into the RISC complex, and if so do they have specific targets?

requirements we have observed. One potential explanation is that the structure and stability of the Central Domain, and therefore the three-helix junction, is particularly sensitive to mutation. This explanation is supported by the fact that the point mutations that most impair VA RNA₁ activity are clustered around the junction itself, and disrupt base-pair interactions likely to impact the overall structure of the RNA. In addition, the importance of the orientation of the conserved tetranucleotide sequence (GGGU/ACCC) is not in total agreement with our observations (1,2,6), e.g. mutating one of the G-C pairs to a C-G pair significantly attenuates VA RNA₁ activity. This observation was the foundation of the hypothesis that the Central Domain harbors tertiary interactions important for inhibition, and can be viewed as inconsistent with the idea that the junction is indeed the minimal requirement. While this is an important consideration, it is possible that the identity of the bases themselves are important for base-stacking interactions required for optimal stability of the junction and its inhibitory action in cooperation with the Apical Stem, which is the main PKR binding site. In order to fully reconcile these bodies of work, high-resolution crystallographic data that allow for direct visualization of VA RNA₁ bound to full-length PKR would be invaluable.

In broader terms, the discovery that a three-helix junction is the minimal requirement for PKR inhibition by VA RNA₁ raises the question of whether this is the same minimal requirement for other efficient RNA inhibitors of PKR such as EBER-1. For PKR inhibiting RNAs which lack a three-helix junction, such as the cellular nc886 RNA, what are the structural features that enable inhibition? More generally, will any three-helix junction-containing RNA capable of binding PKR inhibit the enzyme? These types of

questions are important for defining the general requirement for PKR inhibition. Is the three-helix junction sufficient: Can its presence turn an activator of PKR into an inhibitor? Beyond these questions, we can ask if the three-helix junction can serve as a predictor of RNA structures that will inhibit PKR, and if so, does selectively disrupting these junctions with small molecules hold promise for modulating the activities of these RNAs during infection?

Are a defined set of interdomain contacts required for PKR inhibition?

Though our work demonstrating the necessity of the three-helix junction of VA RNA_I clearly illustrates the aspects of the VA RNA_I structure important for inhibition, it does not provide a picture of the RNA-protein contacts required for inhibition, or how they may be different from those required for activation. The most current model of PKR activity dictates that VA RNA_I inhibition occurs exclusively from VA RNA_I prevention of PKR dimerization and autophosphorylation (7). Unpublished data from the lab however, indicate that both the RNA-binding and kinase domains of PKR are involved in mediating inhibition, and that the interdomain contacts required for VA RNA_I-mediated inhibition are not the same as those which occur during activation. This finding indicates that simply blocking dimerization is not the complete mechanism of VA RNA_I inhibition of PKR, but that inhibition requires some form of communication between the two protein domains distinct from that which occurs during activation. The nature of this communication remains to be elucidated. Additionally, the evidence from RNA structure probing and SAXS experiments that PKR alters the conformation of VA RNA_I upon binding minimally, if at all (2,8,9), may reflect the fact that VA RNA_I functions by

trapping PKR in state most closely resembling its free and inactive conformation. In contrast, perhaps, activating dsRNA may induce some larger, or at least distinct, conformational changes in PKR. High-resolution structural studies of VA RNA_I and PKR alone and in complex are needed to reveal interdomain contacts unique to inhibition, providing another avenue through which PKR activity may be modulated and allow for new insights into the defining features of an RNA inhibitor of PKR.

DICER PROCESSING OF VA RNA_I

Dicer processing of VA RNA_I produces a fragment that is not identical to TSA21

The TSA21 construct is a small active construct ideal for biochemical characterization and, potentially, structural studies of PKR (2,3). Though TSA21 is similar in size to the Dicer-processed form of VA RNA_I (Figure 2), it is not identical (3,10). Dicer-processed VA RNA_I also closely resembles the VA RNA_I TSA15 truncation mutant, which has significantly diminished inhibitory activity against PKR (3). Discovery that dsRNAs appended with single-stranded sequences can differently modulate both PKR and OAS1 activity (11,12) warrants a more careful examination of the activity of the Dicer-processed form of VA RNA_I. The presence of these single-stranded regions in the Dicer-processed fragment may confer a different activity against OAS1 than that observed for TSA21 (Figure 1). The discovery of the 3'-ssPy motif further highlights the potential importance of these subtle differences and raises the distinct possibility that OAS1 may not be inhibited to the same degree by the actual product of Dicer processing as it is by TSA21 (11). One reason to suspect that this may be the case is that Dicer processing

produces an RNA with five 3'-end single-stranded nucleotides, the first of which is a pyrimidine, while the TS Δ 21 construct terminates with a base paired G. Additionally, only one OAS1 activation consensus sequence is retained in TS Δ 21, while both are retained in the Dicer-processed VA RNA_I fragment.

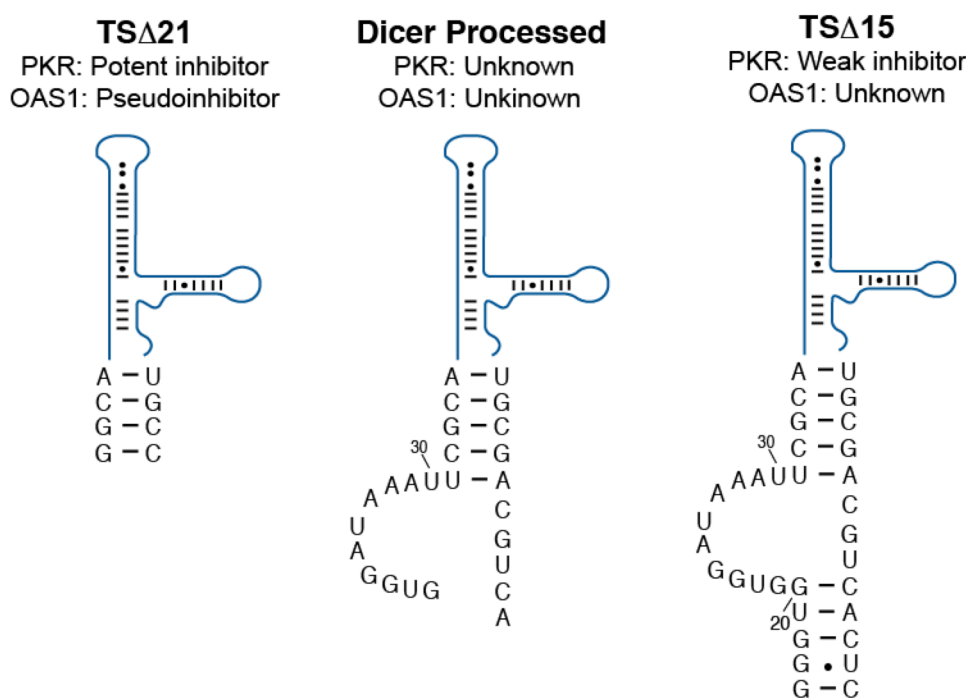


Figure 2. The Dicer-processed VA RNA_I is not identical to TS Δ 21. Comparison of the sequences and structures present at the termini of the TS Δ 21 deletion, the Dicer-processed fragment (mivaRNA138), and the TS Δ 15 deletion mutant. Known activities of each variant are listed.

These open questions may be easily addressed by testing an *in vitro* transcribed RNA designed to exactly mimic the VA RNA_I product of Dicer processing using the kinase and chromogenic assays described in this work. Such studies are important for continuing to connect *in vitro* findings to cellular processes. In addition to resolving this discrepancy, the function of the Dicer-processed VA RNA_I fragment must include an

evaluation of the stability of the fragment *in vivo*. While a great deal of effort has been focused upon identifying the targets of the miRNAs derived from the Terminal Stem, little has been done to show that the remaining Apical Stem-Central Domain fragment is stable or if it is bound by cellular proteins. While one group has reported that the fragment is indeed unstable (13), and not present in cellular extracts of AdV-infected cells, this was not the focus of their investigation, and the specific data is not presented. Additionally, to detect this fragment, this group used a labeled probe to the Apical Stem of the RNA, which is incredibly stable (14). It is possible that the extreme denaturation required to unfold the Apical Stem and allow hybridization was not applied. To best move forward with investigations of the Dicer-processed fragment, its presence in the cell must be assessed and the RNAs utilized in *in vitro* experiments must better reflect the actual Dicer-cleavage product and its activities against PKR and OAS in the cell.

FUNCTIONAL IMPLICATIONS OF THE 3'-ssPy MOTIF

What is the mechanism of potentiation of OAS1 by the 3'-ssPy motif?

Further investigation of how the 3'-ssPy motif modulates OAS1 activity is required to build an understanding of its mechanism. In addition to being both simple and potent, the model duplex system used in studies in Chapter 5 presents a unique opportunity to investigate how the 3'-ssPy motif exerts its effect. The 18 bp dsNA possesses two overlapping consensus sequences, one on each strand running in antiparallel orientation (Figure 3A). Previous work from another lab shows that OAS1 does not tolerate mutations in the final G of the consensus sequence (15), providing an avenue through which we can independently assess contributions of each consensus sequence and the

effect of the 3'-ssPy motif on OAS1 activation. Assuming that these consensus sequences are equivalent, we will be able to determine if the 3'-ssPy motif is driving OAS1 to bind to one activation sequence at the expense of the other. For example, a consensus sequence inactivated by a G to U mutation appended with a 3'-ssPy will display activity lower than the dsRNA without the 3'-ssPy motif. Further, moving the 3'-ssPy motif to the reverse strand containing an intact activation sequence should restore activity. Alternatively, a 3'-ssPy may augment OAS1 activation through an alternative unknown mechanism, presenting the possibility that appending a 3'-ssPy to both ends of the model RNA may increase activity beyond that observed with a single 3'-ssPy. RNAs designed to test the relative contributions of the consensus sequences and the effects of appending the 3'-ssPy motif to each are shown in Figure 3B, (group 1).

While the above experiments make the assumption that the sequences are equivalent, there is some evidence in the literature which suggest that the activation potential of these consensus sequences are context dependent (16), and there are some differences which may make them functionally non-equivalent. First, the consensus sequence on the forward strand is located only one nucleotide before the 3'-terminus of the RNA, while on the reverse strand there are two nucleotides following the final consensus sequence G (Figure 3A). Not only does this difference change the distance of the consensus sequence from the end of the RNA, but it changes the number of nucleotides between the consensus sequence and an appended 3'-ssPy.

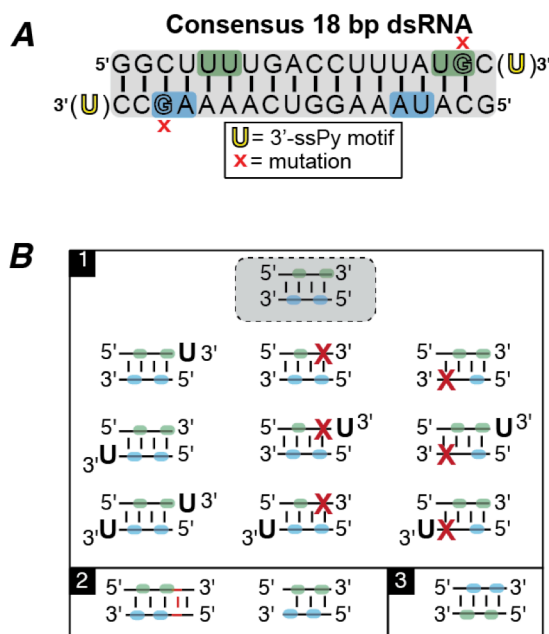


Figure 3. OAS1 binding orientation and potency is derived from the context-specific effects of the activation consensus sequence and the 3'-ssPy motif. (a) The 18 bp model duplex RNA with the consensus sequence highlighted in each strand (shaded blue or green boxes) with sites of mutations and 3'-ssPy motif indicated. (b) Design of constructs to test **1**. The context in which the consensus sequences and the 3'-ssPy motif exert an effect on OAS1 activity, **2**. Placement of the consensus sequences in respect to the dsRNA ends by insertion (left) or deletion (right), and **3**. The effect of sequence context.

To address these potential disparities, we have designed dsRNA variants to evaluate potential contributions of these differences to non-equivalence of OAS1 binding and orientations (Figure 3B, group 2). Second, the nine nucleotides between the defining components of the consensus sequence are different. While work from other labs indicates that these sequences are unlikely to exert an effect, they should be considered if the consensus sequences are found to behave dissimilarly. Finally, while both the forward and reverse strand possess an activation consensus sequence (WWN₉WG) (17), the sequence in the forward strand is UU(N₉)UG, while the reverse is UA(N₉)AG. The

difference in the identity of these bases may also contribute to any differences in the ability of the forward- and reverse-strand sequences to activate OAS1 (Figure 3B, group 3). Because dsRNA binding and activation are non-equivalent for OAS1 activation (16), non-equivalence of the two consensus sequences may provide a simple model system in which to assess the relationship between binding and activation within the same molecule. To assess the equivalence of the activation sequences, the G shown to be important in OAS1 activation in each strand may be mutated to evaluate the contribution of each to the ability of the 18 bp dsRNA model duplex to activate OAS1.

Upon discerning the ‘rules’ that govern OAS1 activation by the 18 bp dsRNA, their application to a more highly structured RNA such as VA RNA_I may allow for dissection of how an additional layer of structural complexity can further modulate OAS1 regulation. Alternatively, the rules may be in part or entirely different, in which case the

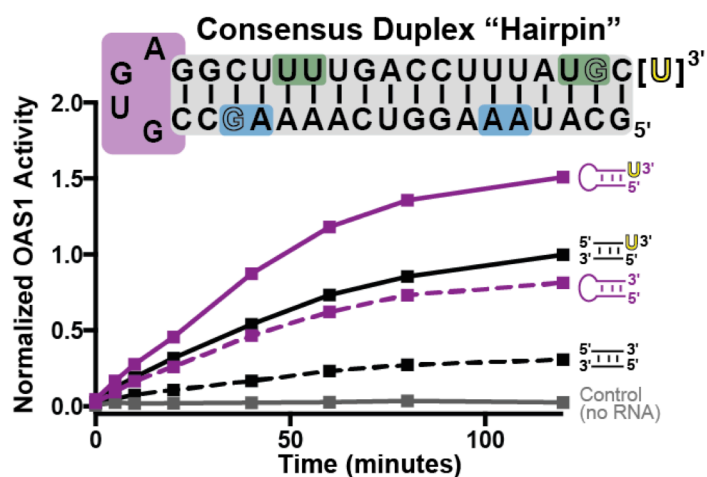


Figure 4. A 40 nt hairpin RNA construct containing the 18 bp model duplex RNA for cell-based studies. The new RNA (top) was cloned, transcribed, and found to both strongly activate OAS1 relative to the equivalent dsRNA (compare purple and black lines) and to retain dependence of the 3'-ssPy motif for optimal activation (compare purple solid and dashed lines).

changes in how OAS is activated introduced by RNA structure must be evaluated.

What are the functional implications of the 3'-ssPy motif *in vivo*?

While the 3'-ssPy motif consistently potentiates OAS1 activation by both duplex and highly structured RNAs *in vitro* (11), its functional consequences *in vivo* have not been explored. To facilitate these types of experiments, we have cloned and transcribed a 40 nt hairpin which contains the 18 bp consensus activation sequence, which is both capable of activating OAS *in vitro*, and also sensitive to the 3'-ssPy motif (Figure 4). Experiments which monitor the activity of OAS1 in cells transfected with a 40 nt duplex hairpin which contains the 18 bp duplex sequences, with and without the 3'-ssPy motif, will be an important first step for understanding how the 3'-ssPy motif ties into the cell's anti-viral response. We hypothesize that cells transfected with 40 nt hairpin RNA with the 3'-ssPy motif will show higher RNase L-mediated degradation of rRNA, an established read out for cellular OAS activity, than cells transfected with 40 nt hairpin lacking the 3'-ssPy motif. This effect would correlate with *in vitro* activity of OAS1 to alterations in OAS1/RNase L pathway activity.

RNase L amplifies the innate immune signals by generating RIG-I-activating fragments by cleaving self mRNA (18). Because RNase L cleaves primarily after single-stranded UU and UA dinucleotides within otherwise highly structured RNA (19,20), it likely produces dsRNAs with the 3'-ssPy motif. These RNase L-derived dsRNAs may therefore further increase activation of OAS1 in a positive feedback loop, directly amplifying innate immune signaling through the OAS1/RNase L pathway in addition to the effects of

RNase L products on RIG-I (Figure 1). In support of this hypothesis, unpublished observations indicate that the effect of the 3'-ssPy motif may be concentration dependent, raising the possibility that the 3'-ssPy motif is especially important for detection of limited viral dsRNA early in infection.

Does VA RNA_I activate OAS1 *in vivo*?

To date, work describing VA RNA_I activation of OAS1 is limited to *in vitro* experiments. VA RNA_I is a comparatively weak activator of OAS1: dsRNA of the same length is over ten times as active (21). Whether the degree to which OAS1 is activated by VA RNA_I is sufficient to elicit an anti-viral response is unknown. Furthermore, while experiments which address the basic ability of VA RNA_I to activate OAS1 *in vivo* are certainly needed, a recent study showing that OAS1 antiviral activity is strongly correlated with the level of OAS1 mRNA (22), introduces a complicating factor. This study showed that OAS1 mRNA levels are highest in the cells which give rise to nervous tissues, and that knocking down OAS1 in myocytes has a far greater effect on the outcome of virus infection than in other cell types. This finding supports the idea that OAS1 ability to limit virus replication is linked to its expression level. Further, that myocytes are the cells in which OAS1 is most highly expressed makes sense, as nearly all of the viruses for which OAS1 polymorphisms are detrimental to the host are neurotropic (23-25). Thus, in addition to determining whether VA RNA_I is capable of activating OAS1 *in vivo*, experiments addressing the likely impact of this ability on the outcome of infection within different cell types are important.

Is VA RNA_I activation of OAS1 beneficial to the virus?

While much remains unknown about the degree to which VA RNA_I activates OAS1 *in vivo* it is possible that low-level activation of OAS1 is beneficial to the virus. Much of the work on OAS1 monitors the effect on the cell of large amounts of pppA(2'-5'A)_n, overexpression of RNase L, or the effect of poly(I).(C) RNA, an extraordinarily potent activator of OAS1. Though high-level activation of the OAS1/ RNase L pathway leads to degradation of rRNA and cell death (26), the effects of intermediate or low-level activation of the pathway are underexplored. RNase L is known to behave in a dose-dependent manner (27), and to degrade different types of RNA: host mRNA, rRNA, and virus genome and mRNA (28-30). It stands to reason that the targets of RNase L are context dependent, and that low-level activation of RNase L may lead to more specific target degradation. Therefore, what at first appears to be a counterproductive activity, may in fact be a way for the virus to control gene expression. For example, low-level activation of RNase L might permit rapid degradation of early viral gene mRNA in favor of late gene mRNA. Accumulation of VA RNA_I at later stages in infection might coincide with a need to rapidly shift gene expression. The secondary structures of target mRNAs in which UU and UA dinucleotides are exposed or occluded may also serve as another level of control over RNase L-mediated mRNA degradation.

ADDITIONAL POTENTIAL PROVIRAL ROLES FOR VA RNA_I**Is VA RNA_I an inhibitor of RNase L?**

The only known target of the pppA(2'-5'A)_n oligos synthesized by OAS1 upon binding to dsRNA is RNase L. Though the true targets of RNase L during virus infection are unknown, the net effect is cessation of protein synthesis (31). In addition to halting translation directly, through degradation of RNA, RNase L activity has a secondary function: amplifying the innate immune response through generation of host mRNA fragments shown to be capable of activating RIG-I and MDA5 (18,20). We hypothesize that AdV is able to overcome its low-level activation of OAS1, and the potentially disastrous amplification of innate immune signals, through direct inhibition of RNase L. Further, we hypothesize that VA RNA_I itself may be a competitive inhibitor of RNase L (Figure 1). While viruses have evolved a number of mechanisms to inhibit RNase L, there is only one example of a competitive RNA inhibitor, a structured RNA located within the poliovirus protein-coding region (32). Should our hypothesis regarding the inhibitory effect of VA RNA_I on RNase L prove to be correct, VA RNA_I will possess yet another pro-viral function in addition to its inhibition of both PKR and the RNAi machinery.

THE FUNCTIONS OF EBV EBER-1 REMAIN UNCLEAR

In spite of the structural similarities between VA RNA_I and EBER-1 and their shared ability to inhibit PKR (33-35), the functions of EBER-1 are less defined. EBER-1's localization has been reported to be both nuclear and cytoplasmic, and is likely dependent upon cellular contexts such as cell cycle stage (36-39). During the course of this work, the similarities between VA RNA_I and EBER-1 were expanded to show that they activate OAS1 to the same level (11). In addition, preliminary experiments demonstrated that

EBER-1 is indeed processed by Dicer *in vitro*. While it is clear that VA RNA_I and EBER-1 do not serve identical roles (40), their functions may overlap in previously unappreciated ways. Further research is needed to confirm Dicer processing of EBER-1 *in vivo*, and to evaluate the roles of any fragments produced (Figure 1). Importantly, evaluating the activities of EBER-1 against these cytoplasmic innate immune proteins must be coupled with studies of when EBER-1 is localized to the cytoplasm and available to regulate their activities.

CONCLUSION

Further expanding our understanding of the activation and inhibition requirements for both PKR and OAS1 will allow for development of a clear picture of how these two innate immune systems overlap, and how the interplay between the two systems effects host-pathogen interaction. A complete understanding of the RNA features required for activation or inhibition of these enzymes is critical for the development of general antiviral therapies that selectively potentiate the activities of these proteins. General therapies unreliant on the adaptive immune response are especially important for treating viral infections in the elderly, infants, and immunocompromised people, as well as for treating viral infections for which there are no vaccines or effective treatments.

REFERENCES

1. Ma, Y. and Mathews, M.B. (1996) Secondary and tertiary structure in the central domain of adenovirus type 2 VA RNA I. *RNA*, **2**, 937-951.

2. Wilson, J.L., Vachon, V.K., Sunita, S., Schwartz, S.L. and Conn, G.L. (2014) Dissection of the adenoviral VA RNAI central domain structure reveals minimum requirements for RNA-mediated inhibition of PKR. *J Biol Chem*, **289**, 23233-23245.
3. Wahid, A.M., Coventry, V.K. and Conn, G.L. (2008) Systematic deletion of the adenovirus-associated RNAI terminal stem reveals a surprisingly active RNA inhibitor of double-stranded RNA-activated protein kinase. *J Biol Chem*, **283**, 17485-17493.
4. Bhat, R.A., Domer, P.H. and Thimmappaya, B. (1985) Structural requirements of adenovirus VAI RNA for its translation enhancement function. *Mol Cell Biol*, **5**, 187-196.
5. Rahman, A., Malhotra, P., Dhar, R., Kewalramani, T. and Thimmappaya, B. (1995) Effect of single-base substitutions in the central domain of virus-associated RNA I on its function. *J Virol*, **69**, 4299-4307.
6. Ma, Y. and Mathews, M.B. (1996) Structure, function, and evolution of adenovirus-associated RNA: a phylogenetic approach. *J Virol*, **70**, 5083-5099.
7. Cole, J.L. (2007) Activation of PKR: an open and shut case? *Trends Biochem Sci*, **32**, 57-62.
8. Wahid, A.M., Coventry, V.K. and Conn, G.L. (2009) The PKR-binding domain of adenovirus VA RNAI exists as a mixture of two functionally non-equivalent structures. *Nucleic Acids Res*, **37**, 5830-5837.
9. Dzananovic, E., Patel, T.R., Chojnowski, G., Boniecki, M.J., Deo, S., McEleney, K., Harding, S.E., Bujnicki, J.M. and McKenna, S.A. (2014) Solution conformation of

- adenovirus virus associated RNA-I and its interaction with PKR. *J Struct Biol*, **185**, 48-57.
10. Xu, N., Gkoutela, S., Saeed, K. and Akusjarvi, G. (2009) The 5'-end heterogeneity of adenovirus virus-associated RNAI contributes to the asymmetric guide strand incorporation into the RNA-induced silencing complex. *Nucleic Acids Res*, **37**, 6950-6959.
 11. Vachon, V.K., Calderon, B.M. and Conn, G.L. (2015) A novel RNA molecular signature for activation of 2'-5' oligoadenylate synthetase-1. *Nucleic Acids Res*, **43**, 544-552.
 12. Zheng, X. and Bevilacqua, P.C. (2004) Activation of the protein kinase PKR by short double-stranded RNAs with single-stranded tails. *RNA*, **10**, 1934-1945.
 13. Carnero, E., Sutherland, J.D. and Fortes, P. (2011) Adenovirus and miRNAs. *Biochim Biophys Acta*, **1809**, 660-667.
 14. Coventry, V.K. and Conn, G.L. (2008) Analysis of adenovirus VA RNAI structure and stability using compensatory base pair modifications. *Nucleic Acids Res*, **36**, 1645-1653.
 15. Donovan, J., Dufner, M. and Korennykh, A. (2013) Structural basis for cytosolic double-stranded RNA surveillance by human oligoadenylate synthetase 1. *Proc Natl Acad Sci U S A*, **110**, 1652-1657.
 16. Hartmann, R., Norby, P.L., Martensen, P.M., Jorgensen, P., James, M.C., Jacobsen, C., Moestrup, S.K., Clemens, M.J. and Justesen, J. (1998) Activation of 2'-5' oligoadenylate synthetase by single-stranded and double-stranded RNA aptamers. *J Biol Chem*, **273**, 3236-3246.

17. Kodym, R., Kodym, E. and Story, M.D. (2009) 2'-5'-Oligoadenylate synthetase is activated by a specific RNA sequence motif. *Biochem Biophys Res Commun*, **388**, 317-322.
18. Malathi, K., Dong, B., Gale, M., Jr. and Silverman, R.H. (2007) Small self-RNA generated by RNase L amplifies antiviral innate immunity. *Nature*, **448**, 816-819.
19. Wreschner, D.H., McCauley, J.W., Skehel, J.J. and Kerr, I.M. (1981) Interferon action--sequence specificity of the ppp(A2'p)nA-dependent ribonuclease. *Nature*, **289**, 414-417.
20. Malathi, K., Saito, T., Crochet, N., Barton, D.J., Gale, M., Jr. and Silverman, R.H. (2010) RNase L releases a small RNA from HCV RNA that refolds into a potent PAMP. *RNA*, **16**, 2108-2119.
21. Desai, S.Y., Patel, R.C., Sen, G.C., Malhotra, P., Ghadge, G.D. and Thimmapaya, B. (1995) Activation of interferon-inducible 2'-5' oligoadenylate synthetase by adenoviral VAI RNA. *J Biol Chem*, **270**, 3454-3461.
22. Zhao, L., Birdwell, L.D., Wu, A., Elliott, R., Rose, K.M., Phillips, J.M., Li, Y., Grinspan, J., Silverman, R.H. and Weiss, S.R. (2013) Cell-type-specific activation of the oligoadenylate synthetase-RNase L pathway by a murine coronavirus. *J Virol*, **87**, 8408-8418.
23. Alagarasu, K., Honap, T., Damle, I.M., Mulay, A.P., Shah, P.S. and Cecilia, D. (2013) Polymorphisms in the oligoadenylate synthetase gene cluster and its association with clinical outcomes of dengue virus infection. *Infect Genet Evol*, **14**, 390-395.

24. Lim, J.K., Lisco, A., McDermott, D.H., Huynh, L., Ward, J.M., Johnson, B., Johnson, H., Pape, J., Foster, G.A., Krysztof, D. *et al.* (2009) Genetic variation in OAS1 is a risk factor for initial infection with West Nile virus in man. *PLoS Pathog*, **5**, e1000321.
25. Zhou, A., Paranjape, J., Brown, T.L., Nie, H., Naik, S., Dong, B., Chang, A., Trapp, B., Fairchild, R., Colmenares, C. *et al.* (1997) Interferon action and apoptosis are defective in mice devoid of 2',5'-oligoadenylate-dependent RNase L. *EMBO J*, **16**, 6355-6363.
26. Silverman, R.H., Skehel, J.J., James, T.C., Wreschner, D.H. and Kerr, I.M. (1983) rRNA cleavage as an index of ppp(A2'p)nA activity in interferon-treated encephalomyocarditis virus-infected cells. *J Virol*, **46**, 1051-1055.
27. Nilsen, T.W. and Baglioni, C. (1979) Mechanism for discrimination between viral and host mRNA in interferon-treated cells. *Proc Natl Acad Sci U S A*, **76**, 2600-2604.
28. Andersen, J.B., Mazan-Mamczarz, K., Zhan, M., Gorospe, M. and Hassel, B.A. (2009) Ribosomal protein mRNAs are primary targets of regulation in RNase-L-induced senescence. *RNA Biol*, **6**, 305-315.
29. Baglioni, C., De Benedetti, A. and Williams, G.J. (1984) Cleavage of nascent reovirus mRNA by localized activation of the 2'-5'-oligoadenylate-dependent endoribonuclease. *J Virol*, **52**, 865-871.
30. Li, X.L., Blackford, J.A. and Hassel, B.A. (1998) RNase L mediates the antiviral effect of interferon through a selective reduction in viral RNA during encephalomyocarditis virus infection. *J Virol*, **72**, 2752-2759.

31. Silverman, R.H. (2007) Viral encounters with 2',5'-oligoadenylate synthetase and RNase L during the interferon antiviral response. *J Virol*, **81**, 12720-12729.
32. Keel, A.Y., Jha, B.K. and Kieft, J.S. (2012) Structural architecture of an RNA that competitively inhibits RNase L. *RNA*, **18**, 88-99.
33. Rosa, M.D., Gottlieb, E., Lerner, M.R. and Steitz, J.A. (1981) Striking similarities are exhibited by two small Epstein-Barr virus-encoded ribonucleic acids and the adenovirus-associated ribonucleic acids VAI and VAII. *Mol Cell Biol*, **1**, 785-796.
34. Mathews, M.B. and Shenk, T. (1991) Adenovirus virus-associated RNA and translation control. *J Virol*, **65**, 5657-5662.
35. Clarke, P.A., Sharp, N.A. and Clemens, M.J. (1990) Translational control by the Epstein-Barr virus small RNA EBER-1. Reversal of the double-stranded RNA-induced inhibition of protein synthesis in reticulocyte lysates. *Eur J Biochem*, **193**, 635-641.
36. Fok, V., Friend, K. and Steitz, J.A. (2006) Epstein-Barr virus noncoding RNAs are confined to the nucleus, whereas their partner, the human La protein, undergoes nucleocytoplasmic shuttling. *J Cell Biol*, **173**, 319-325.
37. Howe, J.G. and Steitz, J.A. (1986) Localization of Epstein-Barr virus-encoded small RNAs by in situ hybridization. *Proc Natl Acad Sci U S A*, **83**, 9006-9010.
38. Young, L.S. and Rickinson, A.B. (2004) Epstein-Barr virus: 40 years on. *Nat Rev Cancer*, **4**, 757-768.
39. Schwemmle, M., Clemens, M.J., Hilse, K., Pfeifer, K., Troster, H., Muller, W.E. and Bachmann, M. (1992) Localization of Epstein-Barr virus-encoded RNAs EBER-1

- and EBER-2 in interphase and mitotic Burkitt lymphoma cells. *Proc Natl Acad Sci U S A*, **89**, 10292-10296.
40. Bhat, R.A. and Thimmappaya, B. (1983) Two small RNAs encoded by Epstein-Barr virus can functionally substitute for the virus-associated RNAs in the lytic growth of adenovirus 5. *Proc Natl Acad Sci U S A*, **80**, 4789-4793.